

# MONITORING COINTEGRATING POLYNOMIAL REGRESSIONS

## SUPPLEMENTARY APPENDIX B: LOCAL ASYMPTOTIC POWER

FABIAN KNORRE, MARTIN WAGNER AND MAXIMILIAN GRUPE

### Local Asymptotic Power

In this appendix we consider local asymptotic power (LAP) in models of the form in (1) in the main document with the following specifications: Intercept and intercept plus linear trend, up to four integrated regressors and consecutive powers of up to order three of one of the integrated regressors. Denote as in the main text, w.l.o.g.,  $x_{kt}$  as the I(1) regressor considered to enter the regression model with powers larger than one. The LAP results are based on 10,000 replications using time series of length 1,000 of i.i.d. standard normals to approximate the limiting distributions. The limiting distributions underlying LAP, as discussed in Proposition 3(b), are based on the functional central limit theorems for the scaled partial sum residual processes under the local alternatives discussed in Appendix A. In particular these FCLTs are given in:

- Local I(1) breaks ( $\{u_t\}$  changes its behavior from I(0) to I(1)): Equation (A2) in Appendix A.
- Local trend breaks: Equation (A3) in Appendix A.
- Local slope breaks: Equation (A4) in Appendix A.

For local I(1) breaks the limiting distribution depends, in addition to the break magnitude parameter  $\delta$ , on the ratio of the long-run variance  $\omega_\gamma^2$  of the additional error component  $\{\gamma_t\}$  and the conditional long-run variance  $\omega_{u.v}^2$ .<sup>1</sup> We set this ratio to  $\frac{\omega_\gamma^2}{\omega_{u.v}^2} := 1$ . Similarly, the limiting distribution in case of local slope breaks depends on the long-run covariance matrix  $\Omega_{vv}$  of the regressors. We set  $\Omega_{vv} := I_k$ . The parameter  $\delta$  determines the magnitude of a local I(1) break and

<sup>1</sup>Note: The limiting distribution underlying LAP in case of local I(1) breaks in Equation (30) of Wagner and Wied (2017) contains a typo. The long-run variance  $\omega^2$  must be replaced by the *conditional* long-run variance  $\omega_{u.v}^2$ . This also holds for the corresponding discussion in the main text and in Supplementary Appendix B, where  $\omega_\xi/\omega$  must be replaced by  $\omega_\xi/\omega_{u.v}$ .

varies in 1001 equidistant steps over the interval  $[0, 10000]$ . The value  $\delta = 0$  corresponds to the null hypothesis. Similarly,  $\Delta_{\theta_D}$  indicates the magnitude of a local break in the coefficient of the linear trend.<sup>2</sup> The parameter  $\Delta_{\theta_D}$  varies in 751 equidistant steps over the interval  $[0, 1500]$ , with  $\Delta_{\theta_D} = 0$  corresponding to the null hypothesis. In case of local slope breaks, the magnitude of a local break in the slope parameter is given by  $\Delta_{\theta_X}$ .<sup>3</sup> We consider 1001 equally spaced values of  $\Delta_{\theta_X}$  in the interval  $[0, 10000]$ , with  $\Delta_{\theta_X} = 0$  corresponding to the null hypothesis. For local slope breaks we consider a local break either in the coefficient corresponding to  $x_{kt}$  or in the coefficient corresponding to  $x_{kt}^2$ . All simulations are performed at the 5% significance level.

With respect to the stochastic regressors, LAP depends upon  $k$ , the number of I(1) regressors, and  $p_k$ , the highest power of  $x_{kt}$ . Figure S1 displays for different values of  $k$  and  $p_k$  LAP against local I(1) breaks in the intercept and linear trend case using  $\hat{H}^m$ . As expected, LAP decreases when further I(1) regressors or higher powers are included. With this observation in mind, for the sake of brevity all other LAP results are presented only for the case including a single I(1) regressor and its square (i.e.,  $k = 1$  and  $p_k = 2$ ), considering both deterministic specifications, intercept and intercept and linear trend. This case also covers the quadratic EKC model, which we use in addition to the linear and cubic model in the empirical application in Section 4 in the main document.

In most considered settings the two detectors  $\hat{H}^m$  and  $\hat{H}_d^m$  lead to nearly identical LAP. In a few cases, however, LAP of  $\hat{H}_d^m$  is considerably lower than that of  $\hat{H}^m$ . Therefore, we neglect  $\hat{H}_d^m$  in our LAP analysis and focus on  $\hat{H}^m$ ,  $\hat{H}_{sn}^m$ ,  $\hat{H}_{mov}^{m,n}$  and  $\hat{H}_{mov,sn}^{m,n}$ , for  $n = 0.1, 0.2, 0.3$ .

We start with local I(1) breaks and compare LAP with respect to the estimation method. Figure S2 displays LAP against local I(1) breaks in the intercept only case for FM-/D-OLS and IM-OLS using the four detectors  $\hat{H}^m$ ,  $\hat{H}_{sn}^m$ ,  $\hat{H}_{mov}^{m,0.1}$  and  $\hat{H}_{mov,sn}^{m,0.1}$ . Calibration and break fraction are set to  $m = 0.5$  and  $r = 0.75$ , respectively. For each of the four detectors FM-/D-OLS leads to higher LAP than IM-OLS. This result is independent of the choice of the window size, deterministic specification, calibration and break fraction and is in line with standard asymptotic theory concerning estimator efficiency. The next aspect considered is the impact of the window size on LAP and in addition the comparison to a detector without moving window. Figure S3 displays

---

<sup>2</sup>In Proposition 3(b)  $\Delta_{\theta_D}$  refers to a vector defining changes of all elements of  $\theta_D \in \mathbb{R}^q$ , with  $\Delta_{\theta_D} \in \mathbb{R}^q$ . In the LAP analysis only a single element of  $\theta_D$  changes. To avoid overloaded notation,  $\Delta_{\theta_D}$  denotes in the LAP analysis only the change in a single element, thus  $\Delta_{\theta_D} \in \mathbb{R}$ .

<sup>3</sup>The parameter  $\Delta_{\theta_X}$  refers in the LAP analysis – in a similar fashion as  $\Delta_{\theta_D}$  – to a scalar value, in contrast to Proposition 3(b) where  $\Delta_{\theta_X} \in \mathbb{R}^p$ .

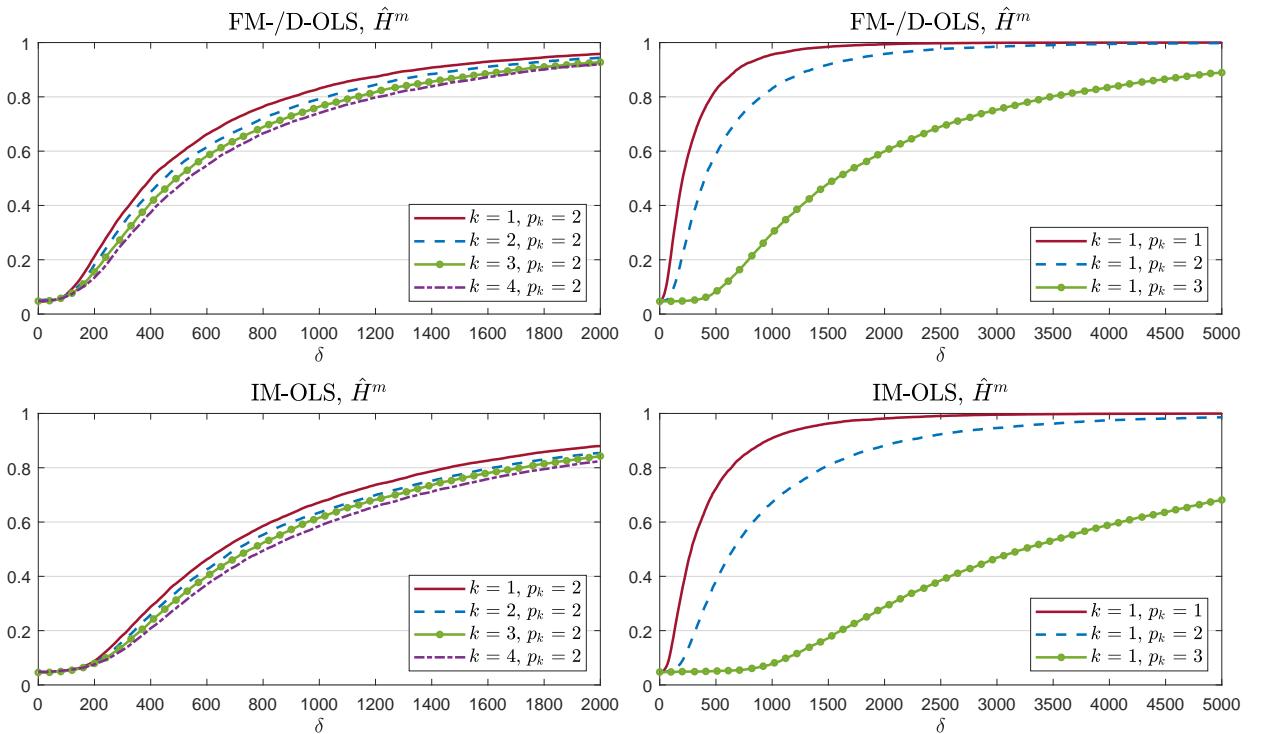


Figure S1: Local asymptotic power against I(1) breaks in the intercept and linear trend case for  $\hat{H}^m$ . The upper two plots correspond to FM-/D-OLS and the lower plots to IM-OLS. Calibration and break fraction are set to  $m = 0.5$  and  $r = 0.75$ , respectively.

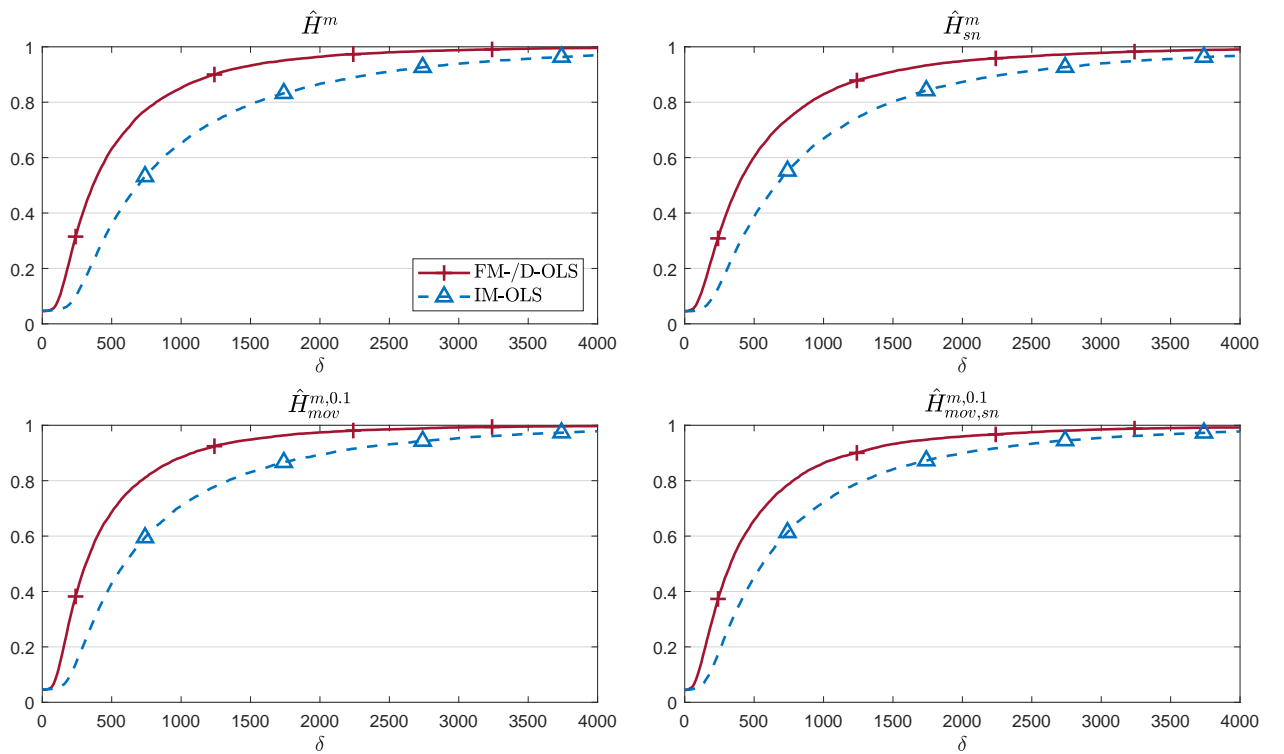


Figure S2: Local asymptotic power against  $I(1)$  breaks in the intercept only case for FM-/D-OLS and IM-OLS using  $\hat{H}^m$ ,  $\hat{H}_{sn}^m$ ,  $\hat{H}_{mov}^{m,0.1}$  and  $\hat{H}_{mov,sn}^{m,0.1}$ . Calibration and break fraction are set to  $m = 0.5$  and  $r = 0.75$ , respectively.

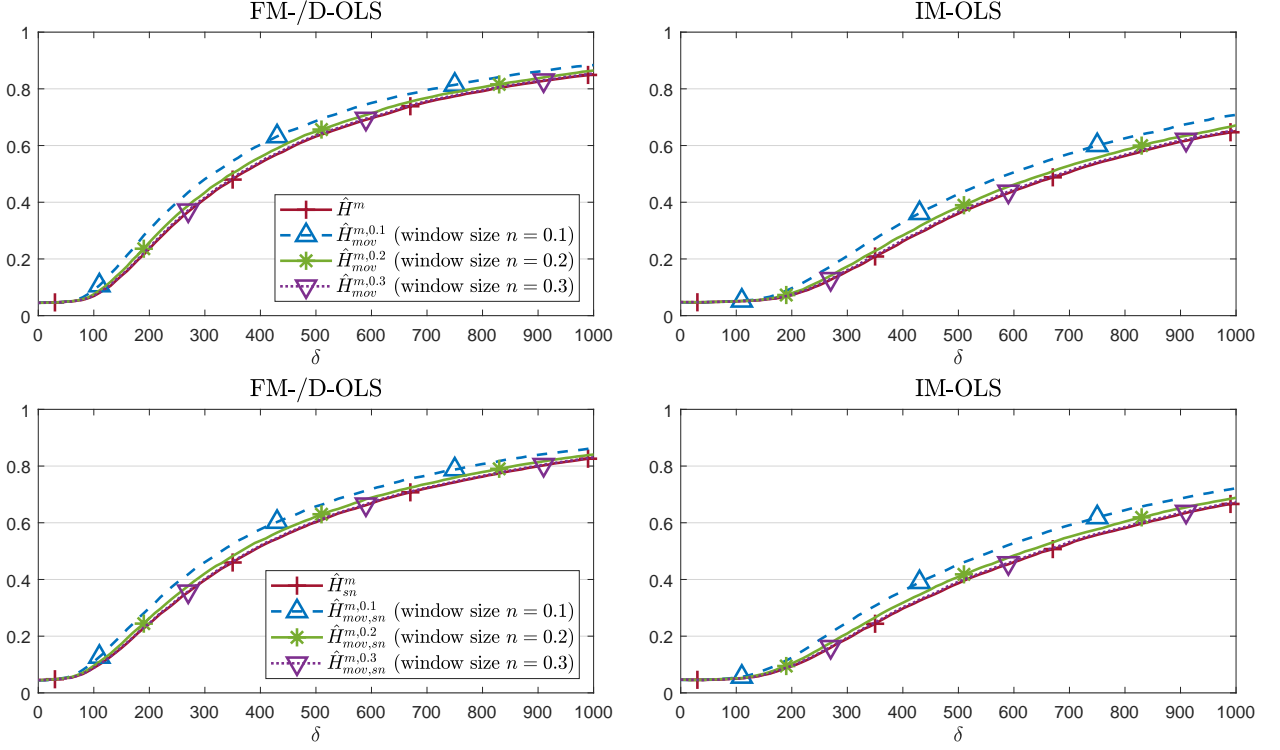


Figure S3: Local asymptotic power against I(1) breaks in the intercept only case for  $\hat{H}^m$ ,  $\hat{H}_{sn}^m$ ,  $\hat{H}_{mov}^{m,n}$  and  $\hat{H}_{mov,sn}^{m,n}$ , for  $n = 0.1, 0.2, 0.3$ . The upper two plots correspond to standardized detectors, the lower two plots correspond to self-normalized detectors. Calibration and break fraction are set to  $m = 0.5$  and  $r = 0.75$ , respectively.

LAP against local I(1) breaks in the intercept only case for  $\hat{H}^m$  and  $\hat{H}_{mov}^{m,n}$ , and their corresponding self-normalized counterparts  $\hat{H}_{sn}^m$  and  $\hat{H}_{mov,sn}^{m,n}$ , for  $n = 0.1, 0.2, 0.3$ . Calibration and break fraction are set to  $m = 0.5$  and  $r = 0.75$ , respectively. LAP is highest for the smallest window size  $n = 0.1$ , decreases with increasing window size and is lowest for the detector without moving window. This result is independent of estimator choice, self-normalization and also the choices of calibration and break fraction. However, the differences in LAP between the detectors are sometimes very small. Including a linear trend in the model does not cause any qualitative changes in the above results. The last aspect we consider for LAP against local I(1) breaks is the impact of self-normalization in comparison to standardization. Figure S4 shows the results for  $\hat{H}_{sn}^m$  and  $\hat{H}_{mov,sn}^{m,1}$ , each compared to its standardized counterpart  $\hat{H}^m$  and  $\hat{H}_{mov}^{m,0.1}$ , respectively, in case of local I(1) breaks with intercept only. Calibration and break fraction are set to  $m = 0.5$  and  $r = 0.75$ . Self-normalization by and large reduces LAP for FM-/D-OLS and increases LAP for IM-OLS. Figure S5 displays the corresponding results if additionally a linear trend is included in the model. In this case, when

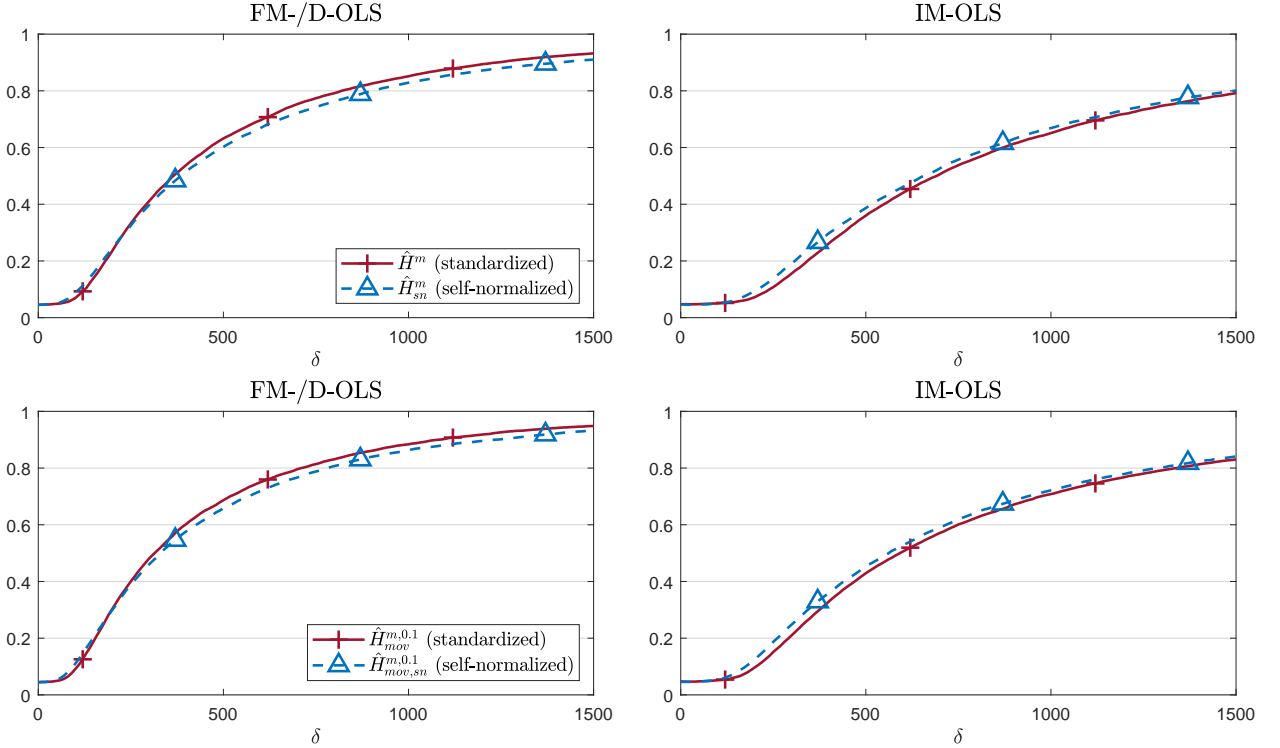


Figure S4: Local asymptotic power against local I(1) breaks in the intercept only case. The upper two plots correspond to  $\hat{H}^m$  and  $\hat{H}_{sn}^m$ . The lower two plots correspond to  $\hat{H}_{mov}^{m,0.1}$  and  $\hat{H}_{mov,sn}^{m,0.1}$ . Calibration and break fraction are set to  $m = 0.5$  and  $r = 0.75$ , respectively.

using IM-OLS the advantage of self-normalization over standardization disappears. Changes in the window size or calibration and break fraction have no qualitative influence on the differences in LAP between standardized and self-normalized detectors.

We now turn briefly to LAP against local slope breaks. The results are qualitatively the same as in case of local I(1) breaks with respect to the estimation method, self-normalization, window size and deterministic specification and are independent of the calibration and break fraction. Corresponding LAP figures are available upon request.

Finally, we consider LAP in case of local trend breaks. The overall results are very similar to both cases, local I(1) and local slope breaks, but with two major differences: The first difference is that now calibration and break fraction influence which detector leads to the highest LAP. Figure S6 displays LAP for standardized detectors for  $m = 0.5$  and  $r \in \{0.5, 0.75\}$ , with either  $\hat{H}^m$  or  $\hat{H}_{mov}^{m,0.1}$  leading to the highest LAP, depending on the choice of  $m$  and  $r$ . We obtain similar results for self-normalized detectors, with either  $\hat{H}_{sn}^m$  or  $\hat{H}_{mov,sn}^{m,0.1}$  leading to the highest LAP. The second difference in case of local trend breaks is the impact of self-normalization compared to standardization on

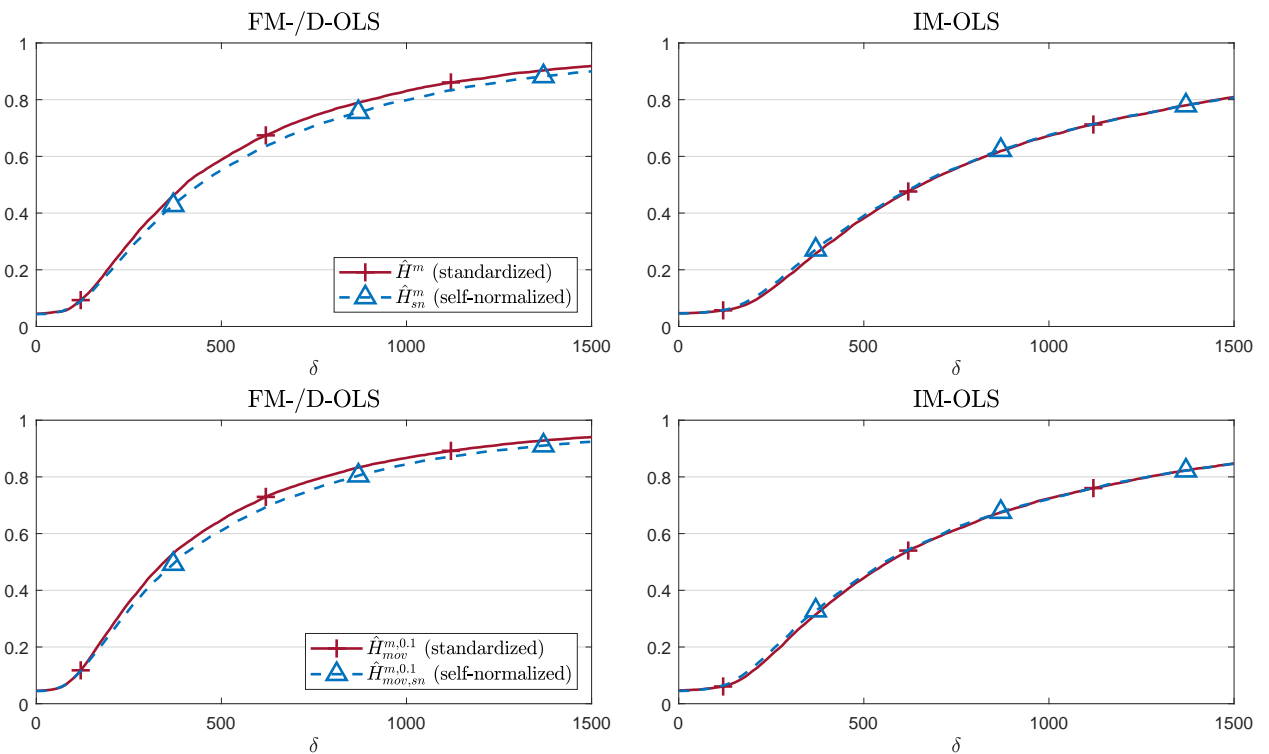


Figure S5: Local asymptotic power against local  $I(1)$  breaks in the intercept and linear trend case. For further explanations see notes for Figure S4.

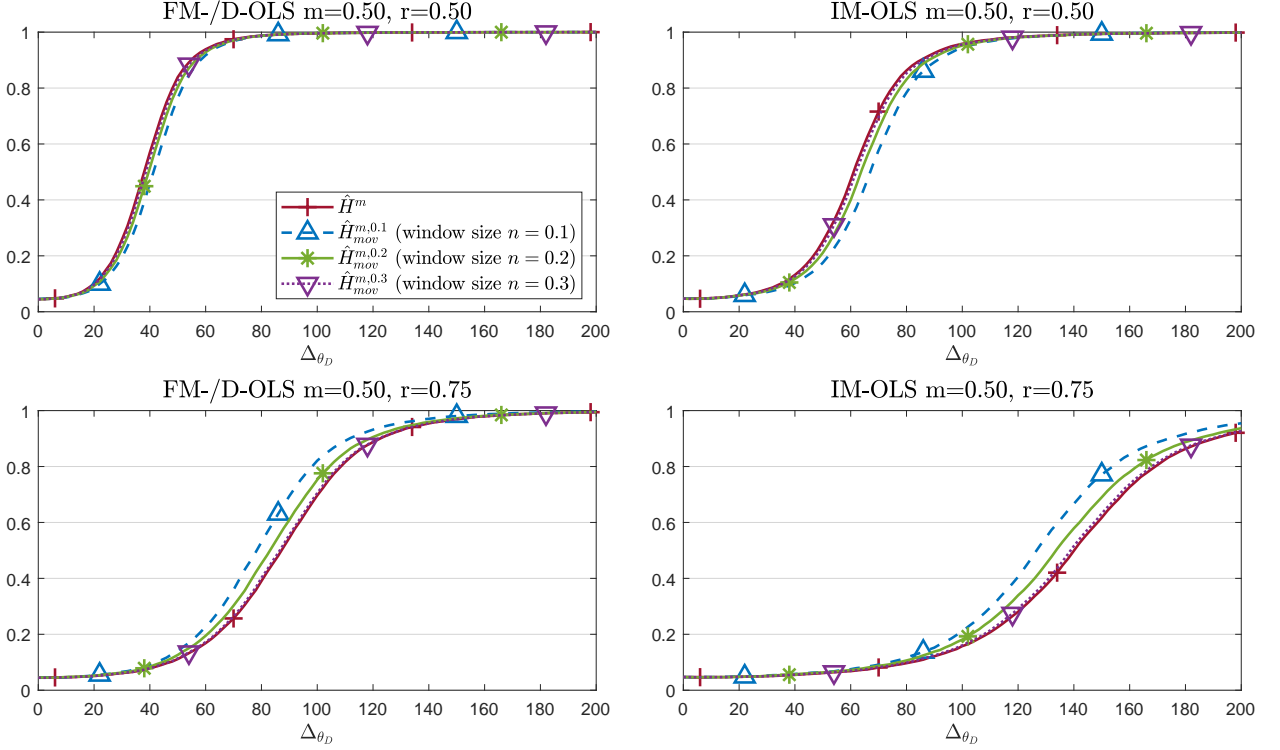


Figure S6: Local asymptotic power against local trend breaks for  $\hat{H}^m$  and  $\hat{H}_{mov}^{m,n}$  in the intercept and linear trend case. The upper two plots correspond to  $m = r = 0.5$ . The lower two plots correspond to  $m = 0.5$  and  $r = 0.75$ .

LAP for IM-OLS. Figure S7 displays LAP in case of local trend breaks for  $\hat{H}^m$ ,  $\hat{H}_{sn}^m$ ,  $\hat{H}_{mov}^{m,0.1}$  and  $\hat{H}_{mov,sn}^{m,0.1}$ , with  $m = 0.5$  and  $r = 0.75$ . For IM-OLS, the two self-normalized detectors, each compared to its standardized counterpart, lead to higher LAP at smaller break magnitudes at the expense of lower LAP at larger break magnitudes. In contrast, in case of local I(1) or local slope breaks, self-normalization either leads to higher or nearly the same LAP as standardization for IM-OLS, regardless of the break magnitude. For FM-/D-OLS, standardization still leads to higher LAP than self-normalization, as is the case with local I(1) or local slope breaks.

In conclusion, the LAP results can be summarized as follows: First, given a certain detector, break type, calibration and break fraction, LAP is higher for FM-/D-OLS than for IM-OLS. This stems from the fact that for the linear case FM-/D-OLS is asymptotically conditionally more efficient than IM-OLS from a standard asymptotic theory point of view (see Vogelsang and Wagner, 2014a, Proposition 2). A similar result can be obtained for the CPR case. Second, moving window detectors with  $n = 0.1$  are the best choice in case of local I(1) and local slope breaks. In case of local trend breaks there is no clear ranking. Third, self-normalization by  $\sqrt{n}$  reduces LAP for

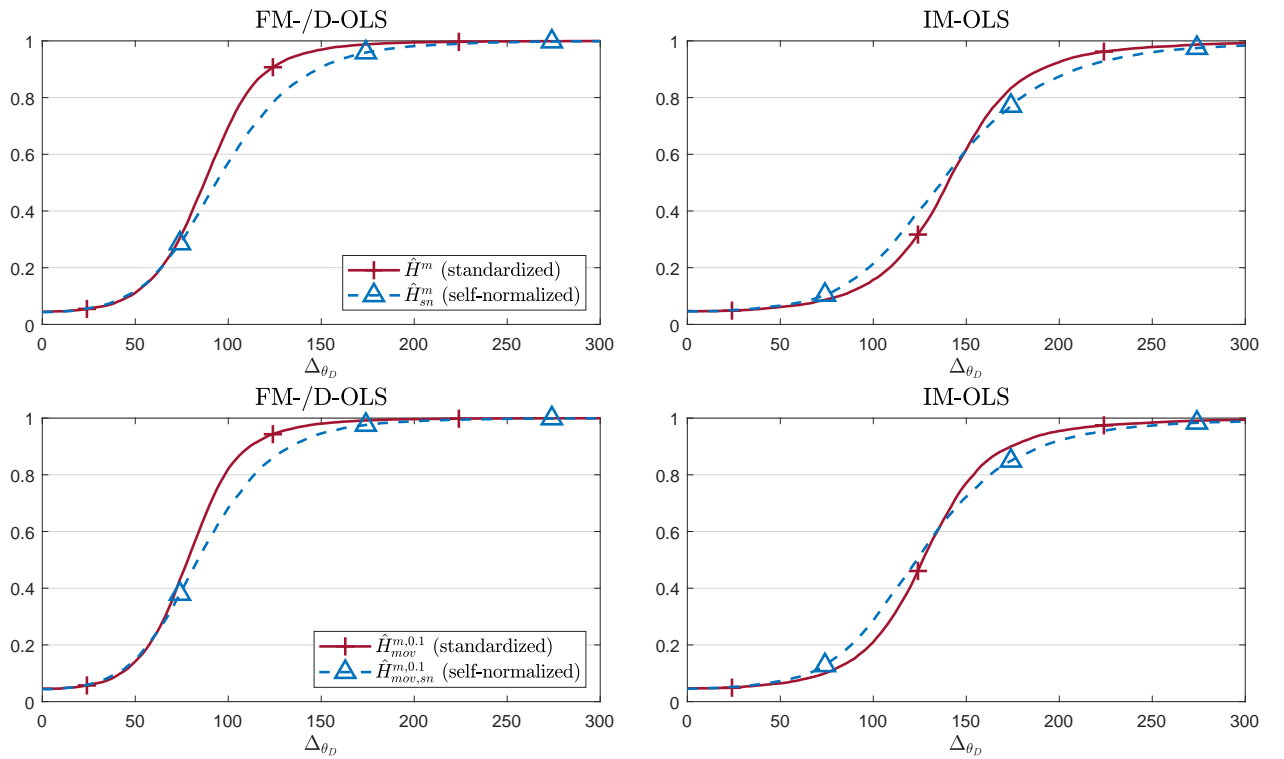


Figure S7: Local asymptotic power against local trend breaks in the model with intercept and linear trend. The upper two plots correspond to  $\hat{H}^m$  and  $\hat{H}_{sn}^m$ . The lower two plots correspond to  $\hat{H}_{mov}^{m,0.1}$  and  $\hat{H}_{mov,sn}^{m,0.1}$ . Calibration and break fraction are set to  $m = 0.5$  and  $r = 0.75$ , respectively.

FM-/D-OLS. In contrast, for IM-OLS self-normalization is by and large advantageous, in case of local trend breaks at least for small break magnitudes. Fourth, local slope breaks lead, as expected, to almost identical LAP patterns as local I(1) breaks. Wagner and Wied (2017, p. 967) explain for the cointegrating linear regression model that the asymptotic behavior in case of slope breaks is similar to the case of I(1) breaks. The same holds for the CPR model when there is only a (local) break in the coefficient corresponding to one I(1) regressor: The slope coefficient after the break,  $\theta_{X,1}$ , can be separated into  $\theta_X$  and  $\theta_{X,1} - \theta_X$ . The additional post break term  $X_t'(\theta_{X,1} - \theta_X)$  is an I(1) process – since the coefficient corresponding to one I(1) regressors changes – and thus leads to similar asymptotic behavior as in case of local I(1) breaks, where  $\{u_t\}$  changes its behavior from I(0) to I(1). Fifth,  $\hat{H}^m$  is preferable to  $\hat{H}_d^m$ , since  $\hat{H}^m$  performs either better or at least as good as  $\hat{H}_d^m$  in all considered cases. Finally, regardless of the choice of estimation method and detector, the LAP results suggest to choose the calibration fraction  $m$  as large as possible.

The LAP analysis reveals indications about the behavior of the monitoring procedures in finite samples. In fact, we find by and large very similar relative performance results in the finite sample simulations in Section 3 in the main document as in the LAP analysis.

# MONITORING COINTEGRATING POLYNOMIAL REGRESSIONS

## SUPPLEMENTARY APPENDIX C: ADDITIONAL FINITE SAMPLE PERFORMANCE RESULTS

FABIAN KNORRE, MARTIN WAGNER AND MAXIMILIAN GRUPE

### Finite Sample Performance

#### Null Rejection Probabilities

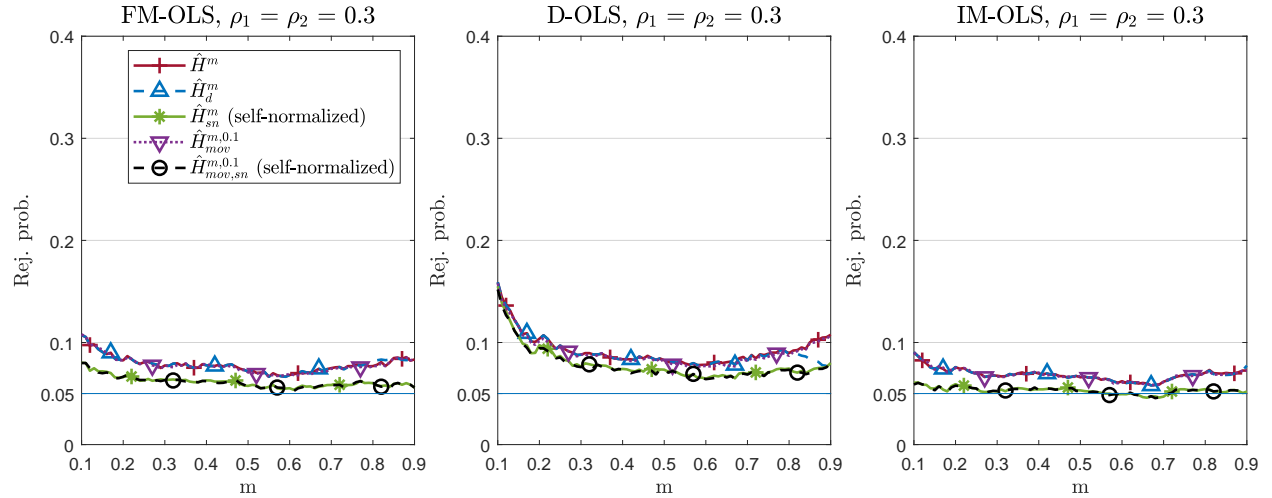


Figure S8: Empirical null rejection probabilities for a grid of values of  $m$ , with  $T = 500$  and  $\rho_1 = \rho_2 = 0.3$ .

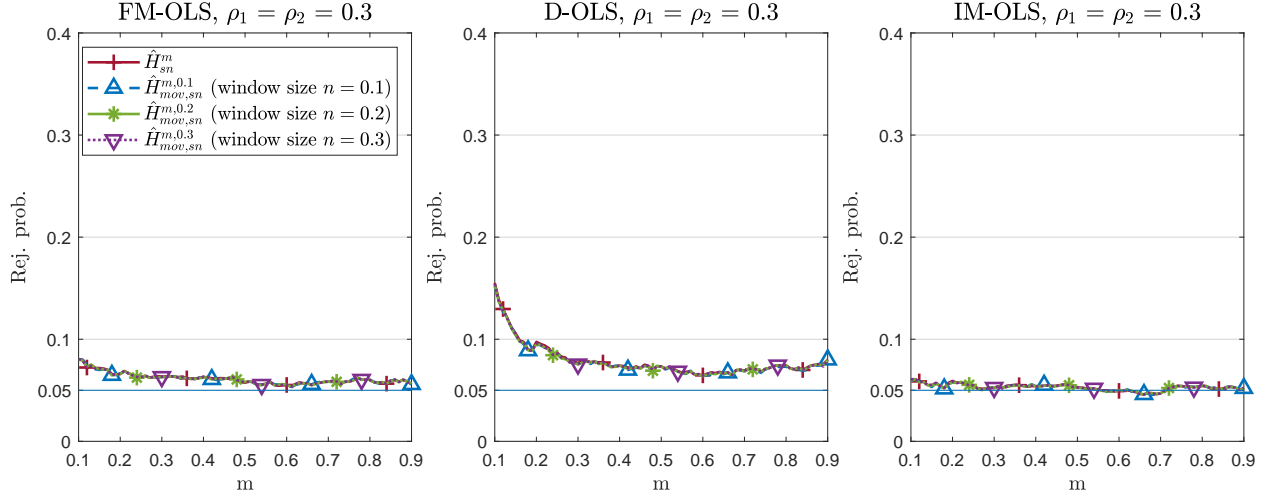


Figure S9: Empirical null rejection probabilities for a grid of values of  $m$ , with  $T = 500$  and  $\rho_1 = \rho_2 = 0.3$ .

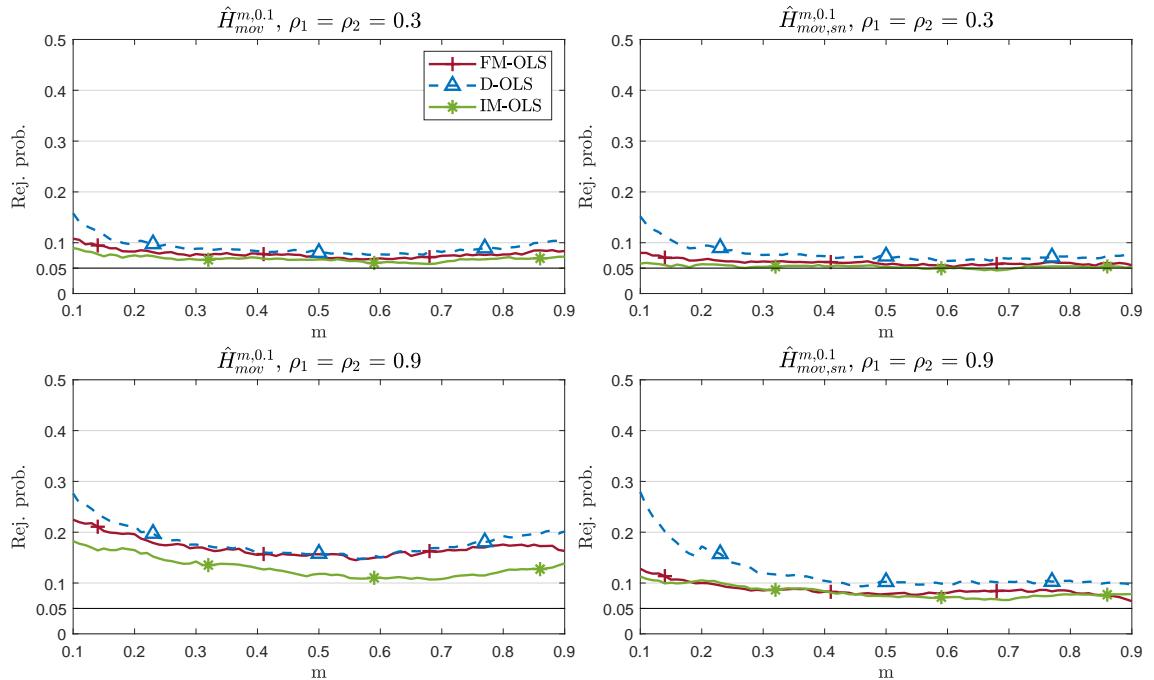


Figure S10: Empirical null rejection probabilities for a grid of values of  $m$  and  $T = 500$ . The left panel displays results for  $\hat{H}_{mov}^{m,0.1}$ . The right panel displays results for  $\hat{H}_{mov,sn}^{m,0.1}$ .

## Size-Corrected Power – I(1) Breaks

In addition to Section 3 in the main document, Table S1 displays the size-corrected power results in case of I(1) breaks for  $\rho_1 = \rho_2 = 0.3$  and  $T = 500$ . Furthermore, Tables S2 to S7 display the corresponding results for  $\rho_1 = \rho_2 \in \{0, 0.6, 0.9\}$  and  $T \in \{200, 500\}$ . The findings are similar as for  $\rho_1 = \rho_2 = 0.3$  in the main text: Size-corrected power is by and large highest for  $\hat{H}_{mov}^{m,0.1}$  or  $\hat{H}_{mov,sn}^{m,0.1}$  and lower for IM-OLS than for FM-OLS and D-OLS.

$\rho_1 = \rho_2 = 0.3$		$r$	m = 0.25			m = 0.5			m = 0.75		
			0.25	0.5	0.75	0.25	0.5	0.75	0.25	0.5	0.75
$\hat{H}^m$	FM	0.67	0.24	0.06	0.44	0.93	0.46	0.45	0.57	0.97	
	D	0.62	0.21	0.06	0.42	0.92	0.42	0.46	0.58	0.96	
	IM	0.42	0.11	0.05	0.34	0.82	0.25	0.43	0.52	0.91	
$\hat{H}_d^m$	FM	0.67	0.24	0.06	0.44	0.93	0.46	0.45	0.58	0.97	
	D	0.62	0.21	0.06	0.42	0.92	0.42	0.45	0.57	0.96	
	IM	0.42	0.11	0.05	0.34	0.82	0.25	0.43	0.52	0.91	
$\hat{H}_{sn}^m$	FM	0.65	0.25	0.06	0.21	0.91	0.44	0.18	0.30	0.96	
	D	0.59	0.20	0.06	0.21	0.89	0.40	0.20	0.32	0.95	
	IM	0.43	0.12	0.05	0.23	0.83	0.28	0.24	0.36	0.91	
$\hat{H}_{mov}^{m,0.1}$	FM	0.70	0.25	0.06	0.44	0.94	0.53	0.45	0.57	0.97	
	D	0.66	0.22	0.06	0.42	0.93	0.49	0.47	0.58	0.96	
	IM	0.43	0.11	0.05	0.33	0.84	0.31	0.43	0.52	0.91	
$\hat{H}_{mov}^{m,0.2}$	FM	0.68	0.25	0.06	0.44	0.93	0.48	0.45	0.57	0.97	
	D	0.64	0.22	0.06	0.42	0.92	0.44	0.46	0.58	0.96	
	IM	0.42	0.11	0.05	0.34	0.83	0.27	0.43	0.52	0.91	
$\hat{H}_{mov}^{m,0.3}$	FM	0.67	0.25	0.06	0.44	0.93	0.47	0.45	0.57	0.97	
	D	0.63	0.22	0.06	0.42	0.92	0.42	0.46	0.58	0.96	
	IM	0.42	0.11	0.05	0.34	0.82	0.26	0.43	0.52	0.91	
$\hat{H}_{mov,sn}^{m,0.1}$	FM	0.68	0.26	0.06	0.21	0.93	0.51	0.18	0.30	0.96	
	D	0.63	0.21	0.06	0.21	0.91	0.47	0.20	0.32	0.95	
	IM	0.45	0.12	0.05	0.22	0.85	0.34	0.24	0.36	0.91	
$\hat{H}_{mov,sn}^{m,0.2}$	FM	0.66	0.26	0.06	0.21	0.92	0.47	0.18	0.30	0.96	
	D	0.60	0.20	0.06	0.21	0.90	0.42	0.20	0.32	0.95	
	IM	0.44	0.12	0.05	0.23	0.83	0.30	0.24	0.36	0.91	
$\hat{H}_{mov,sn}^{m,0.3}$	FM	0.65	0.26	0.06	0.21	0.91	0.45	0.18	0.30	0.96	
	D	0.60	0.20	0.06	0.21	0.89	0.40	0.20	0.32	0.95	
	IM	0.43	0.12	0.05	0.23	0.83	0.28	0.24	0.36	0.91	

Table S1: Size-corrected power against I(1) breaks for  $T = 500$  and  $\rho_1 = \rho_2 = 0.3$ .

$\rho_1 = \rho_2 = 0.0$		$m = 0.25$			$m = 0.5$			$m = 0.75$		
	$r$	0.25	0.5	0.75	0.25	0.5	0.75	0.25	0.5	0.75
$\hat{H}^m$	FM	0.26	0.08	0.05	0.37	0.76	0.21	0.38	0.51	0.87
	D	0.19	0.06	0.05	0.37	0.71	0.17	0.39	0.51	0.85
	IM	0.15	0.06	0.05	0.32	0.61	0.11	0.38	0.47	0.77
$\hat{H}_d^m$	FM	0.26	0.08	0.05	0.37	0.76	0.21	0.37	0.50	0.87
	D	0.19	0.06	0.05	0.37	0.71	0.17	0.39	0.51	0.85
	IM	0.15	0.06	0.05	0.32	0.61	0.11	0.38	0.47	0.77
$\hat{H}_{sn}^m$	FM	0.28	0.08	0.05	0.18	0.73	0.21	0.17	0.27	0.85
	D	0.20	0.07	0.05	0.23	0.69	0.17	0.22	0.33	0.83
	IM	0.18	0.06	0.05	0.22	0.62	0.12	0.23	0.34	0.77
$\hat{H}_{mov}^{m,0.1}$	FM	0.26	0.07	0.05	0.37	0.77	0.26	0.38	0.51	0.87
	D	0.18	0.06	0.05	0.36	0.73	0.22	0.39	0.51	0.85
	IM	0.14	0.06	0.05	0.32	0.63	0.14	0.37	0.46	0.78
$\hat{H}_{mov}^{m,0.2}$	FM	0.26	0.08	0.05	0.37	0.76	0.23	0.38	0.51	0.87
	D	0.18	0.07	0.05	0.36	0.72	0.19	0.39	0.51	0.85
	IM	0.15	0.06	0.05	0.32	0.62	0.12	0.38	0.47	0.77
$\hat{H}_{mov}^{m,0.3}$	FM	0.26	0.08	0.05	0.37	0.75	0.21	0.38	0.51	0.87
	D	0.18	0.06	0.05	0.36	0.71	0.17	0.39	0.51	0.85
	IM	0.15	0.06	0.05	0.32	0.61	0.11	0.38	0.47	0.77
$\hat{H}_{mov,sn}^{m,0.1}$	FM	0.29	0.08	0.05	0.18	0.75	0.26	0.17	0.28	0.86
	D	0.21	0.07	0.05	0.23	0.71	0.21	0.22	0.33	0.84
	IM	0.17	0.06	0.05	0.21	0.63	0.15	0.22	0.33	0.77
$\hat{H}_{mov,sn}^{m,0.2}$	FM	0.29	0.08	0.05	0.18	0.74	0.23	0.17	0.27	0.85
	D	0.21	0.07	0.05	0.23	0.69	0.18	0.22	0.33	0.83
	IM	0.17	0.06	0.05	0.22	0.63	0.14	0.23	0.34	0.76
$\hat{H}_{mov,sn}^{m,0.3}$	FM	0.29	0.08	0.05	0.18	0.73	0.22	0.17	0.27	0.85
	D	0.21	0.07	0.05	0.23	0.69	0.17	0.22	0.33	0.83
	IM	0.17	0.06	0.05	0.22	0.62	0.13	0.23	0.34	0.77

Table S2: Size-corrected power against  $I(1)$  breaks for  $T = 200$  and  $\rho_1 = \rho_2 = 0.0$ .

$\rho_1 = \rho_2 = 0.6$		$m = 0.25$			$m = 0.5$			$m = 0.75$		
	$r$	0.25	0.5	0.75	0.25	0.5	0.75	0.25	0.5	0.75
$\hat{H}^m$	FM	0.11	0.06	0.05	0.24	0.44	0.08	0.27	0.36	0.64
	D	0.09	0.05	0.05	0.23	0.40	0.07	0.29	0.38	0.61
	IM	0.07	0.05	0.05	0.19	0.27	0.06	0.26	0.32	0.48
$\hat{H}_d^m$	FM	0.11	0.06	0.05	0.24	0.44	0.08	0.27	0.36	0.64
	D	0.09	0.05	0.05	0.23	0.40	0.07	0.28	0.37	0.61
	IM	0.07	0.05	0.05	0.19	0.27	0.06	0.26	0.32	0.48
$\hat{H}_{sn}^m$	FM	0.12	0.06	0.05	0.15	0.42	0.08	0.14	0.23	0.62
	D	0.10	0.06	0.05	0.17	0.38	0.07	0.17	0.25	0.58
	IM	0.07	0.05	0.05	0.15	0.29	0.06	0.18	0.27	0.48
$\hat{H}_{mov}^{m,0.1}$	FM	0.10	0.06	0.05	0.23	0.45	0.09	0.27	0.36	0.64
	D	0.09	0.05	0.05	0.22	0.41	0.08	0.29	0.38	0.62
	IM	0.06	0.05	0.05	0.18	0.26	0.06	0.25	0.31	0.48
$\hat{H}_{mov}^{m,0.2}$	FM	0.10	0.06	0.05	0.24	0.45	0.08	0.27	0.36	0.64
	D	0.09	0.05	0.05	0.22	0.40	0.07	0.29	0.38	0.61
	IM	0.07	0.05	0.05	0.19	0.27	0.06	0.26	0.32	0.48
$\hat{H}_{mov}^{m,0.3}$	FM	0.11	0.06	0.05	0.24	0.44	0.08	0.27	0.36	0.64
	D	0.09	0.05	0.05	0.22	0.40	0.07	0.29	0.38	0.61
	IM	0.07	0.05	0.05	0.19	0.27	0.06	0.26	0.32	0.48
$\hat{H}_{mov,sn}^{m,0.1}$	FM	0.12	0.06	0.05	0.15	0.43	0.10	0.15	0.23	0.62
	D	0.10	0.06	0.05	0.17	0.39	0.08	0.17	0.25	0.59
	IM	0.07	0.05	0.05	0.14	0.27	0.06	0.18	0.26	0.49
$\hat{H}_{mov,sn}^{m,0.2}$	FM	0.12	0.06	0.05	0.15	0.42	0.09	0.14	0.23	0.62
	D	0.09	0.06	0.05	0.17	0.38	0.08	0.17	0.25	0.58
	IM	0.07	0.05	0.05	0.15	0.28	0.06	0.18	0.26	0.48
$\hat{H}_{mov,sn}^{m,0.3}$	FM	0.12	0.06	0.05	0.15	0.42	0.08	0.14	0.23	0.62
	D	0.09	0.06	0.05	0.17	0.38	0.07	0.17	0.25	0.58
	IM	0.07	0.05	0.05	0.15	0.28	0.06	0.18	0.27	0.48

Table S3: Size-corrected power against  $I(1)$  breaks for  $T = 200$  and  $\rho_1 = \rho_2 = 0.6$ .

$\rho_1 = \rho_2 = 0.9$		$m = 0.25$			$m = 0.5$			$m = 0.75$		
	$r$	0.25	0.5	0.75	0.25	0.5	0.75	0.25	0.5	0.75
$\hat{H}^m$	FM	0.06	0.05	0.05	0.10	0.10	0.05	0.13	0.13	0.17
	D	0.06	0.05	0.05	0.10	0.10	0.06	0.14	0.15	0.16
	IM	0.05	0.05	0.05	0.08	0.06	0.05	0.12	0.12	0.11
$\hat{H}_d^m$	FM	0.06	0.05	0.05	0.10	0.10	0.05	0.13	0.13	0.17
	D	0.06	0.05	0.05	0.10	0.10	0.06	0.14	0.15	0.16
	IM	0.05	0.05	0.05	0.08	0.06	0.05	0.12	0.12	0.11
$\hat{H}_{sn}^m$	FM	0.06	0.05	0.05	0.08	0.09	0.05	0.08	0.10	0.15
	D	0.06	0.05	0.05	0.08	0.10	0.05	0.10	0.11	0.15
	IM	0.05	0.05	0.05	0.07	0.07	0.05	0.11	0.11	0.12
$\hat{H}_{mov}^{m,0.1}$	FM	0.06	0.05	0.05	0.09	0.09	0.05	0.13	0.13	0.17
	D	0.06	0.05	0.05	0.10	0.10	0.06	0.14	0.15	0.16
	IM	0.05	0.05	0.05	0.08	0.06	0.05	0.12	0.12	0.11
$\hat{H}_{mov}^{m,0.2}$	FM	0.06	0.05	0.05	0.10	0.10	0.05	0.13	0.13	0.17
	D	0.06	0.05	0.05	0.10	0.10	0.06	0.14	0.15	0.16
	IM	0.05	0.05	0.05	0.08	0.06	0.05	0.12	0.12	0.11
$\hat{H}_{mov}^{m,0.3}$	FM	0.06	0.05	0.05	0.10	0.10	0.05	0.13	0.13	0.17
	D	0.06	0.05	0.05	0.10	0.10	0.05	0.14	0.15	0.16
	IM	0.05	0.05	0.05	0.08	0.06	0.05	0.12	0.12	0.11
$\hat{H}_{mov,sn}^{m,0.1}$	FM	0.06	0.05	0.05	0.08	0.10	0.06	0.09	0.10	0.15
	D	0.06	0.05	0.05	0.09	0.10	0.06	0.10	0.11	0.15
	IM	0.05	0.05	0.05	0.07	0.07	0.05	0.11	0.11	0.12
$\hat{H}_{mov,sn}^{m,0.2}$	FM	0.06	0.05	0.05	0.08	0.09	0.05	0.08	0.10	0.15
	D	0.06	0.05	0.05	0.09	0.10	0.06	0.10	0.11	0.15
	IM	0.05	0.05	0.05	0.07	0.07	0.05	0.11	0.11	0.12
$\hat{H}_{mov,sn}^{m,0.3}$	FM	0.06	0.05	0.05	0.08	0.09	0.05	0.08	0.10	0.15
	D	0.06	0.05	0.05	0.08	0.10	0.05	0.10	0.11	0.15
	IM	0.05	0.05	0.05	0.07	0.07	0.05	0.11	0.11	0.12

Table S4: Size-corrected power against  $I(1)$  breaks for  $T = 200$  and  $\rho_1 = \rho_2 = 0.9$ .

$\rho_1 = \rho_2 = 0.0$		$m = 0.25$			$m = 0.5$			$m = 0.75$		
	$r$	0.25	0.5	0.75	0.25	0.5	0.75	0.25	0.5	0.75
$\hat{H}^m$	FM	0.78	0.36	0.06	0.48	0.97	0.59	0.49	0.61	0.99
	D	0.75	0.33	0.06	0.47	0.96	0.56	0.50	0.62	0.98
	IM	0.58	0.19	0.05	0.38	0.89	0.38	0.48	0.57	0.95
$\hat{H}_d^m$	FM	0.78	0.36	0.06	0.48	0.97	0.59	0.51	0.65	0.99
	D	0.75	0.33	0.06	0.47	0.96	0.56	0.50	0.62	0.98
	IM	0.58	0.19	0.05	0.38	0.89	0.38	0.47	0.57	0.95
$\hat{H}_{sn}^m$	FM	0.76	0.36	0.06	0.21	0.95	0.57	0.18	0.31	0.98
	D	0.74	0.32	0.06	0.23	0.95	0.54	0.21	0.34	0.98
	IM	0.60	0.20	0.05	0.24	0.90	0.41	0.25	0.38	0.95
$\hat{H}_{mov}^{m,0.1}$	FM	0.82	0.38	0.07	0.49	0.98	0.65	0.49	0.61	0.99
	D	0.79	0.34	0.07	0.48	0.97	0.62	0.50	0.62	0.98
	IM	0.61	0.18	0.06	0.38	0.92	0.45	0.47	0.57	0.96
$\hat{H}_{mov}^{m,0.2}$	FM	0.80	0.37	0.06	0.48	0.97	0.61	0.49	0.61	0.99
	D	0.77	0.34	0.06	0.47	0.96	0.58	0.50	0.62	0.98
	IM	0.60	0.19	0.05	0.38	0.90	0.40	0.47	0.57	0.95
$\hat{H}_{mov}^{m,0.3}$	FM	0.79	0.37	0.06	0.48	0.97	0.59	0.49	0.61	0.99
	D	0.76	0.33	0.06	0.47	0.96	0.57	0.50	0.62	0.98
	IM	0.58	0.19	0.05	0.38	0.89	0.38	0.48	0.57	0.95
$\hat{H}_{mov,sn}^{m,0.1}$	FM	0.80	0.38	0.07	0.21	0.96	0.63	0.19	0.31	0.98
	D	0.78	0.34	0.07	0.22	0.96	0.59	0.21	0.33	0.98
	IM	0.63	0.20	0.05	0.23	0.92	0.47	0.25	0.38	0.96
$\hat{H}_{mov,sn}^{m,0.2}$	FM	0.77	0.37	0.07	0.21	0.96	0.59	0.18	0.31	0.98
	D	0.76	0.33	0.06	0.22	0.95	0.56	0.21	0.34	0.98
	IM	0.61	0.21	0.05	0.23	0.90	0.43	0.25	0.38	0.95
$\hat{H}_{mov,sn}^{m,0.3}$	FM	0.76	0.36	0.06	0.21	0.95	0.58	0.18	0.31	0.98
	D	0.74	0.33	0.06	0.23	0.95	0.55	0.21	0.34	0.98
	IM	0.60	0.20	0.05	0.24	0.90	0.41	0.25	0.38	0.95

Table S5: Size-corrected power against  $I(1)$  breaks for  $T = 500$  and  $\rho_1 = \rho_2 = 0.0$ .

$\rho_1 = \rho_2 = 0.6$		$m = 0.25$			$m = 0.5$			$m = 0.75$		
	$r$	0.25	0.5	0.75	0.25	0.5	0.75	0.25	0.5	0.75
$\hat{H}^m$	FM	0.44	0.13	0.05	0.40	0.82	0.27	0.42	0.53	0.91
	D	0.40	0.11	0.05	0.38	0.80	0.24	0.43	0.54	0.89
	IM	0.21	0.07	0.05	0.31	0.66	0.13	0.40	0.49	0.80
$\hat{H}_d^m$	FM	0.44	0.13	0.05	0.40	0.82	0.27	0.41	0.53	0.90
	D	0.40	0.11	0.05	0.38	0.80	0.24	0.41	0.53	0.89
	IM	0.21	0.07	0.05	0.31	0.66	0.13	0.40	0.49	0.80
$\hat{H}_{sn}^m$	FM	0.43	0.13	0.05	0.19	0.79	0.26	0.17	0.28	0.88
	D	0.39	0.12	0.05	0.20	0.78	0.24	0.18	0.29	0.87
	IM	0.23	0.07	0.05	0.21	0.67	0.15	0.23	0.34	0.79
$\hat{H}_{mov}^{m,0.1}$	FM	0.46	0.13	0.05	0.40	0.85	0.34	0.42	0.53	0.91
	D	0.42	0.11	0.05	0.38	0.83	0.30	0.43	0.54	0.90
	IM	0.21	0.07	0.05	0.30	0.67	0.16	0.40	0.48	0.81
$\hat{H}_{mov}^{m,0.2}$	FM	0.45	0.13	0.05	0.40	0.83	0.29	0.42	0.53	0.90
	D	0.42	0.12	0.05	0.38	0.81	0.26	0.43	0.54	0.89
	IM	0.21	0.07	0.05	0.30	0.66	0.14	0.40	0.49	0.80
$\hat{H}_{mov}^{m,0.3}$	FM	0.44	0.13	0.05	0.40	0.82	0.28	0.42	0.53	0.91
	D	0.41	0.11	0.05	0.38	0.80	0.24	0.43	0.54	0.89
	IM	0.21	0.07	0.05	0.31	0.66	0.13	0.41	0.49	0.80
$\hat{H}_{mov,sn}^{m,0.1}$	FM	0.46	0.14	0.06	0.20	0.82	0.32	0.18	0.28	0.89
	D	0.41	0.12	0.06	0.20	0.80	0.29	0.18	0.29	0.88
	IM	0.23	0.07	0.05	0.21	0.69	0.18	0.23	0.34	0.81
$\hat{H}_{mov,sn}^{m,0.2}$	FM	0.45	0.14	0.05	0.20	0.80	0.28	0.17	0.28	0.88
	D	0.40	0.12	0.05	0.20	0.79	0.25	0.18	0.29	0.87
	IM	0.23	0.07	0.05	0.21	0.68	0.16	0.23	0.34	0.79
$\hat{H}_{mov,sn}^{m,0.3}$	FM	0.44	0.14	0.05	0.19	0.80	0.26	0.17	0.28	0.88
	D	0.39	0.12	0.05	0.20	0.78	0.24	0.18	0.29	0.87
	IM	0.23	0.07	0.05	0.21	0.67	0.15	0.23	0.34	0.79

Table S6: Size-corrected power against  $I(1)$  breaks for  $T = 500$  and  $\rho_1 = \rho_2 = 0.6$ .

$\rho_1 = \rho_2 = 0.9$		$m = 0.25$			$m = 0.5$			$m = 0.75$		
	$r$	0.25	0.5	0.75	0.25	0.5	0.75	0.25	0.5	0.75
$\hat{H}^m$	FM	0.09	0.06	0.05	0.23	0.30	0.07	0.27	0.33	0.47
	D	0.09	0.06	0.05	0.24	0.30	0.06	0.29	0.34	0.46
	IM	0.06	0.05	0.05	0.17	0.16	0.05	0.29	0.30	0.33
$\hat{H}_d^m$	FM	0.09	0.06	0.05	0.23	0.30	0.07	0.27	0.32	0.47
	D	0.09	0.06	0.05	0.24	0.30	0.06	0.28	0.33	0.46
	IM	0.06	0.05	0.05	0.17	0.16	0.05	0.29	0.30	0.33
$\hat{H}_{sn}^m$	FM	0.09	0.06	0.05	0.15	0.28	0.07	0.13	0.18	0.42
	D	0.09	0.06	0.05	0.15	0.28	0.07	0.14	0.19	0.41
	IM	0.06	0.05	0.05	0.13	0.17	0.05	0.18	0.23	0.33
$\hat{H}_{mov}^{m,0.1}$	FM	0.09	0.06	0.05	0.22	0.30	0.07	0.28	0.32	0.47
	D	0.09	0.06	0.05	0.23	0.30	0.07	0.29	0.34	0.47
	IM	0.06	0.05	0.05	0.16	0.15	0.05	0.28	0.30	0.33
$\hat{H}_{mov}^{m,0.2}$	FM	0.09	0.06	0.05	0.23	0.30	0.07	0.27	0.33	0.47
	D	0.09	0.06	0.05	0.23	0.30	0.07	0.29	0.34	0.46
	IM	0.06	0.05	0.05	0.16	0.16	0.05	0.29	0.30	0.33
$\hat{H}_{mov}^{m,0.3}$	FM	0.09	0.06	0.05	0.23	0.30	0.07	0.27	0.33	0.47
	D	0.09	0.06	0.05	0.23	0.30	0.06	0.29	0.34	0.46
	IM	0.06	0.05	0.05	0.17	0.16	0.05	0.29	0.30	0.33
$\hat{H}_{mov,sn}^{m,0.1}$	FM	0.09	0.06	0.05	0.14	0.28	0.07	0.13	0.18	0.42
	D	0.09	0.06	0.05	0.15	0.28	0.08	0.14	0.19	0.41
	IM	0.06	0.05	0.05	0.13	0.17	0.06	0.18	0.23	0.33
$\hat{H}_{mov,sn}^{m,0.2}$	FM	0.09	0.06	0.05	0.14	0.28	0.07	0.13	0.18	0.42
	D	0.09	0.06	0.05	0.15	0.28	0.07	0.14	0.19	0.41
	IM	0.06	0.05	0.05	0.13	0.17	0.06	0.18	0.23	0.33
$\hat{H}_{mov,sn}^{m,0.3}$	FM	0.09	0.06	0.05	0.14	0.28	0.07	0.13	0.18	0.42
	D	0.09	0.06	0.05	0.15	0.28	0.07	0.14	0.19	0.41
	IM	0.06	0.05	0.05	0.13	0.17	0.05	0.18	0.23	0.33

Table S7: Size-corrected power against  $I(1)$  breaks for  $T = 500$  and  $\rho_1 = \rho_2 = 0.9$ .

## Size-Corrected Power – Trend Breaks

The size-corrected power results in case of trend breaks complement the results for the case of I(1) breaks from Section 3 in the main document. The parameter  $\theta_{D_1}$  varies in 101 equidistant steps over the interval [1, 1.5], including the corresponding null hypothesis value  $\theta_{D_1} = 1$ . Figure S11 displays size-corrected power against trend breaks using  $\hat{H}^m$ ,  $\hat{H}_{sn}^m$ ,  $\hat{H}_{mov}^{m,0.1}$  and  $\hat{H}_{mov,sn}^{m,0.1}$ . The sample size is  $T = 200$ , calibration and break fraction are set to  $m = 0.5$  and  $r = 0.75$  with  $\rho_1 = \rho_2 = 0.3$ . FM-OLS leads to the highest size-corrected power and IM-OLS to the lowest, with D-OLS in between. Figure S12 displays the corresponding results for  $T = 500$ . Size-corrected power increases with increasing sample size  $T$ . Differences in size-corrected power between FM-OLS and D-OLS become very small for  $T = 500$  compared to  $T = 200$ , reflecting the asymptotic equivalence between FM-OLS and D-OLS. The size-corrected power ranking with respect to FM-OLS, D-OLS and IM-OLS remains unchanged for larger window sizes and other combinations of  $m$  and  $r$ . Next, consider the impact of different window sizes and in addition the comparison to one expanding window detector. Figure S13 displays size-corrected power for  $\hat{H}^m$ ,  $\hat{H}_{mov}^{m,0.1}$ ,  $\hat{H}_{mov}^{m,0.2}$  and  $\hat{H}_{mov}^{m,0.3}$  in case of trend breaks. The sample size is  $T = 200$  with  $\rho_1 = \rho_2 = 0.3$ ,  $m = 0.5$  and  $r = 0.75$ . Size-corrected power is highest either for  $\hat{H}^m$  or  $\hat{H}_{mov}^{m,0.1}$ . The same holds for other combinations of  $m$  and  $r$ . Figures S14 and S15 display size-corrected power against trend breaks using  $\hat{H}_{mov}^{m,0.1}$  and  $\hat{H}_{mov,sn}^{m,0.1}$  and focus on the effect of self-normalization for several combinations of  $m$  and  $r$  with  $\rho_1 = \rho_2 = 0.3$ . Self-normalization leads, compared to standardization, by and large to higher size-corrected power for small breaks in  $\theta_{D_1}$  and to lower size-corrected power for large breaks in  $\theta_{D_1}$ . For small breaks in  $\theta_{D_1}$  the differences in size-corrected power between self-normalization and standardization are larger for IM-OLS than for FM-OLS and D-OLS.

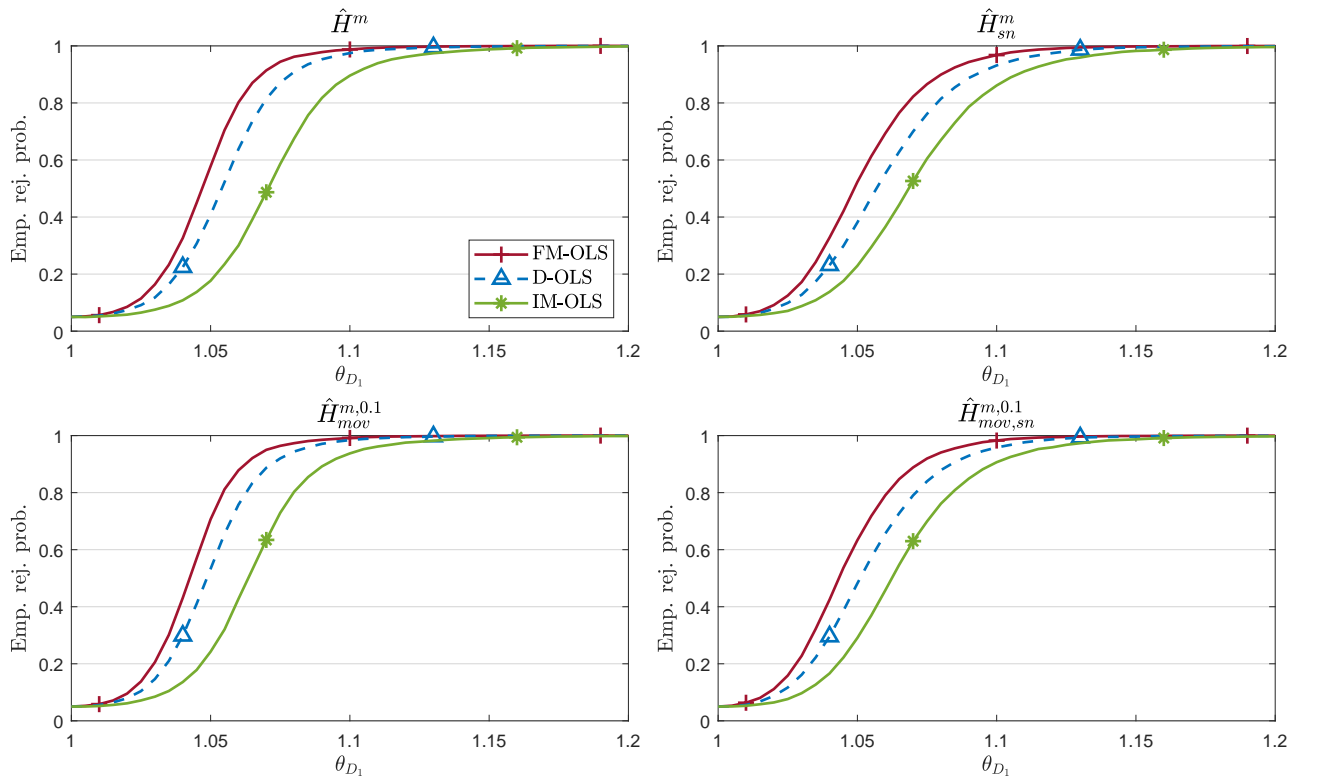


Figure S11: Size-corrected power against trend breaks for  $T = 200$ ,  $m = 0.5$ ,  $r = 0.75$  and  $\rho_1 = \rho_2 = 0.3$ .

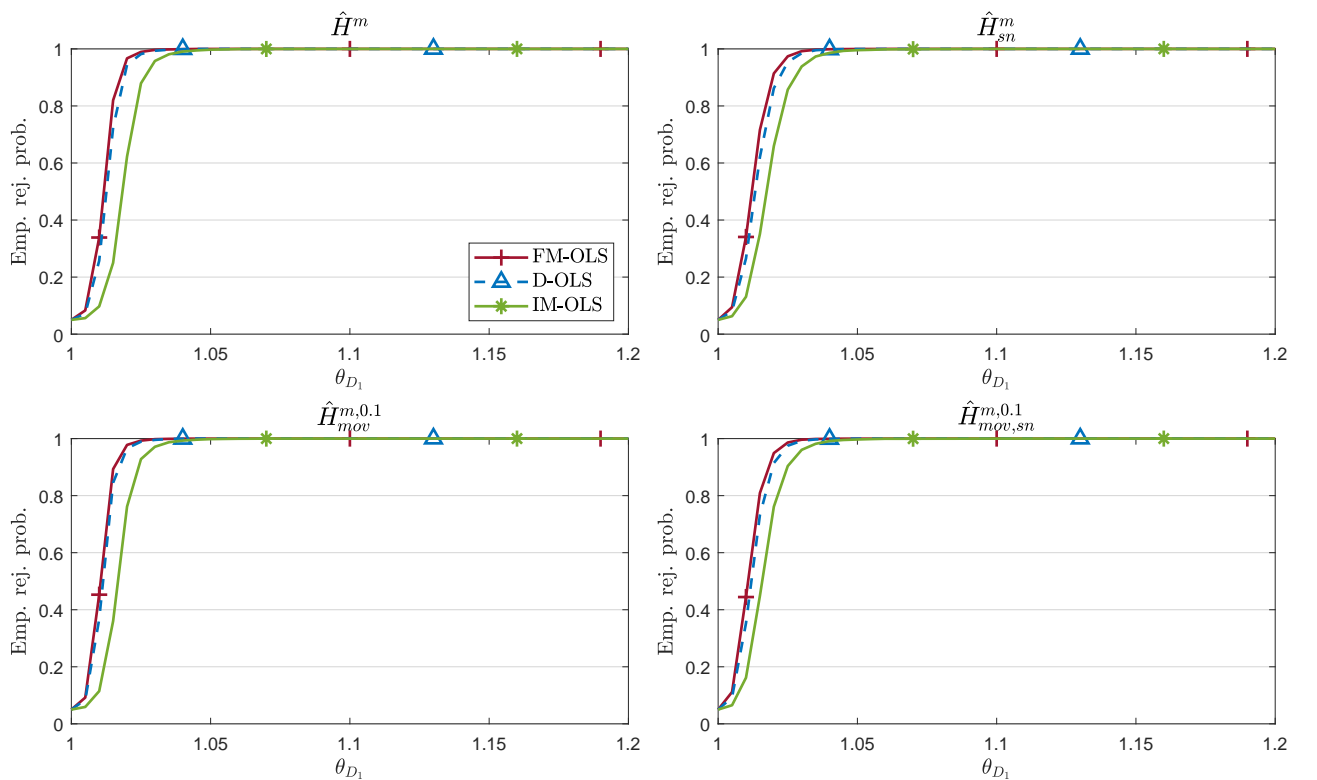


Figure S12: Size-corrected power against trend breaks for  $T = 500$ ,  $m = 0.5$ ,  $r = 0.75$  and  $\rho_1 = \rho_2 = 0.3$ .

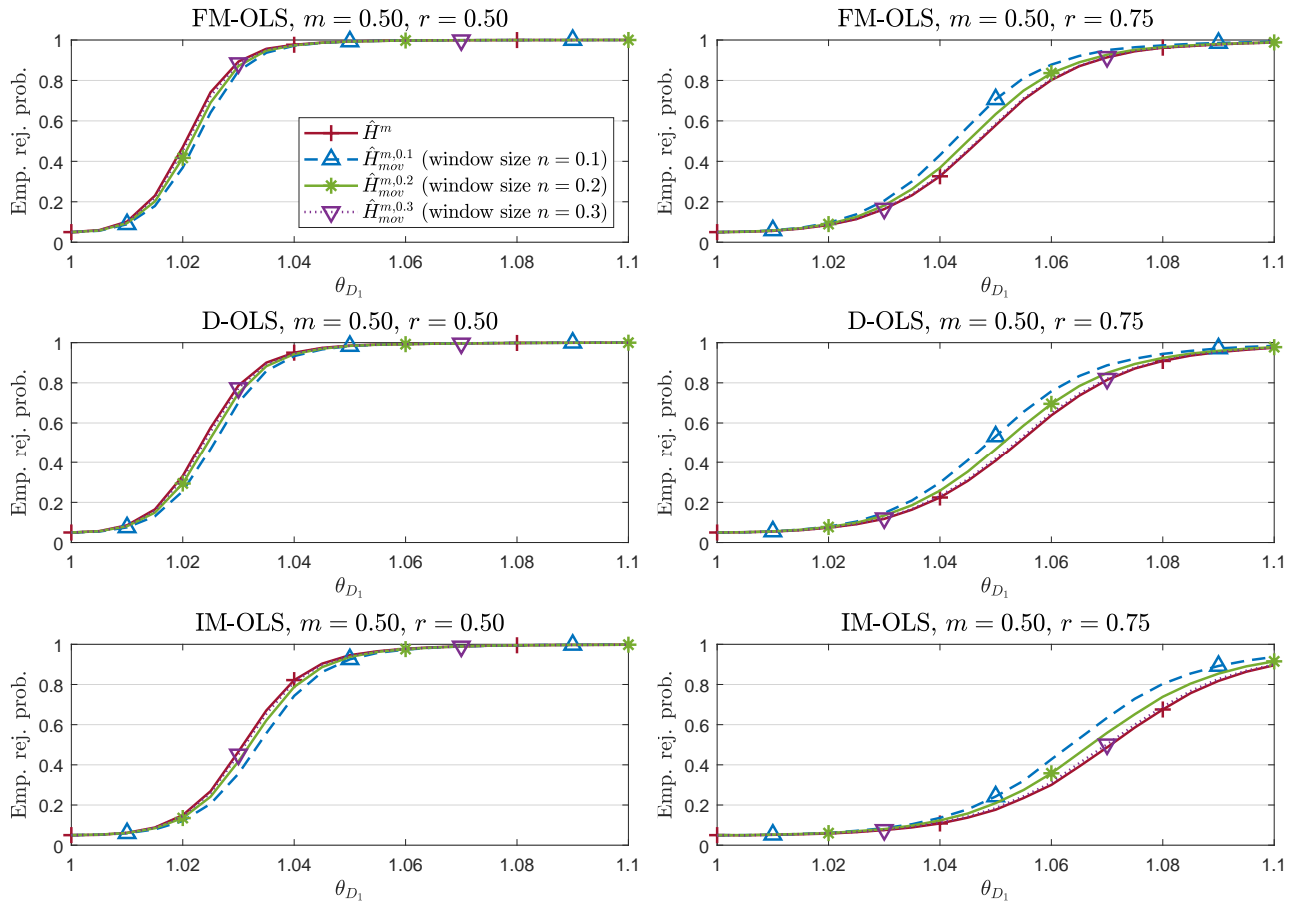


Figure S13: Size-corrected power against trend breaks for  $T = 200$  and  $\rho_1 = \rho_2 = 0.3$ .

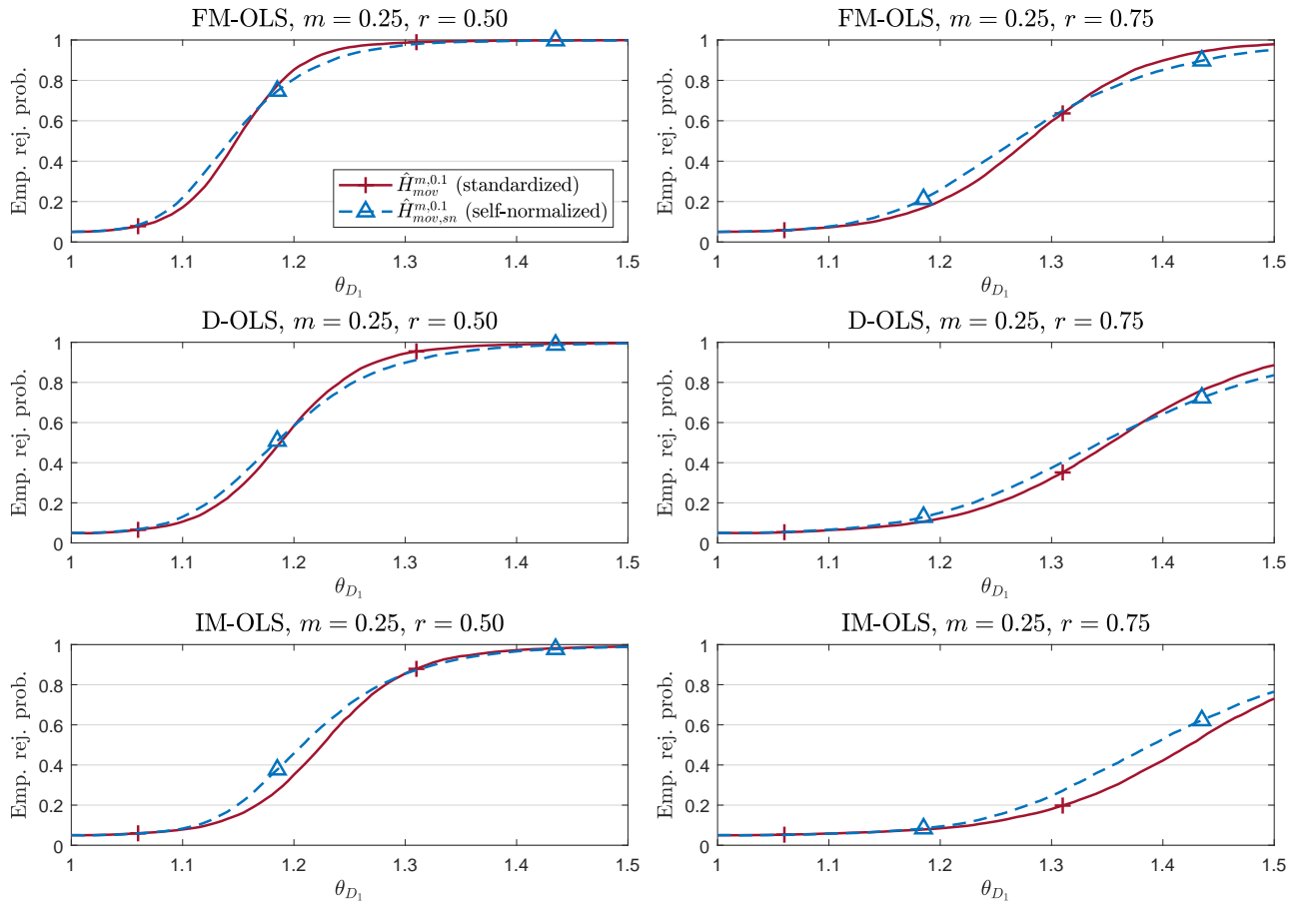


Figure S14: Size-corrected power against trend breaks for  $T = 200$  and  $\rho_1 = \rho_2 = 0.3$ .

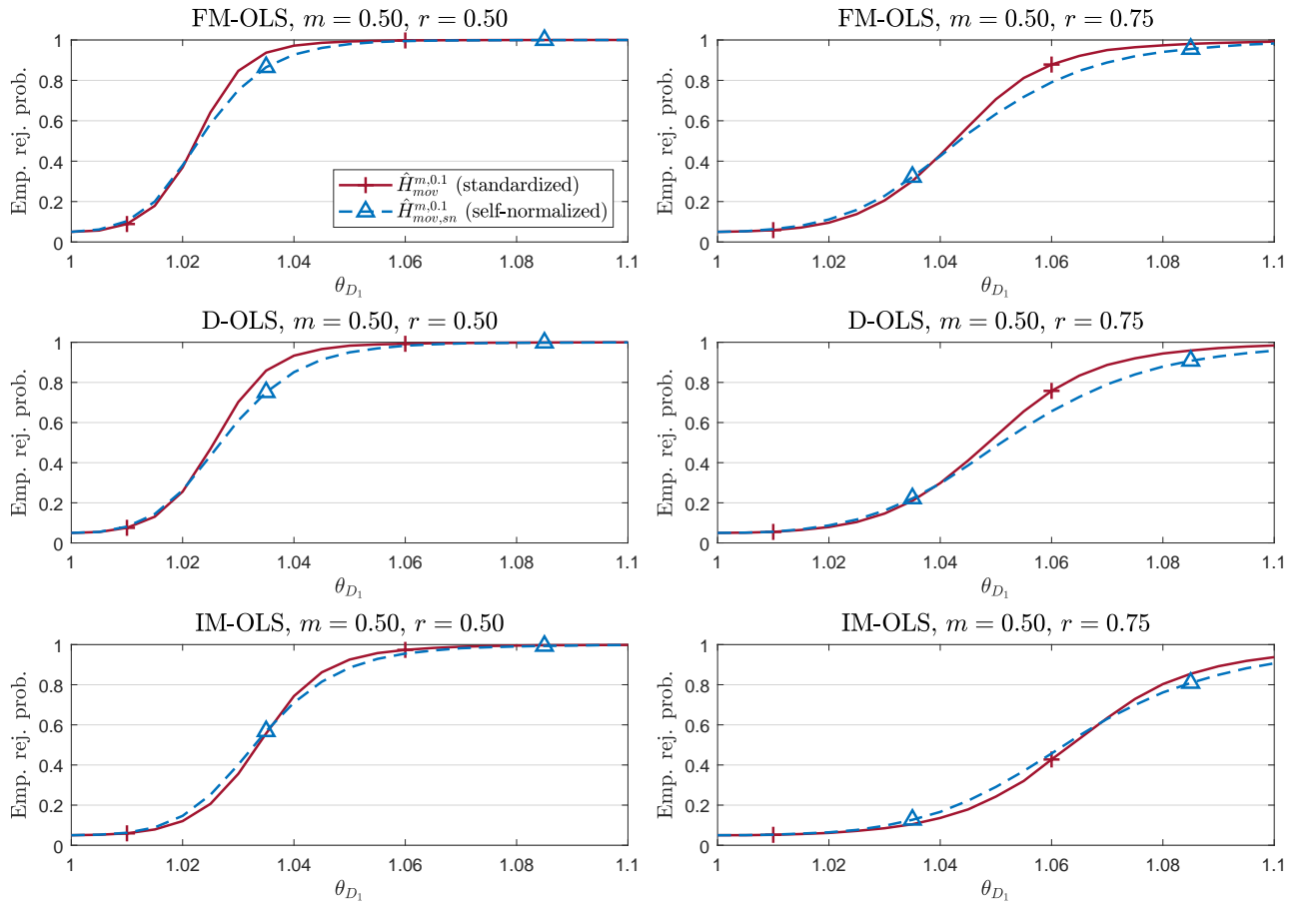


Figure S15: Size-corrected power against trend breaks for  $T = 200$  and  $\rho_1 = \rho_2 = 0.3$ .

## Size-Corrected Power – Slope Breaks

We next consider size-corrected power in case of slope breaks, where either  $\theta_{X_{1,1}}$  or  $\theta_{X_{1,2}}$  changes. The parameter  $\theta_{X_{1,1}}$  varies in 26 equidistant steps over the interval [5, 10] and  $\theta_{X_{1,2}}$  varies in 27 equidistant steps over the interval [-0.3, 1]. The two intervals each include the corresponding null hypothesis value  $\theta_{X_{1,1}} = 5$  and  $\theta_{X_{1,2}} = -0.3$ , respectively. Figures S16 (slope break in  $\theta_{X_{1,1}}$ ) and S17 (slope break in  $\theta_{X_{1,2}}$ ) display size-corrected power for  $\hat{H}^m$ ,  $\hat{H}_{mov}^{m,0.1}$ ,  $\hat{H}_{mov}^{m,0.2}$  and  $\hat{H}_{mov}^{m,0.3}$ . The sample size is  $T = 200$  with  $\rho_1 = \rho_2 = 0.3$ ,  $m = 0.5$  and  $r = 0.75$ . Similar to the case of I(1) breaks, size-corrected power is by and large highest for the moving window detector with  $n = 0.1$ . To assess the impact of self-normalization, Figures S18 ( $m = 0.25$ ) and S19 ( $m = 0.5$ ) display size-corrected power against slope breaks in  $\theta_{X_{1,1}}$  using  $\hat{H}_{mov}^{m,0.1}$  and  $\hat{H}_{mov,sn}^{m,0.1}$ , for  $T = 200$ ,  $\rho_1 = \rho_2 = 0.3$  and  $r \in \{0.5, 0.75\}$ . In case of  $m = 0.25$ , self-normalization leads for small breaks in  $\theta_{X_{1,1}}$  to slightly higher size-corrected power than standardization, especially for IM-OLS. In case of  $m = 0.5$ , standardization leads for FM-OLS and D-OLS to slightly higher size-corrected power than self-normalization, with the exception of very small break magnitudes (i.e.,  $\theta_{X_{1,1}} < 5.5$ ) where both standardization and self-normalization lead to equal size-corrected power. For IM-OLS, size-corrected power is almost equal for standardization and self-normalization when  $m = 0.5$ . The observed results are qualitatively similar for larger sample sizes and other values of  $\rho_1, \rho_2$  and are available upon request.

As expected and already mentioned in the main text, the finite sample size-corrected power results are in line with the results from the LAP analysis in Supplementary Appendix B.

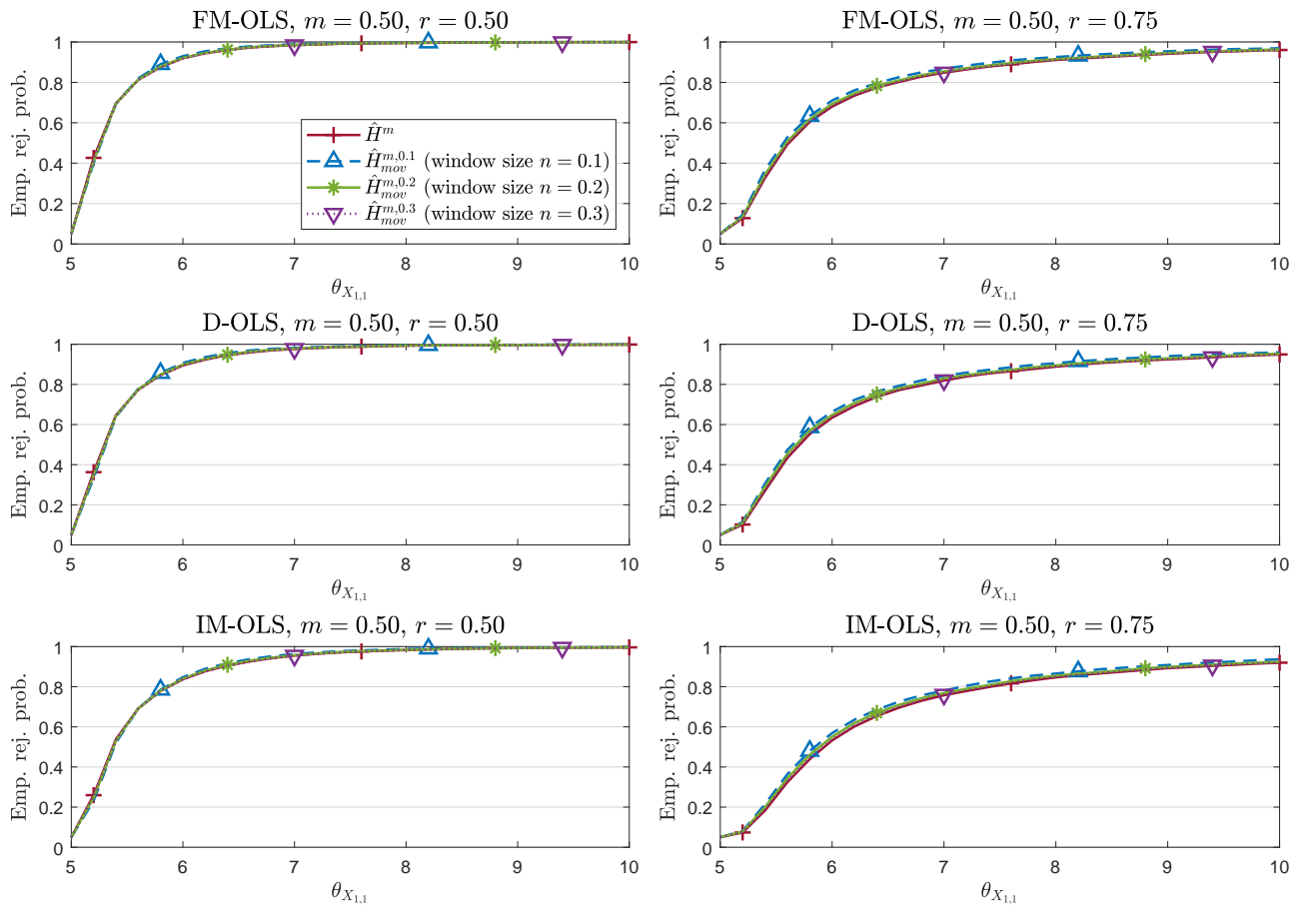


Figure S16: Size-corrected power against slope breaks (in  $\theta_{X_{1,1}}$ ) for  $T = 200$  and  $\rho_1 = \rho_2 = 0.3$ .

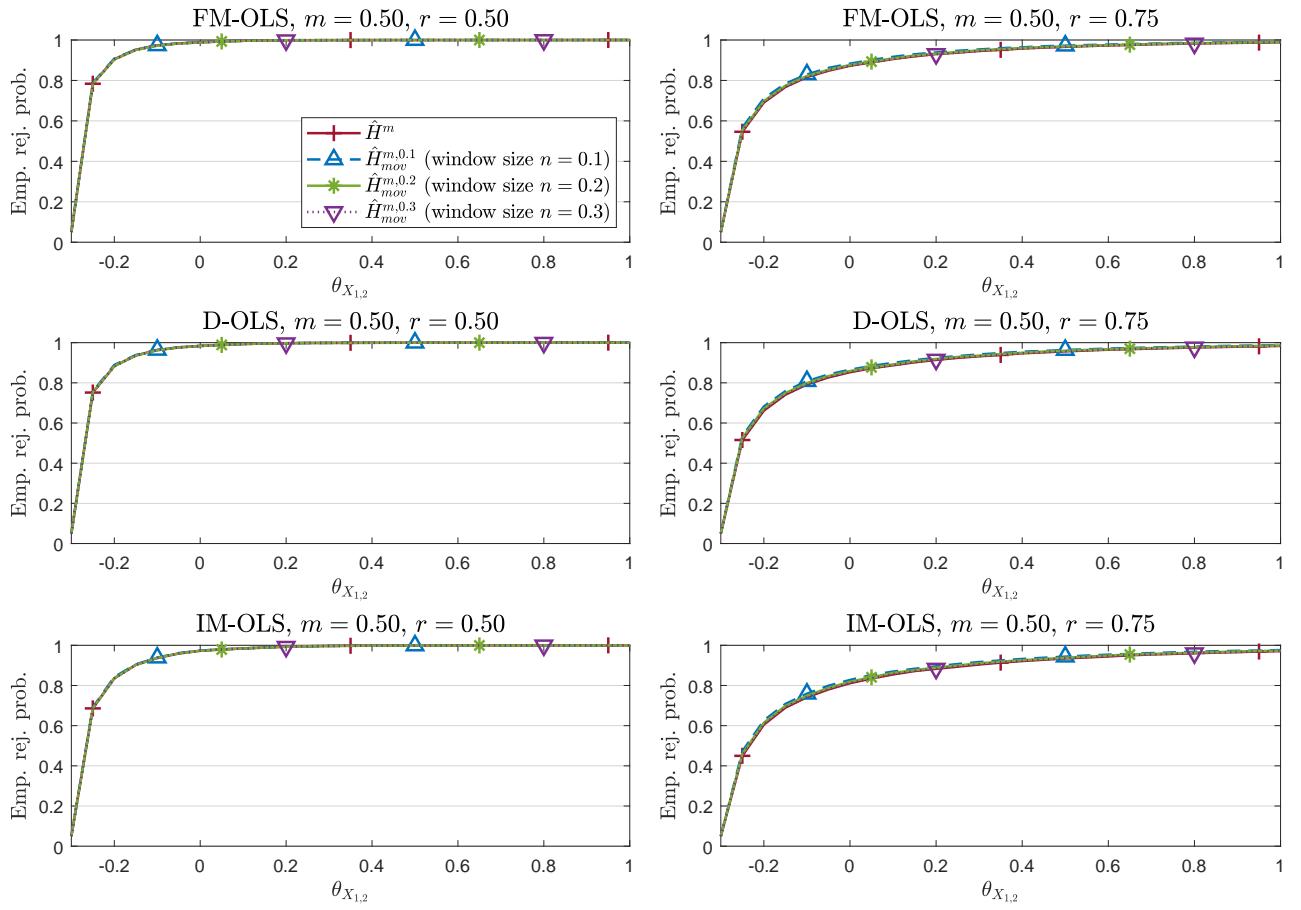


Figure S17: Size-corrected power against slope breaks (in  $\theta_{X_{1,2}}$ ) for  $T = 200$  and  $\rho_1 = \rho_2 = 0.3$ .

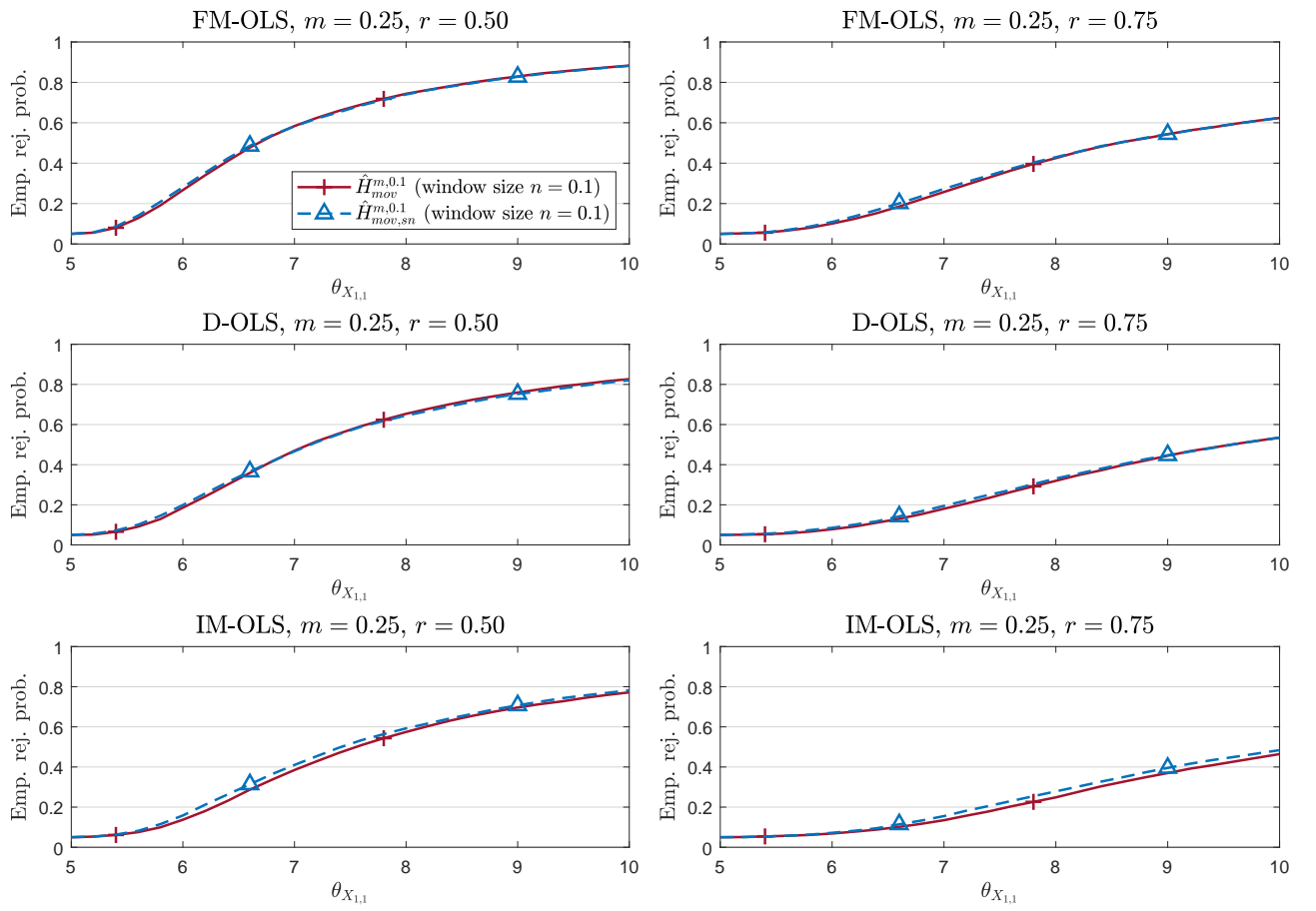


Figure S18: Size-corrected power against slope breaks (in  $\theta_{X_{1,1}}$ ) for  $T = 200$  and  $\rho_1 = \rho_2 = 0.3$ .

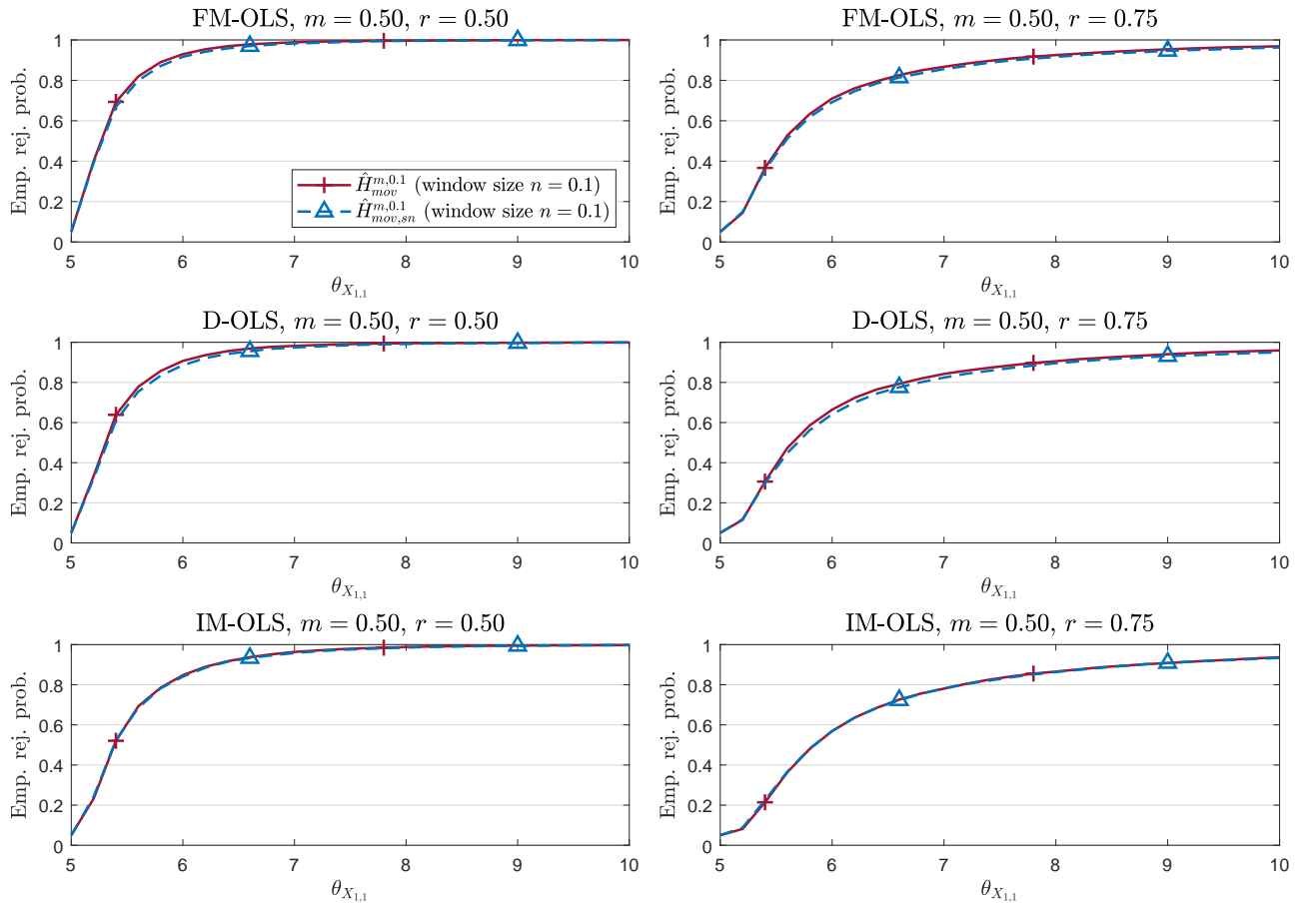


Figure S19: Size-corrected power against slope breaks (in  $\theta_{X_{1,1}}$ ) for  $T = 200$  and  $\rho_1 = \rho_2 = 0.3$ .

## Detection Times

We close Supplementary Appendix C with some additional detection times figures. Figure S20 displays the results for  $T = 500$ ,  $m = 0.5$ ,  $r = 0.5$  and  $\rho_1 = \rho_2 = 0.3$  and complements the results for  $T = 200$  in Figure 4 in the main document. Figures S21 – S25 here in Supplementary Appendix C display the results for  $\rho_1 = \rho_2 = 0.3$ ,  $T \in \{200, 500\}$  and all other combinations of  $m, r \in \{0.25, 0.5, 0.75\}$ , with  $m \leq r$ . In addition, Figure S26 displays detection times for  $\rho_1 = \rho_2 = 0.9$ , with  $m = 0.5$  and  $r = 0.5$ . As expected, increasing  $\rho_1, \rho_2$  leads to larger delays. Further results, e.g., for  $\rho_1 = \rho_2 = 0$ , are available upon request.

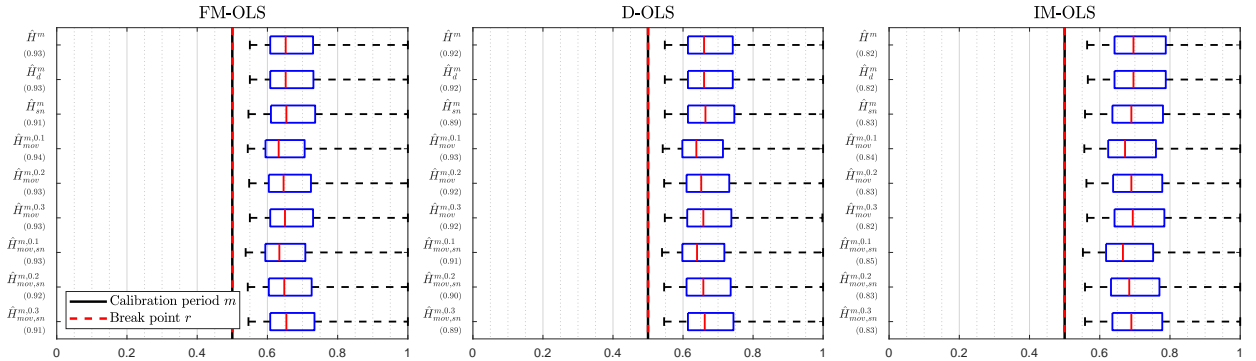


Figure S20: Detection times against  $I(1)$  breaks for  $T = 500$ ,  $m = 0.5$ ,  $r = 0.5$  and  $\rho_1 = \rho_2 = 0.3$ .

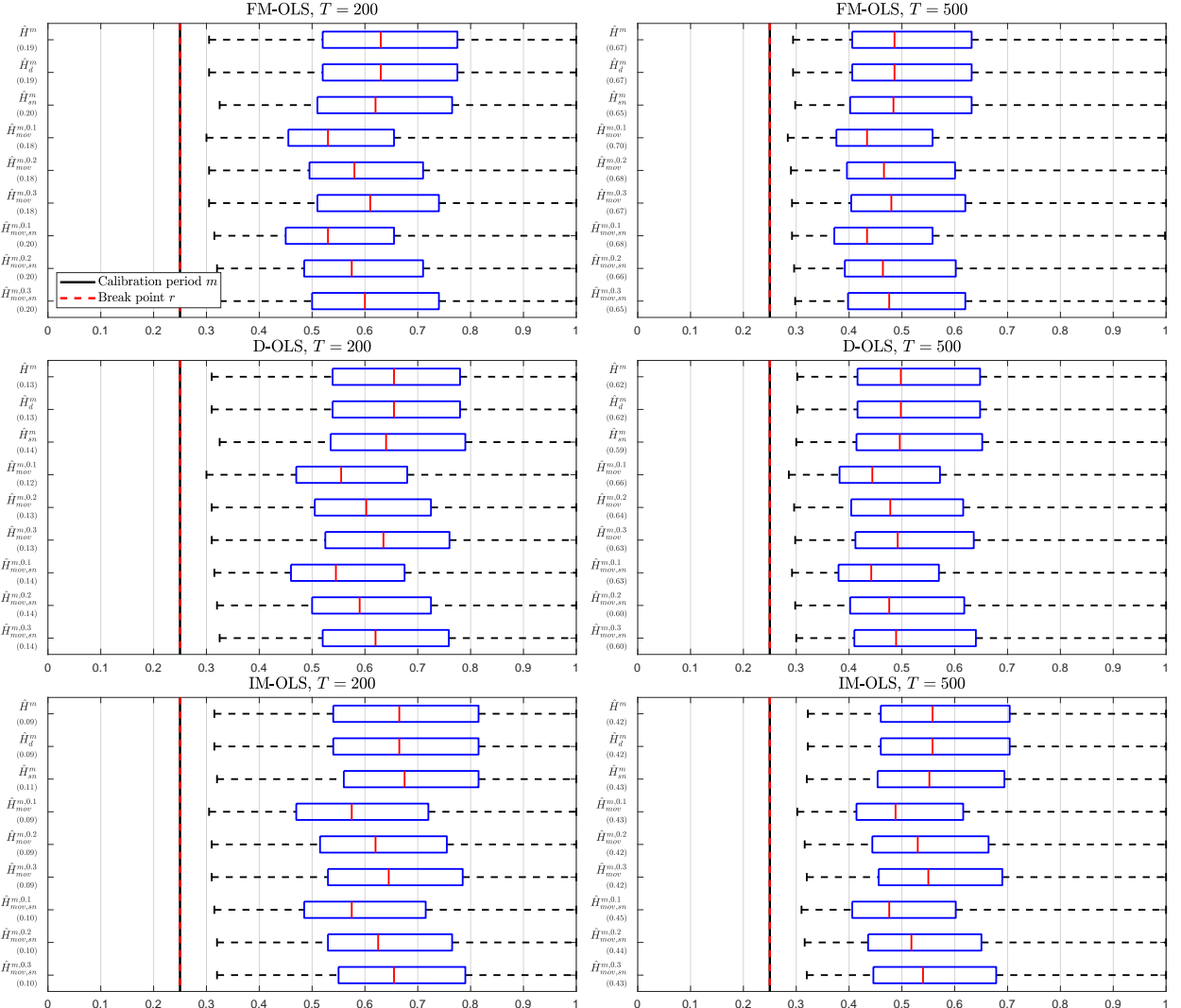


Figure S21: Detection times against  $I(1)$  breaks for  $m = 0.25$ ,  $r = 0.25$  and  $\rho_1 = \rho_2 = 0.3$ .

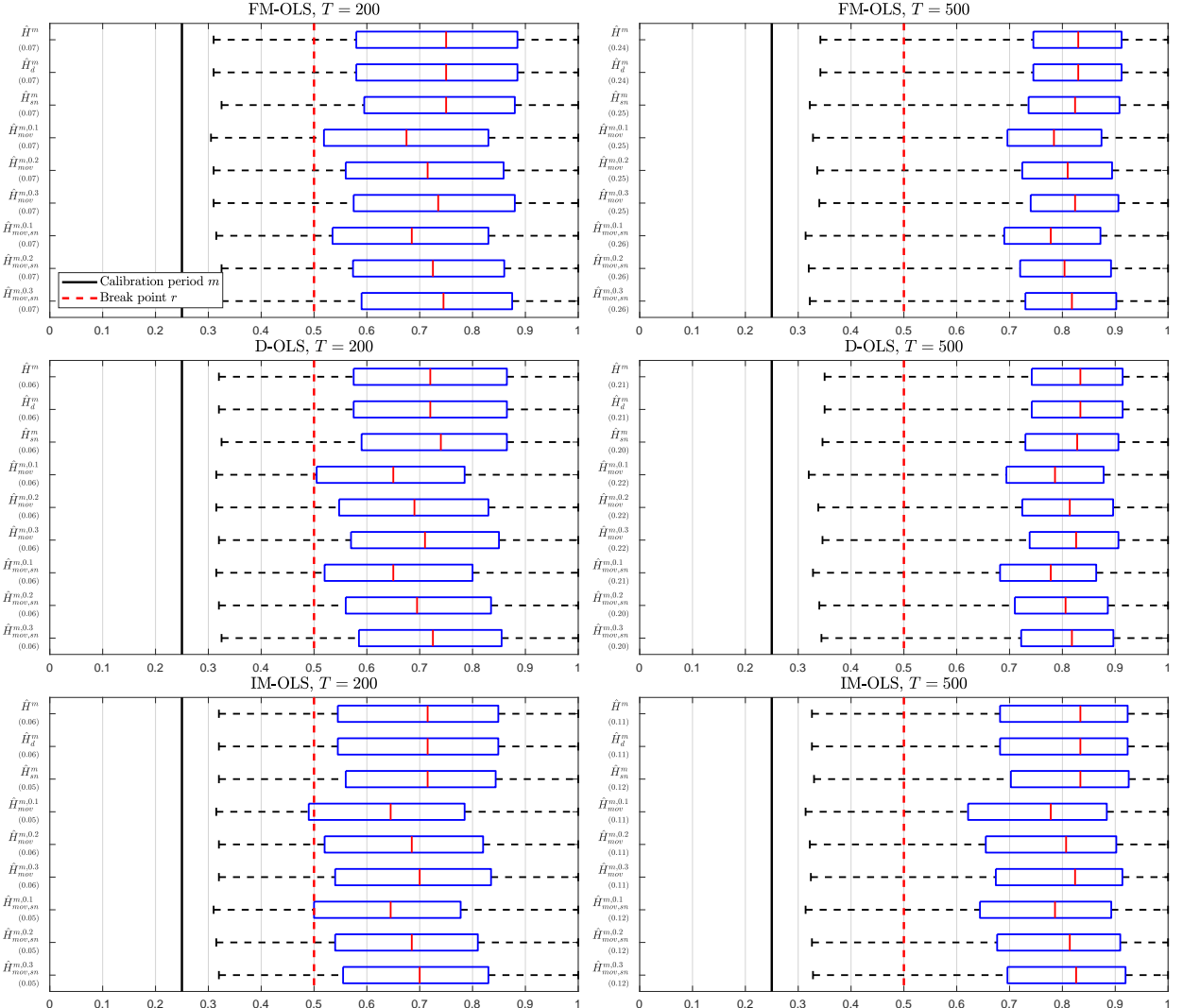


Figure S22: Detection times against  $I(1)$  breaks for  $m = 0.25$ ,  $r = 0.5$  and  $\rho_1 = \rho_2 = 0.3$ .

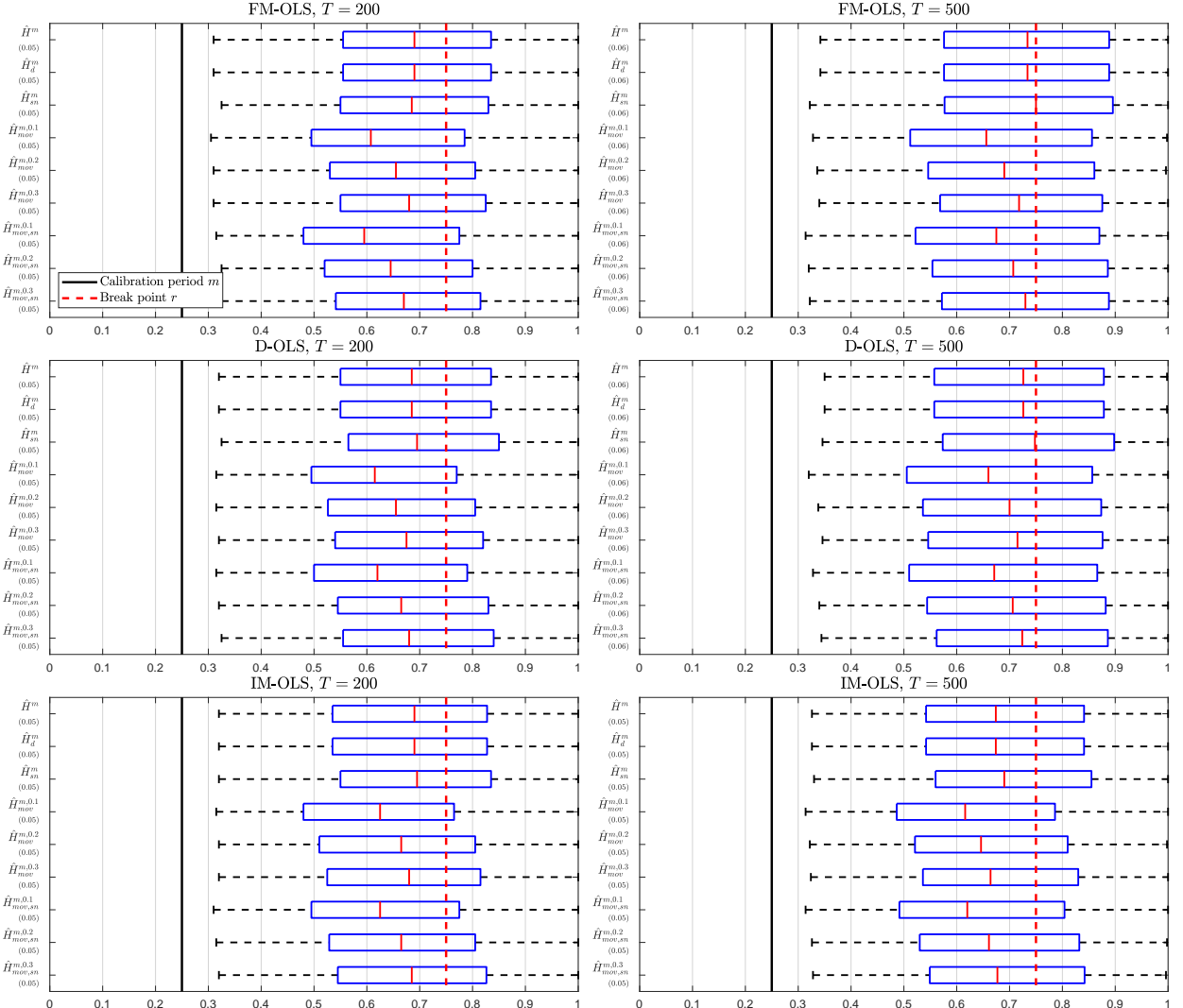


Figure S23: Detection times against  $I(1)$  breaks for  $m = 0.25$ ,  $r = 0.75$  and  $\rho_1 = \rho_2 = 0.3$ .

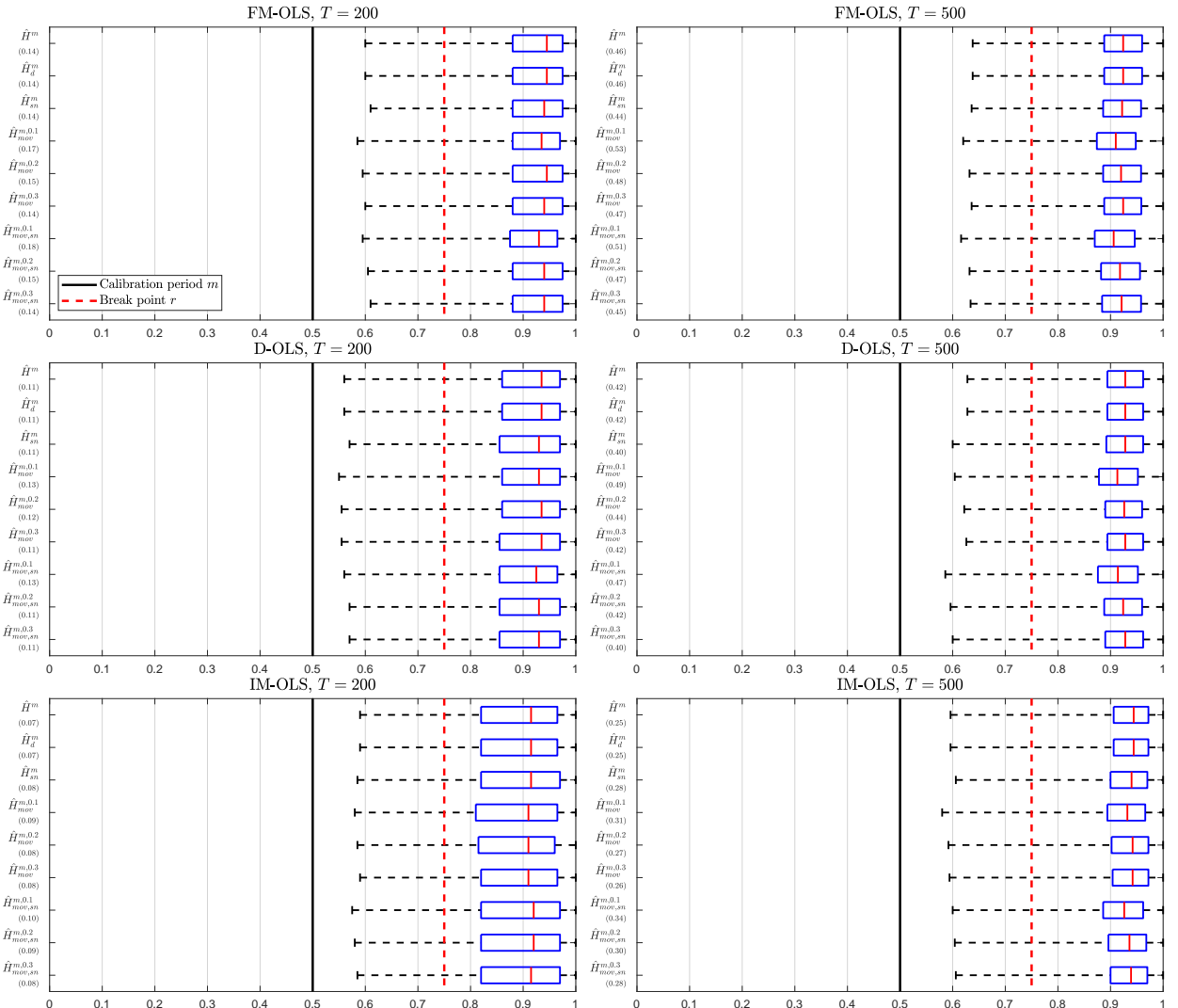


Figure S24: Detection times against  $I(1)$  breaks for  $m = 0.5$ ,  $r = 0.75$  and  $\rho_1 = \rho_2 = 0.3$ .

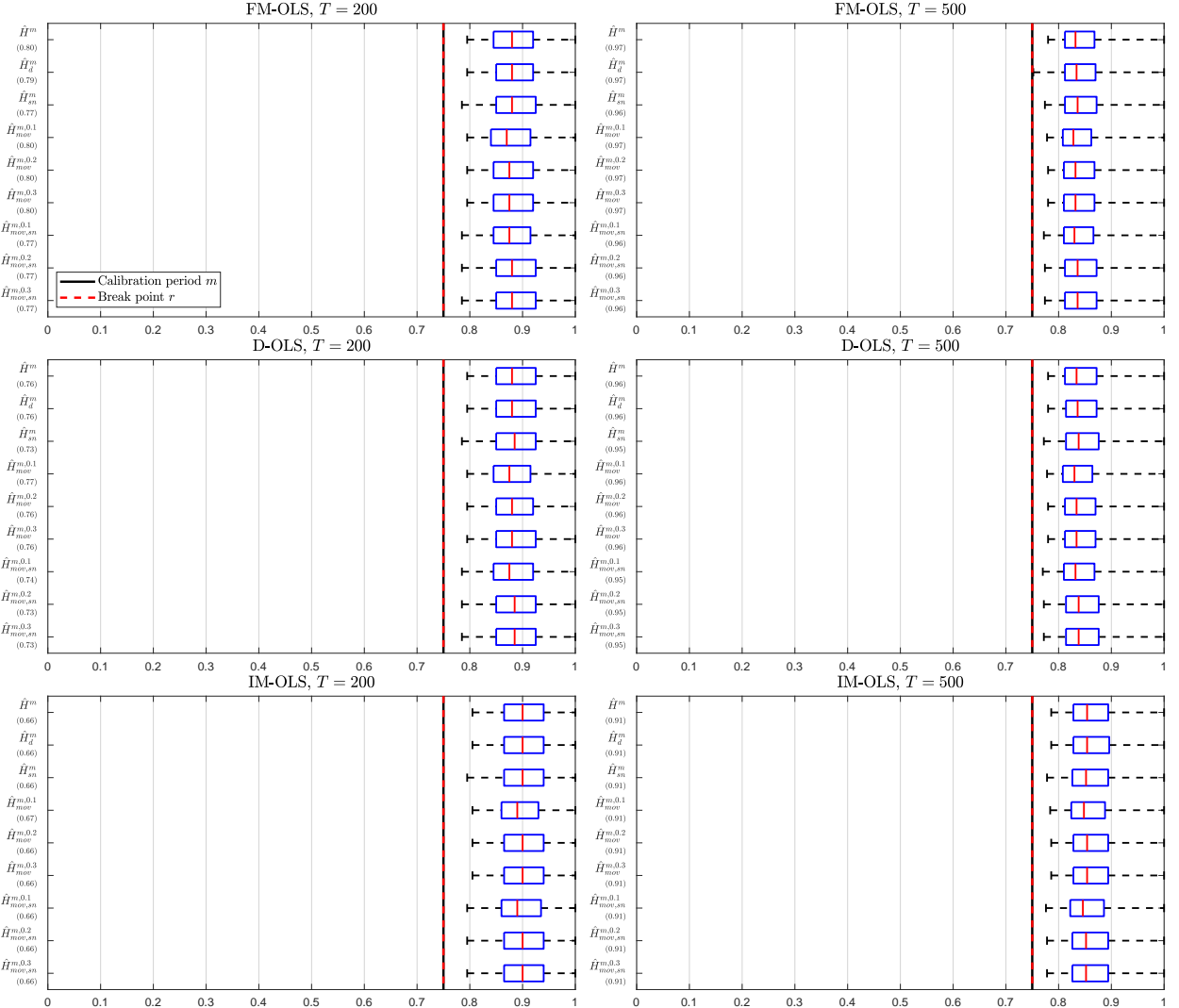


Figure S25: Detection times against  $I(1)$  breaks for  $m = 0.75$ ,  $r = 0.75$  and  $\rho_1 = \rho_2 = 0.3$ .

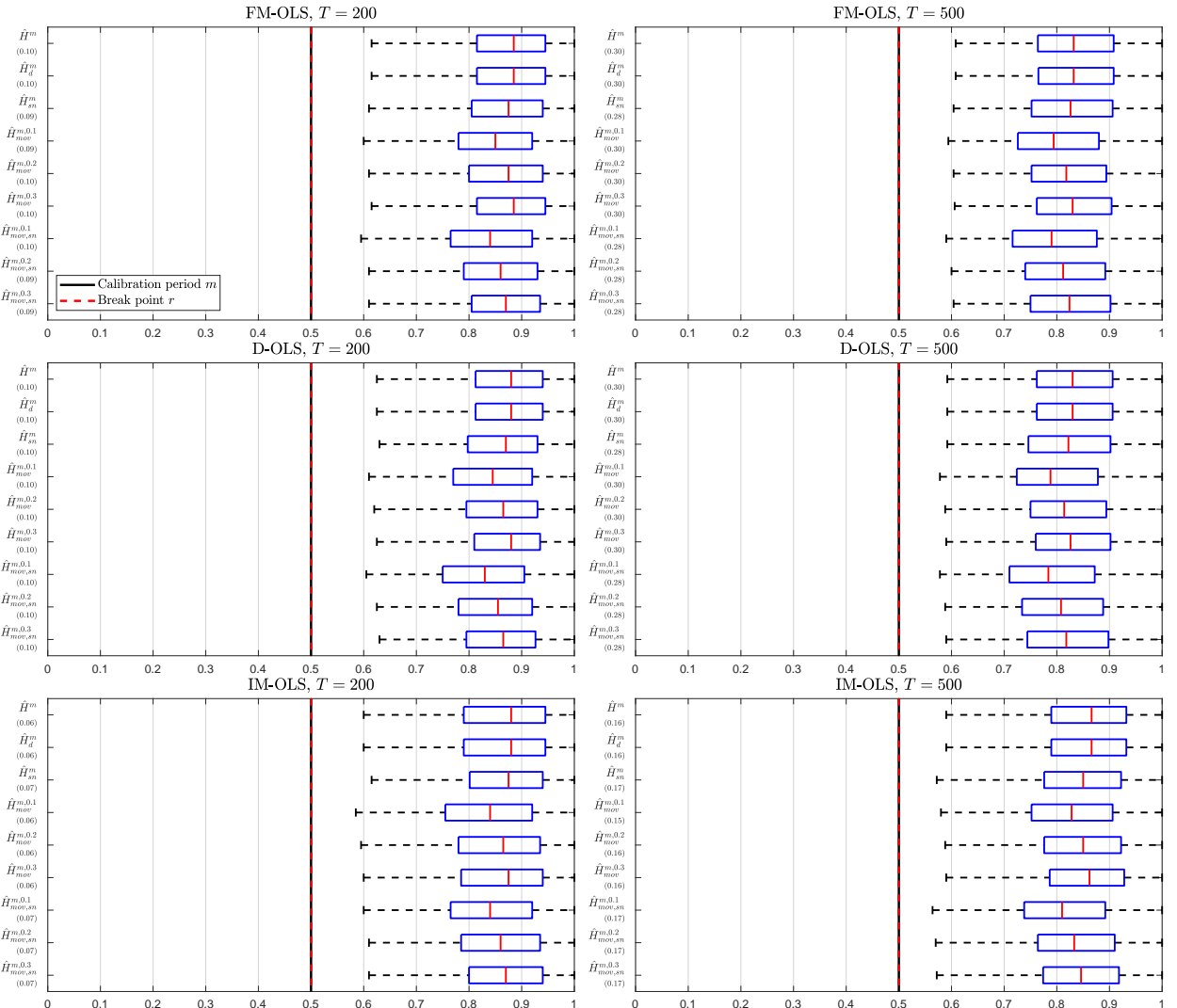


Figure S26: Detection times against  $I(1)$  breaks for  $m = 0.5$ ,  $r = 0.5$  and  $\rho_1 = \rho_2 = 0.9$ .

# MONITORING COINTEGRATING POLYNOMIAL REGRESSIONS

## SUPPLEMENTARY APPENDIX D: ADDITIONAL EMPIRICAL RESULTS

FABIAN KNORRE, MARTIN WAGNER AND MAXIMILIAN GRUPE

### Additional Empirical Results

Country	ln(GDP)	
	ADF	PP
Australia	-1.217	-1.245
Austria	<b>-7.171</b>	<b>-5.324</b>
Belgium	-0.408	-0.485
Canada	-1.182	-1.044
Denmark	-2.422	-2.629
Finland	-2.178	-2.420
France	<b>-6.102</b>	<b>-3.880</b>
Germany	<b>-6.498</b>	<b>-5.337</b>
Italy	<i>-3.283</i>	<b>-4.295</b>
Japan	-1.724	-1.885
New Zealand	<b>-5.436</b>	<b>-6.237</b>
Norway	<b>-5.173</b>	<b>-5.221</b>
Portugal	-0.558	2.010
Spain	-2.415	-2.603
Sweden	-2.460	-2.775
Switzerland	<b>-5.356</b>	<b>-6.322</b>
United Kingdom	-3.221	<i>-3.384</i>
United States	-2.301	-2.547

Table S8: Results of the augmented Dickey and Fuller (1981) and Phillips and Perron (1988) unit root tests for log per capita GDP for the calibration period 1946–1973. The test equation includes intercept and linear trend. For the ADF test, we choose the lag length using the AIC criterion and the maximum lag length is three. *Italic* entries indicate rejection of the null hypothesis at the 10% level and **bold** entries rejection at the 5% level.

Country	ln(GDP)	
	ADF	PP
Australia	-1.146	-1.392
Austria	-2.457	<b>-5.292</b>
Belgium	0.123	0.046
Canada	-0.351	-0.377
Denmark	-0.429	-0.440
Finland	-1.151	-0.199
France	-2.069	-2.061
Germany	<b>-6.960</b>	<b>-32.623</b>
Italy	-0.670	-2.278
Japan	-1.143	-0.878
New Zealand	-2.757	<b>-3.581</b>
Norway	1.198	0.733
Portugal	0.089	0.391
Spain	0.505	0.974
Sweden	-1.900	-1.999
Switzerland	-2.154	-1.101
United Kingdom	-1.999	-1.197
United States	-1.303	-1.484

Table S9: Results of the augmented Dickey and Fuller (1981) and Phillips and Perron (1988) unit root tests for log per capita GDP for the full sample period 1946–2016. For further explanations see notes to Table S8.

Country	$p = 1$		$p = 2$	$p = 3$
	Shin	Johansen		
	r = 0	r = 1	CT	CT
Australia	0.075	<b>73.986</b>	5.418	0.079
Belgium	0.035	<i>23.343</i>	2.296	0.024
Canada	0.072	<i>23.197</i>	7.070	<i>0.091</i>
Denmark	0.056	21.761	3.702	0.057
Finland	<b>0.147</b>	12.999	3.362	0.058
Italy	0.076	<i>23.399</i>	5.211	0.065
Japan	0.045	<b>37.190</b>	3.672	0.021
Portugal	0.052	<b>43.125</b>	7.614	0.049
Spain	<i>0.099</i>	<i>25.045</i>	10.510	0.061
Sweden	0.044	<i>24.473</i>	6.706	0.034
United Kingdom	0.072	<b>30.967</b>	9.082	0.079
United States	<b>0.149</b>	<b>26.274</b>	5.105	0.057

Table S10: Results of the Shin (1994), Johansen (1995) and CT (Wagner, 2020) tests for log per capita CO<sub>2</sub> emissions and log per capita GDP. The (calibration) period is 1946–1973. For the Johansen test the number of lags is determined using the AIC and the maximum lag length is three. *Italic* entries indicate rejection of the null hypothesis at the 10% level and **bold** entries rejection at the 5% level.

Country	$p = 1$		$\frac{p=2}{CT}$	$\frac{p=3}{CT}$	
	Shin	Johansen			
	r = 0	r = 1			
Australia	0.060	<b>38.564</b>	11.952	0.059	0.055
Belgium	<i>0.100</i>	11.945	2.082	<i>0.104</i>	0.022
Canada	0.047	<b>29.940</b>	5.195	0.046	0.022
Denmark	<b>0.137</b>	17.271	4.976	0.086	0.033
Finland	<b>0.132</b>	23.552	5.571	0.063	0.031
Italy	<i>0.111</i>	<b>35.603</b>	5.176	<i>0.091</i>	0.028
Japan	<b>0.145</b>	14.479	5.003	0.059	0.049
Portugal	0.085	<b>29.134</b>	3.959	0.064	0.068
Spain	<i>0.099</i>	25.004	4.024	0.082	0.076
Sweden	<b>0.178</b>	<b>25.901</b>	8.170	0.053	0.050
United Kingdom	0.095	<b>26.260</b>	4.719	0.054	0.046
United States	<b>0.142</b>	<b>38.707</b>	<b>13.683</b>	<b>0.113</b>	0.047

Table S11: Results of the Shin (1994), Johansen (1995) and CT (Wagner, 2020) tests for log per capita SO<sub>2</sub> emissions and log per capita GDP. The (calibration) period is 1946–1973. For further explanations see notes to Table S10.

Country	Polynomial degree	
	CO <sub>2</sub>	SO <sub>2</sub>
Australia	2	1
Belgium	1	1
Canada	1	1
Denmark	1	3
Finland	1	1
Italy	2	1
Japan	1	2
Portugal	2	1
Spain	1	1
Sweden	1	1
United Kingdom	2	3
United States	1	1

Table S12: Minimal polynomial degrees for cointegrating EKCs over the full sample period 1946–2016. The detailed cointegration test results are available in Tables S13 and S14.

Country	$p_1 = 1$		$p_1 = 2$		$p_1 = 3$
	Shin	Johansen		CT	CT
		r = 0	r = 1		
Australia	<b>0.165</b>	<b>55.183</b>	9.001	0.047	0.048
Belgium	0.087	22.624	7.421	0.073	0.058
Canada	0.057	22.511	3.539	0.055	0.053
Denmark	0.039	<b>30.477</b>	10.229	0.030	0.033
Finland	0.068	<b>31.796</b>	<b>14.518</b>	0.051	0.056
Italy	<b>0.121</b>	<b>27.923</b>	4.408	0.082	<i>0.089</i>
Japan	<i>0.111</i>	<b>28.798</b>	7.611	0.073	0.049
Portugal	<b>0.129</b>	9.548	3.273	0.057	0.067
Spain	0.055	23.116	6.730	0.056	0.052
Sweden	0.050	<b>29.520</b>	<i>10.818</i>	0.076	0.054
United Kingdom	<b>0.200</b>	<b>35.167</b>	7.089	0.068	0.041
United States	<i>0.102</i>	20.504	5.966	0.067	0.065

Table S13: Results of the Shin (1994), Johansen (1995) and CT (Wagner, 2020) tests for log per capita CO<sub>2</sub> emissions and log per capita GDP. The (full sample) period is 1946–2016. For further explanations see notes to Table S10.

Country	$p_1 = 1$		$p_1 = 2$		$p_1 = 3$
	Shin	Johansen		CT	CT
		r = 0	r = 1		
Australia	0.064	20.417	3.540	0.047	0.036
Belgium	<i>0.116</i>	20.564	4.520	0.062	0.033
Canada	<i>0.105</i>	<b>29.641</b>	<i>12.067</i>	0.060	0.071
Denmark	0.084	<b>28.038</b>	4.788	<b>0.107</b>	0.057
Finland	<i>0.109</i>	14.953	5.029	<i>0.096</i>	<i>0.100</i>
Italy	<i>0.101</i>	<b>40.453</b>	3.823	0.070	0.050
Japan	<b>0.127</b>	<b>40.635</b>	9.440	0.064	0.066
Portugal	<i>0.100</i>	13.291	5.239	0.068	0.077
Spain	0.089	18.603	8.650	<i>0.088</i>	0.070
Sweden	0.067	<i>23.999</i>	8.783	<i>0.097</i>	0.071
United Kingdom	<b>0.213</b>	<b>33.910</b>	9.928	<b>0.122</b>	0.065
United States	0.080	<b>32.551</b>	<b>14.114</b>	0.041	0.041

Table S14: Results of the Shin (1994), Johansen (1995) and CT (Wagner, 2020) tests for log per capita SO<sub>2</sub> emissions and log per capita GDP. The (full sample) period is 1946–2016. For further explanations see notes to Table S10.

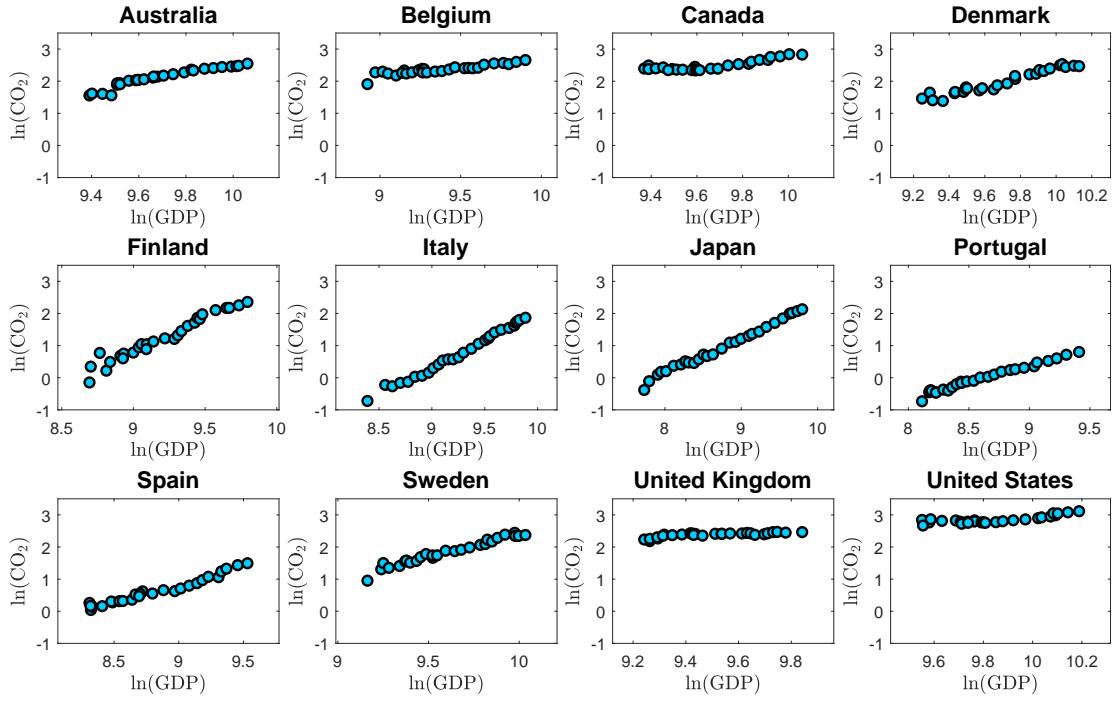


Figure S27: The scatter plots show pairs of observations of log per capita GDP and log per capita CO<sub>2</sub> emissions for the calibration period 1946–1973 for the considered twelve countries.

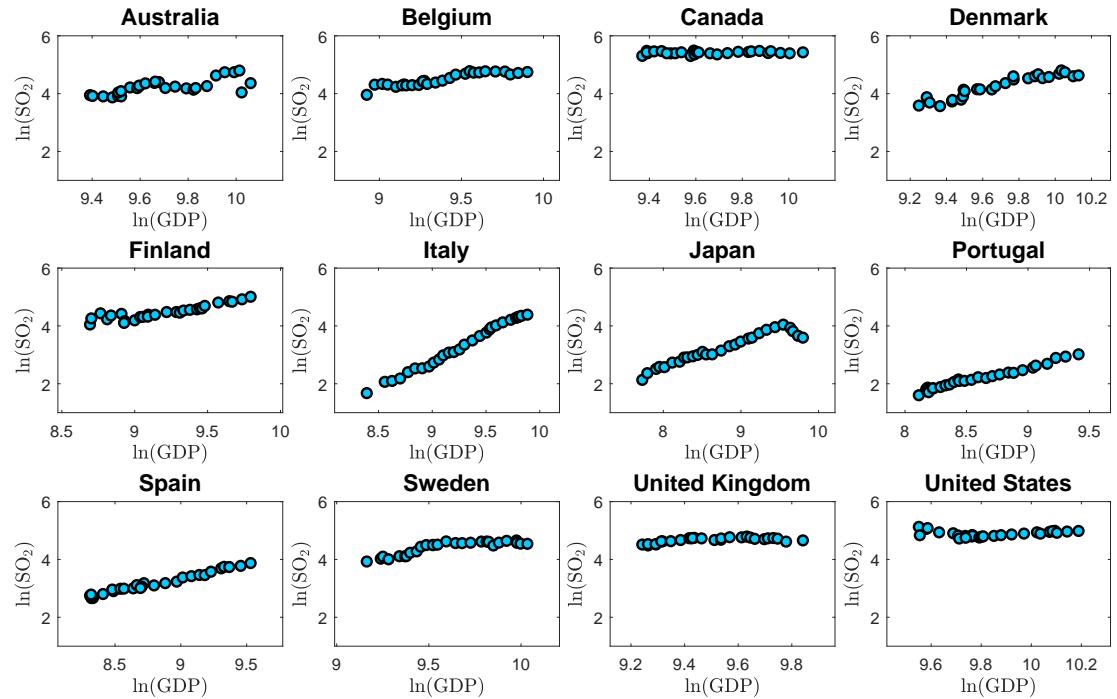


Figure S28: The scatter plots show pairs of observations of log per capita GDP and log per capita SO<sub>2</sub> emissions for the calibration period 1946–1973 for the considered twelve countries.

Country	$p$	$\hat{H}^m$			$\hat{H}_d^m$			$\hat{H}_{sn}^m$			$\hat{H}_{mov}^{m,0.1}$			$\hat{H}_{mov}^{m,0.2}$			$\hat{H}_{mov}^{m,0.3}$			$\hat{H}_{mov,sn}^{m,0.1}$			$\hat{H}_{mov,sn}^{m,0.2}$			$\hat{H}_{mov,sn}^{m,0.3}$			
		FM	D	IM	FM	D	IM	FM	D	IM	FM	D	IM	FM	D	IM	FM	D	IM	FM	D	IM	FM	D	IM	FM	D	IM	
Australia	1	1993	1993	2001	1993	1993	2001	1997	2001	2006	1990	1990	1997	1992	1992	1999	1993	1992	2001	1993	1997	2001	1995	1999	2003	1996	2000	2005	
Belgium	1	1993	1992	2001	1993	1992	2001	1991	1990	1998	1989	1989	1993	1992	1991	1997	1993	1992	1999	1988	1988	1992	1990	1989	1995	1991	1990	1997	
Canada	1	$\infty$	$\infty$	$\infty$	$\infty$	$\infty$	$\infty$	$\infty$	1986	$\infty$	$\infty$	$\infty$	$\infty$	$\infty$	$\infty$	$\infty$	$\infty$	$\infty$	$\infty$	$\infty$	$\infty$	1982	$\infty$	$\infty$	1985	$\infty$	$\infty$	1986	$\infty$
Denmark	1	1993	1991	2006	1993	1991	2006	1996	1992	2014	1989	1988	2003	1992	1990	2004	1993	1991	2005	1991	1988	2011	1994	1990	2012	1995	1991	2013	
Finland	2	1990	1997	1992	1990	1997	1992	1992	2000	1993	1988	1994	1989	1989	1996	1991	1990	1997	1991	1989	1996	1990	1991	1998	1992	1992	1999	1993	
Italy	1	1982	1982	1983	1982	1982	1983	1983	1982	1984	1980	1981	1981	1981	1982	1982	1981	1982	1983	1981	1980	1982	1983	1981	1983	1983	1981	1983	
Japan	1	1985	1984	1985	1985	1984	1985	1985	1982	1982	1982	1981	1982	1984	1983	1984	1985	1983	1984	1984	1982	1980	1980	1984	1981	1981	1985	1981	1982
Portugal	1	2000	$\infty$	$\infty$	2000	$\infty$	$\infty$	2002	$\infty$	$\infty$	1996	$\infty$	$\infty$	1998	$\infty$	$\infty$	1999	$\infty$	$\infty$	1998	$\infty$	$\infty$	2000	$\infty$	$\infty$	2001	$\infty$	$\infty$	
Spain	1	$\infty$	$\infty$	$\infty$	$\infty$	$\infty$	$\infty$	$\infty$	$\infty$	$\infty$	$\infty$	$\infty$	$\infty$	$\infty$	$\infty$	$\infty$	$\infty$	$\infty$	$\infty$	$\infty$	$\infty$	$\infty$	$\infty$	$\infty$	$\infty$	$\infty$	$\infty$	$\infty$	
Sweden	1	1983	1982	1985	1984	1982	1985	1983	1985	1982	1981	1983	1983	1982	1984	1983	1982	1985	1982	1981	1983	1983	1982	1985	1983	1982	1985		
United Kingdom	1	1984	1988	1988	1984	1988	1988	1986	1985	1991	1982	1986	1985	1983	1987	1984	1988	1988	1984	1983	1987	1985	1985	1989	1986	1985	1991		
United States	2	1989	1989	1992	1989	1989	1992	1990	1990	1995	1987	1987	1990	1988	1988	1992	1988	1989	1992	1988	1988	1992	1989	1990	1994	1990	1990	1994	

Table S15: Detection times when monitoring CO<sub>2</sub> emissions using all nine detectors and all three estimation methods FM-OLS, D-OLS and IM-OLS. The column  $p$  indicates the polynomial degree, the calibration period is 1946–1973, the monitoring period is 1974–2016. The nominal significance level is 5%.

Country	$p$	$\hat{H}^m$			$\hat{H}_d^m$			$\hat{H}_{sn}^m$			$\hat{H}_{mov}^{m,0.1}$			$\hat{H}_{mov}^{m,0.2}$			$\hat{H}_{mov}^{m,0.3}$			$\hat{H}_{mov,sn}^{m,0.1}$			$\hat{H}_{mov,sn}^{m,0.2}$			$\hat{H}_{mov,sn}^{m,0.3}$			
		FM	D	IM	FM	D	IM	FM	D	IM	FM	D	IM	FM	D	IM	FM	D	IM	FM	D	IM	FM	D	IM	FM	D	IM	
Australia	1	$\infty$	$\infty$	$\infty$	$\infty$	$\infty$	$\infty$	$\infty$	$\infty$	$\infty$	$\infty$	$\infty$	$\infty$	$\infty$	$\infty$	$\infty$	$\infty$	$\infty$	$\infty$	$\infty$	$\infty$	$\infty$	$\infty$	$\infty$	$\infty$	$\infty$	$\infty$	$\infty$	$\infty$
Belgium	1	1984	1984	1985	1984	1984	1985	1987	1986	1988	1983	1982	1983	1984	1983	1984	1984	1984	1985	1985	1984	1985	1985	1986	1985	1987	1987	1986	1987
Canada	1	1981	1981	1982	1981	1981	1982	1981	1982	1982	1980	1980	1980	1981	1981	1981	1981	1982	1982	1980	1981	1981	1981	1982	1982	1981	1982	1982	
Denmark	2	1994	1999	2007	1994	1999	2007	1999	1990	2009	1991	1997	2005	1993	1998	2006	1993	1999	2006	1997	1987	2006	1998	1989	2008	1999	1990	2008	
Finland	2	1988	1987	1991	1988	1987	1991	1990	1987	1993	1986	1985	1989	1988	1987	1990	1988	1987	1990	1988	1986	1991	1989	1987	1992	1990	1987	1993	
Italy	1	1981	1981	1982	1981	1981	1982	1984	1984	1984	1980	1979	1980	1981	1980	1981	1981	1982	1982	1982	1983	1983	1983	1984	1983	1984	1984		
Japan	2	1991	2005	2004	1991	2005	2004	1993	2007	2007	1989	2002	2002	1991	2004	2003	1991	2004	2004	1991	2005	2004	1992	2007	2006	1993	2007	2007	
Portugal	1	2015	2013	$\infty$	2015	2013	$\infty$	$\infty$	$\infty$	2013	2012	2015	2014	2013	$\infty$	2015	2013	$\infty$	2015	2015	$\infty$	$\infty$	2016	$\infty$	$\infty$	$\infty$	$\infty$	$\infty$	
Spain	1	2003	2002	2011	2003	2002	2011	2007	2007	2013	1983	1983	1984	1986	2002	1987	2003	2002	2011	2005	2005	2012	2007	2013	2007	2007	2014		
Sweden	2	1986	1986	1989	1986	1986	1989	1987	1988	1990	1984	1984	1987	1985	1986	1988	1986	1985	1986	1988	1986	1988	1989	1986	1988	1990			
United Kingdom	1	1982	1983	1984	1982	1983	1984	1985	1989	1985	1981	1981	1982	1982	1983	1982	1983	1983	1985	1983	1984	1987	1984	1985	1988	1985			
United States	3	$\infty$	$\infty$	$\infty$	$\infty$	$\infty$	$\infty$	$\infty$	$\infty$	$\infty$	$\infty$	$\infty$	$\infty$	$\infty$	$\infty$	$\infty$	$\infty$	$\infty$	$\infty$	$\infty$	$\infty$	$\infty$	$\infty$	$\infty$	$\infty$	$\infty$	$\infty$		

Table S16: Detection times when monitoring SO<sub>2</sub> emissions using all nine detectors and all three estimation methods FM-OLS, D-OLS and IM-OLS. The column  $p$  indicates the polynomial degree, the calibration period is 1946–1973, the monitoring period is 1974–2016. The nominal significance level is 5%.

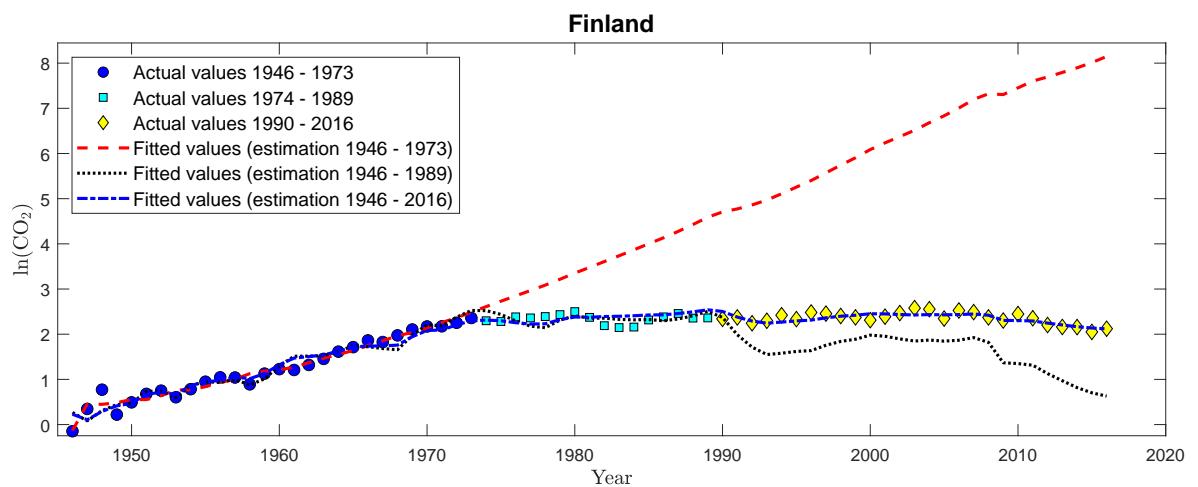


Figure S29: IM-OLS estimation results for a cointegrating quadratic relationship between log per capita GDP and log per capita CO<sub>2</sub> emissions for Finland. The figure shows pairs of observations of log per capita GDP and log per capita CO<sub>2</sub> emissions, for 1946–1973 (blue circles), 1974–1989 (turquoise squares) and 1990–2016 (yellow diamonds). The lines display fitted values over time obtained using different samples for parameter estimation: the dashed red line 1946–1973, the dotted black line 1946–1989 and the dash-dotted blue line 1946–2016.

1946–2016			
	$\theta_{D_1}$	$\theta_{X_1}$	$\theta_{X_2}$
Australia			
FM-OLS	0.004	<b>16.542</b>	<b>-0.786</b>
IM-OLS	0.007	<b>15.218</b>	<b>-0.729</b>
Belgium			
FM-OLS	<b>-0.022</b>	3.355	-0.125
IM-OLS	<b>-0.017</b>	4.869	-0.213
Canada			
FM-OLS	<b>-0.029</b>	0.624	0.056
IM-OLS	<b>-0.027</b>	2.256	-0.030
Denmark			
FM-OLS	<b>-0.053</b>	<b>8.091</b>	<b>-0.265</b>
IM-OLS	<b>-0.051</b>	<b>8.548</b>	<b>-0.291</b>
Finland			
FM-OLS	<b>-0.032</b>	<b>13.660</b>	<b>-0.593</b>
IM-OLS	<b>-0.029</b>	<b>15.157</b>	<b>-0.674</b>
Italy			
FM-OLS	<b>-0.022</b>	<b>5.892</b>	<b>-0.207</b>
IM-OLS	<b>-0.014</b>	<b>11.367</b>	<b>-0.500</b>
Japan			
FM-OLS	<i>-0.009</i>	<b>3.323</b>	<b>-0.123</b>
IM-OLS	<i>-0.004</i>	<b>5.070</b>	<b>-0.222</b>
Portugal			
FM-OLS	<b>-0.021</b>	<b>-3.283</b>	<b>0.272</b>
IM-OLS	<b>-0.025</b>	<b>-4.487</b>	<b>0.343</b>
Spain			
FM-OLS	<b>-0.034</b>	1.488	0.019
IM-OLS	<b>-0.036</b>	1.856	0.003
Sweden			
FM-OLS	<b>-0.052</b>	<b>14.870</b>	<b>-0.621</b>
IM-OLS	<b>-0.066</b>	<b>10.487</b>	<b>-0.373</b>
United Kingdom			
FM-OLS	<b>-0.032</b>	<b>9.229</b>	<b>-0.399</b>
IM-OLS	<b>-0.033</b>	<b>7.205</b>	<b>-0.295</b>
United States			
FM-OLS	<b>-0.030</b>	<b>5.733</b>	<b>-0.204</b>
IM-OLS	<b>-0.023</b>	<b>8.414</b>	<b>-0.350</b>

Table S17: FM-OLS and IM-OLS estimation results for a cointegrating quadratic relationship between log per capita GDP and log per capita CO<sub>2</sub> emissions for the full sample period 1946–2016. *Italic* entries indicate significance of coefficients at the 10% level and **bold** entries significance of coefficients at the 5% level.

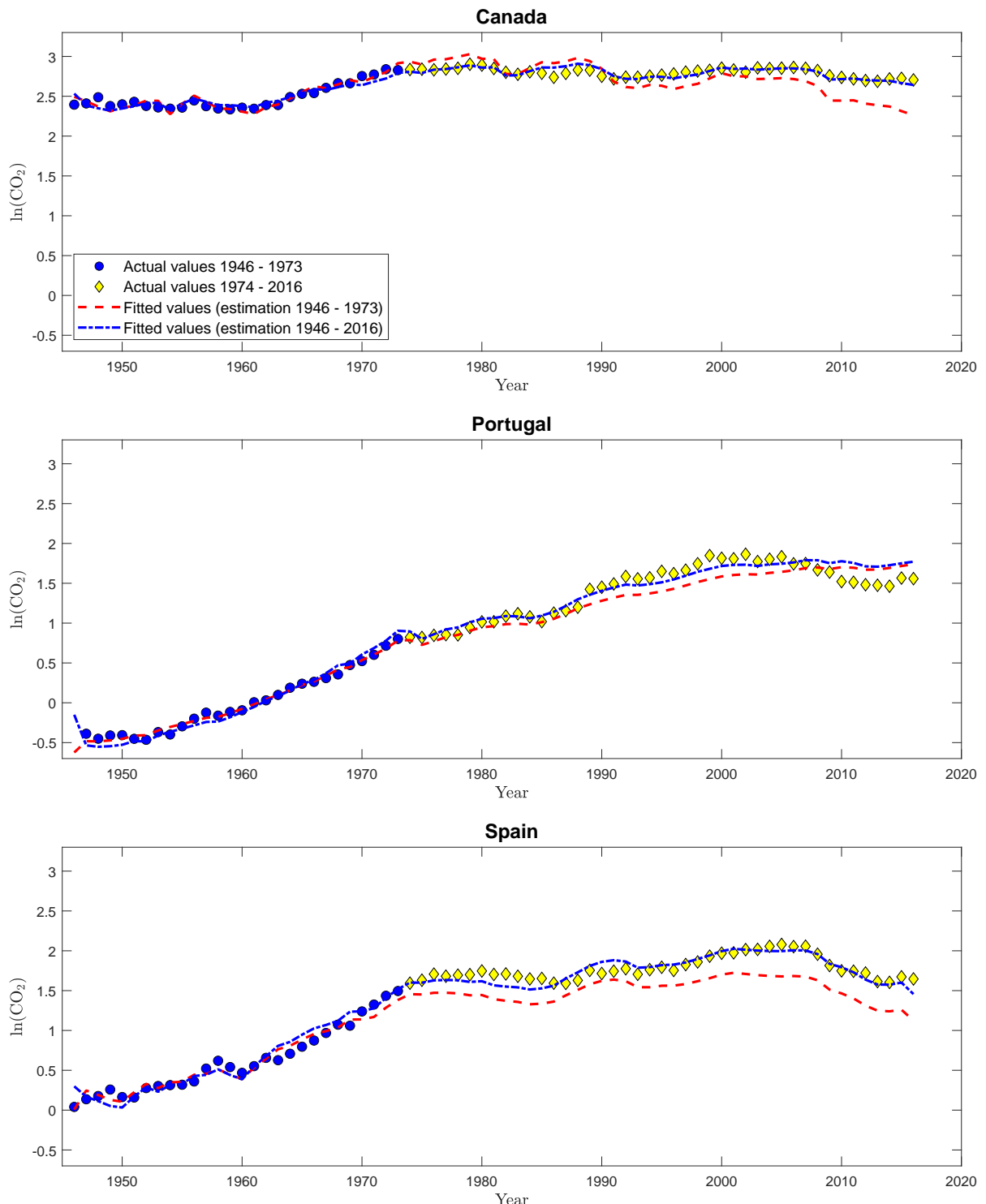


Figure S30: IM-OLS estimation results for a cointegrating linear relationship between log per capita GDP and log per capita CO<sub>2</sub> emissions for Canada, Portugal and Spain. For further explanations see notes to Figure 7 in the main document.

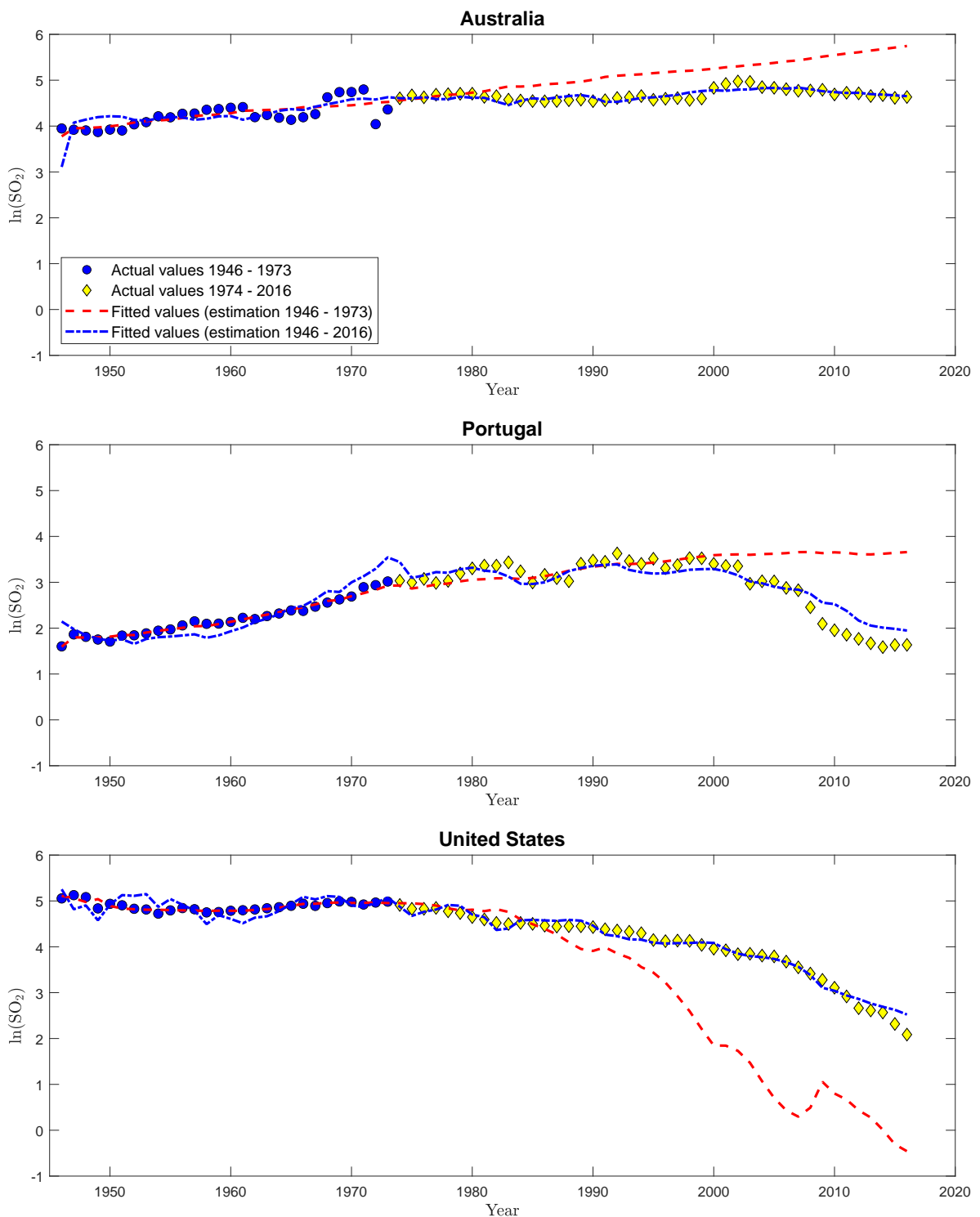


Figure S31: IM-OLS estimation results for a cointegrating linear relationship between log per capita GDP and log per capita  $\text{SO}_2$  emissions for Australia and Portugal, and a cointegrating cubic relationship for the United States. For further explanations see notes to Figure 8 in the main document.

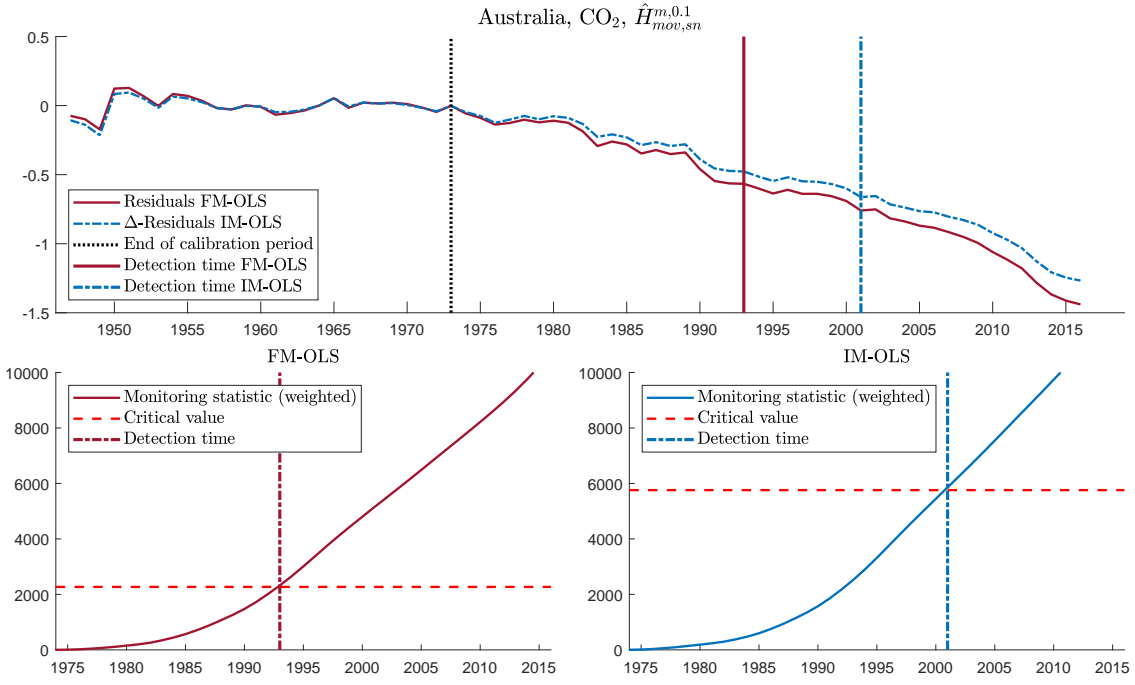


Figure S32: Monitoring results for CO<sub>2</sub> emissions of Australia using  $\hat{H}_{mov,sn}^{m,0.1}$  with both FM-OLS and IM-OLS in the linear specification. The lower panel shows the detectors, the critical values and the detection times for FM-OLS on the left hand side and for IM-OLS on the right hand side.

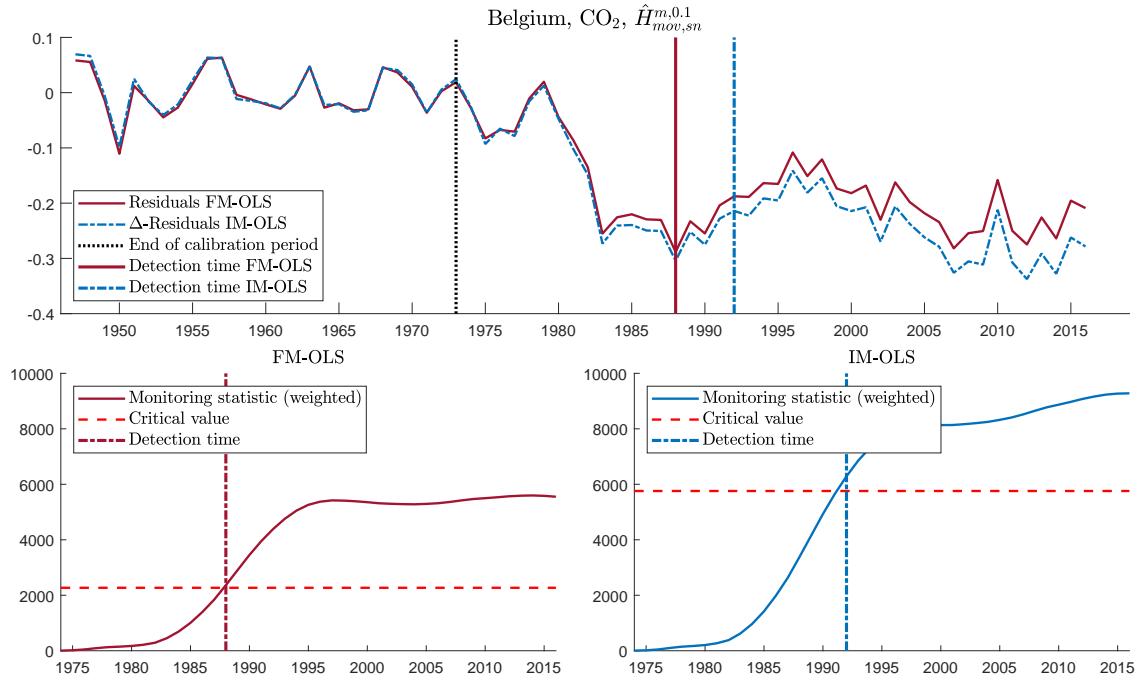


Figure S33: Monitoring results for CO<sub>2</sub> emissions of Belgium using  $\hat{H}_{mov,sn}^{m,0.1}$  with both FM-OLS and IM-OLS in the linear specification. For further explanations see notes to Figure S32.

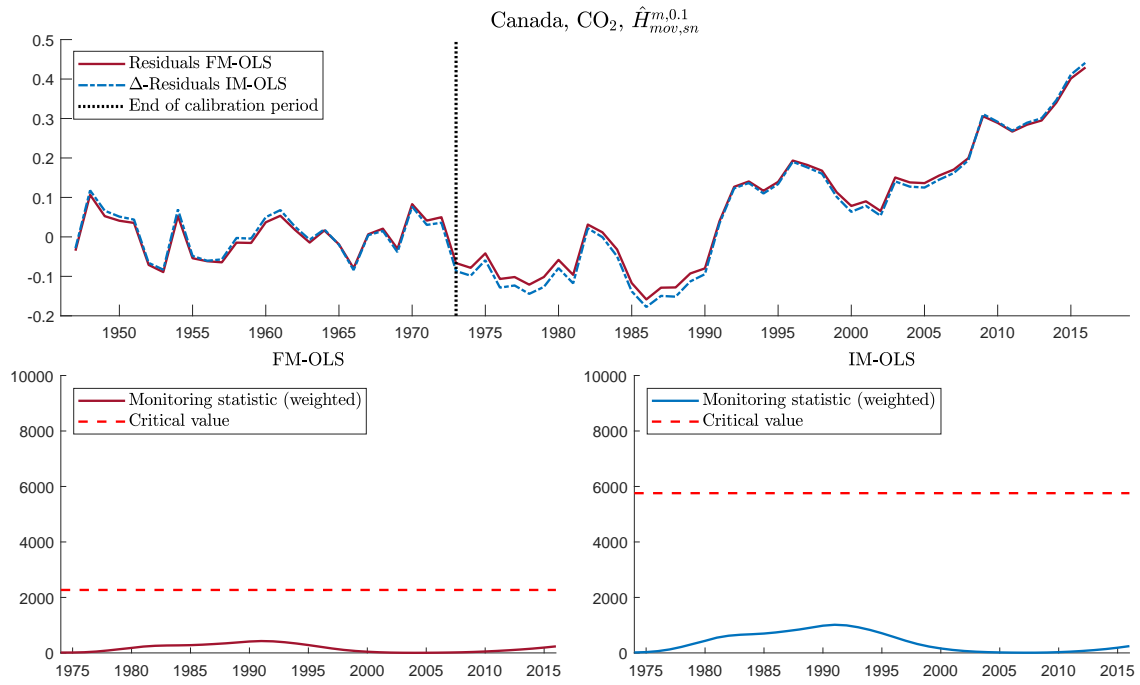


Figure S34: Monitoring results for CO<sub>2</sub> emissions of Canada using  $\hat{H}_{mov,sn}^{m,0.1}$  with both FM-OLS and IM-OLS in the linear specification. For further explanations see notes to Figure S32.

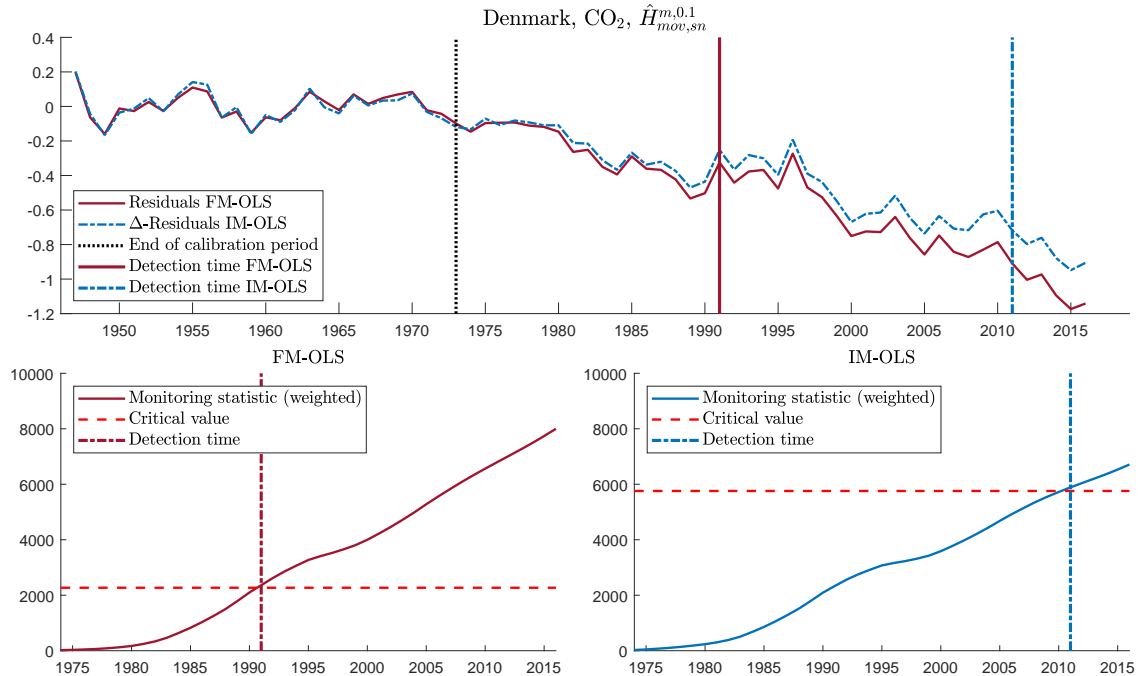


Figure S35: Monitoring results for CO<sub>2</sub> emissions of Denmark using  $\hat{H}_{mov,sn}^{m,0.1}$  with both FM-OLS and IM-OLS in the linear specification. For further explanations see notes to Figure S32.

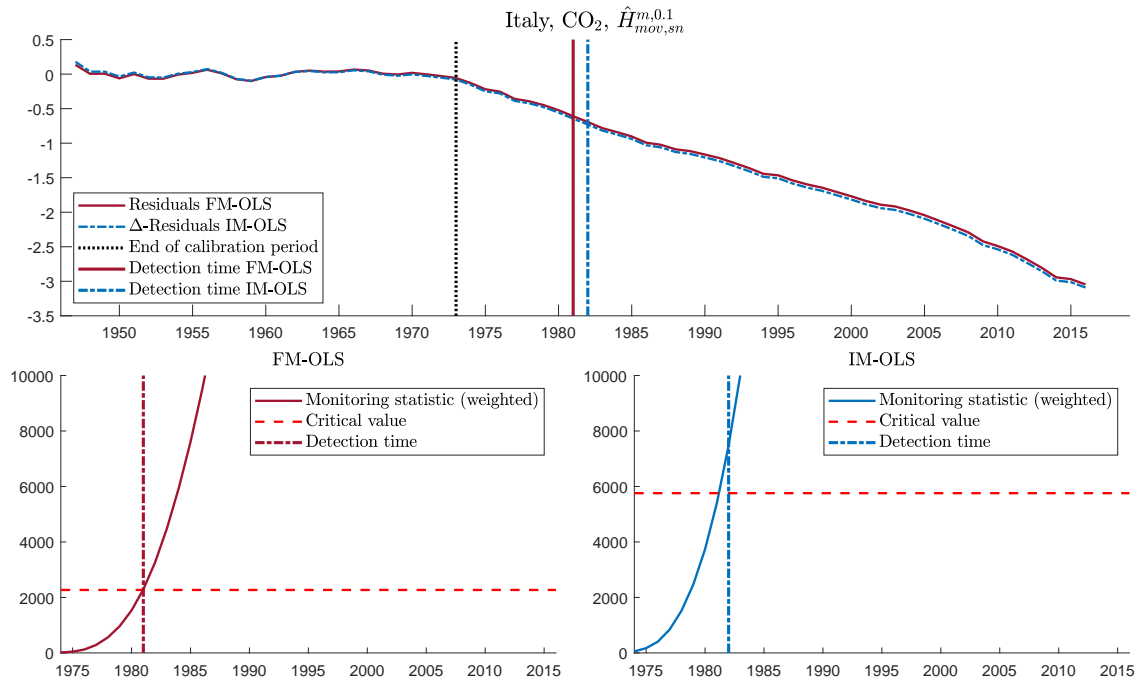


Figure S36: Monitoring results for CO<sub>2</sub> emissions of Italy using  $\hat{H}_{mov,sn}^{m,0.1}$  with both FM-OLS and IM-OLS in the linear specification. For further explanations see notes to Figure S32.

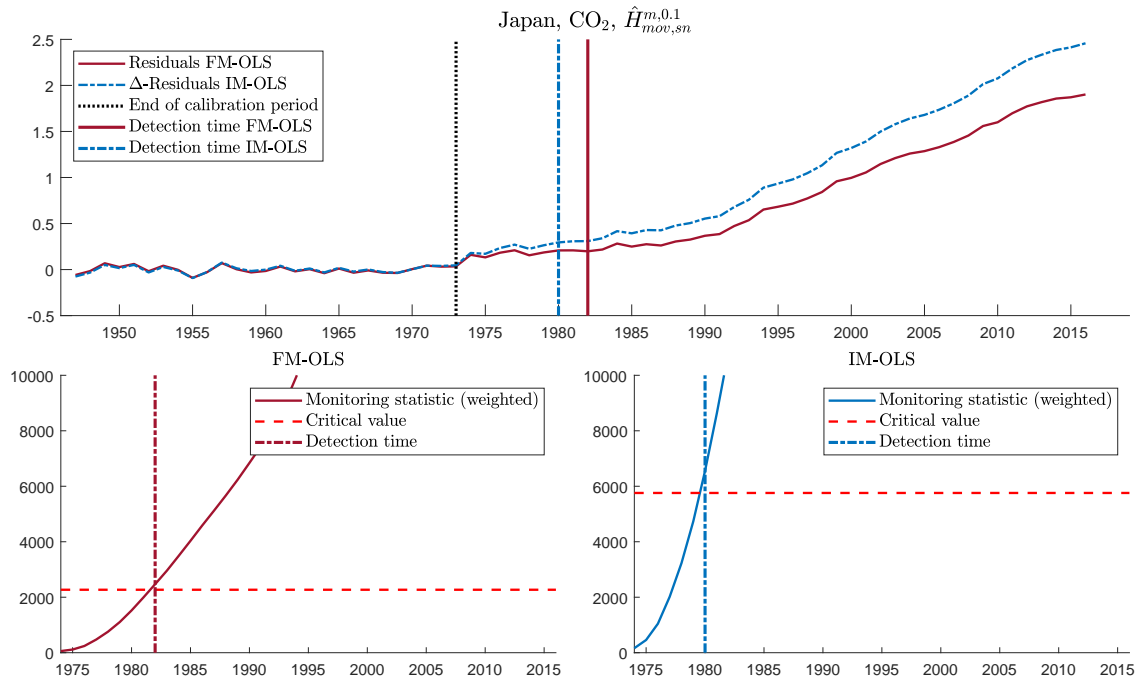


Figure S37: Monitoring results for CO<sub>2</sub> emissions of Japan using  $\hat{H}_{mov,sn}^{m,0.1}$  with both FM-OLS and IM-OLS in the linear specification. For further explanations see notes to Figure S32.

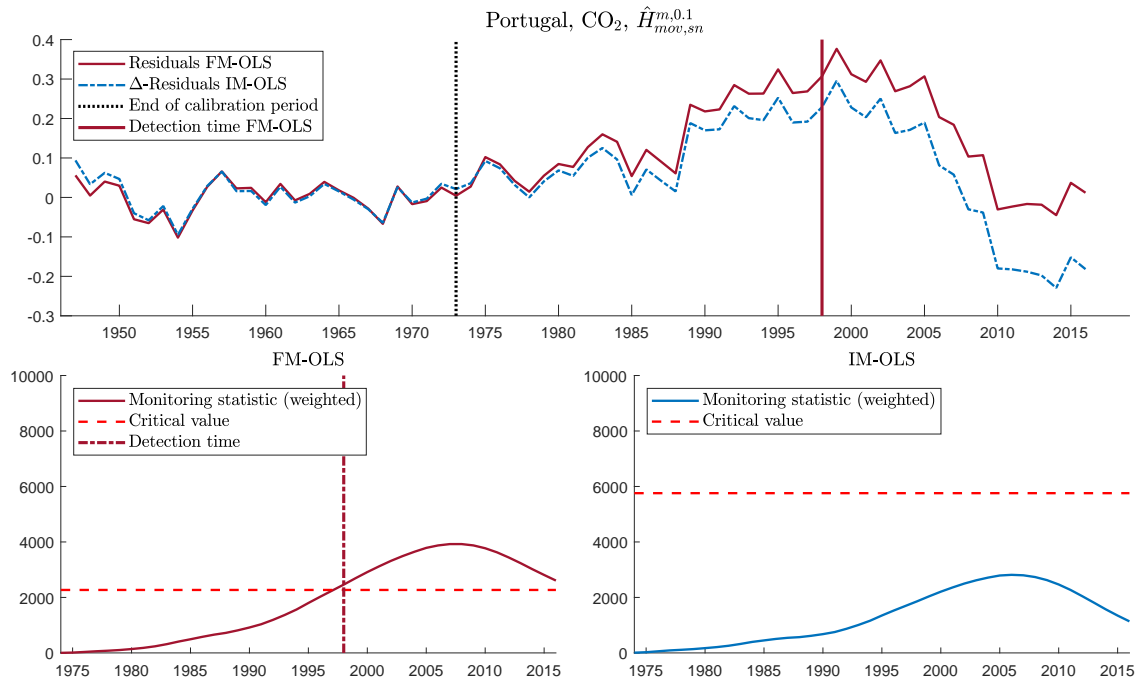


Figure S38: Monitoring results for CO<sub>2</sub> emissions of Portugal using  $\hat{H}_{mov,sn}^{m,0.1}$  with both FM-OLS and IM-OLS in the linear specification. For further explanations see notes to Figure S32.

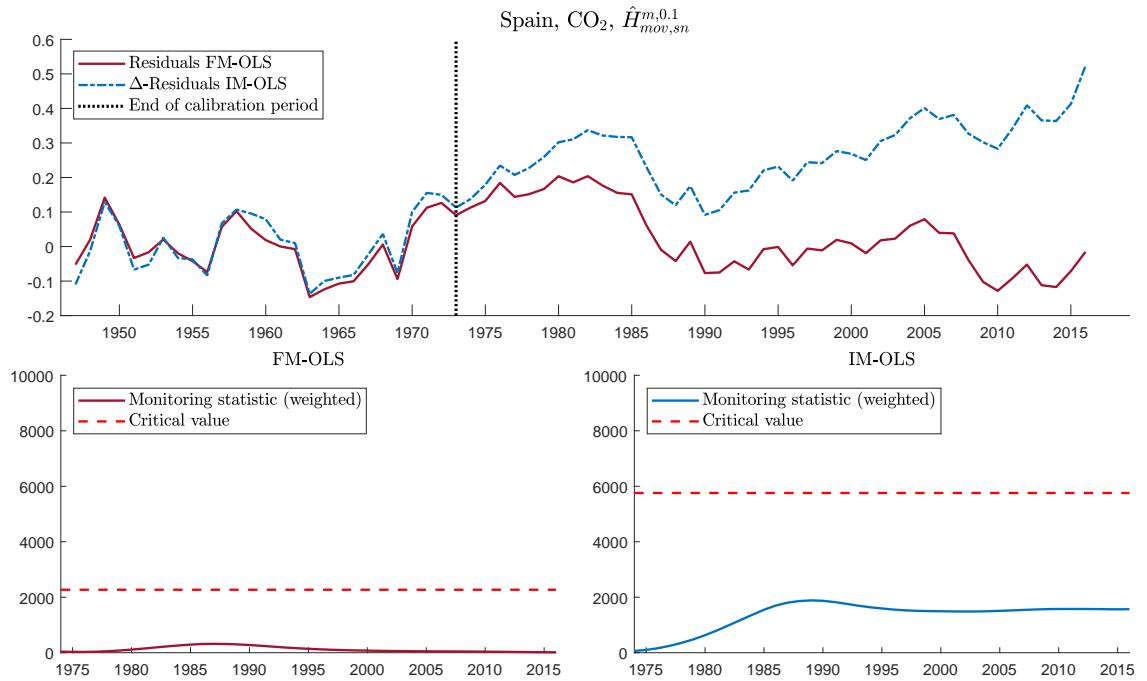


Figure S39: Monitoring results for CO<sub>2</sub> emissions of Spain using  $\hat{H}_{mov,sn}^{m,0.1}$  with both FM-OLS and IM-OLS in the linear specification. For further explanations see notes to Figure S32.

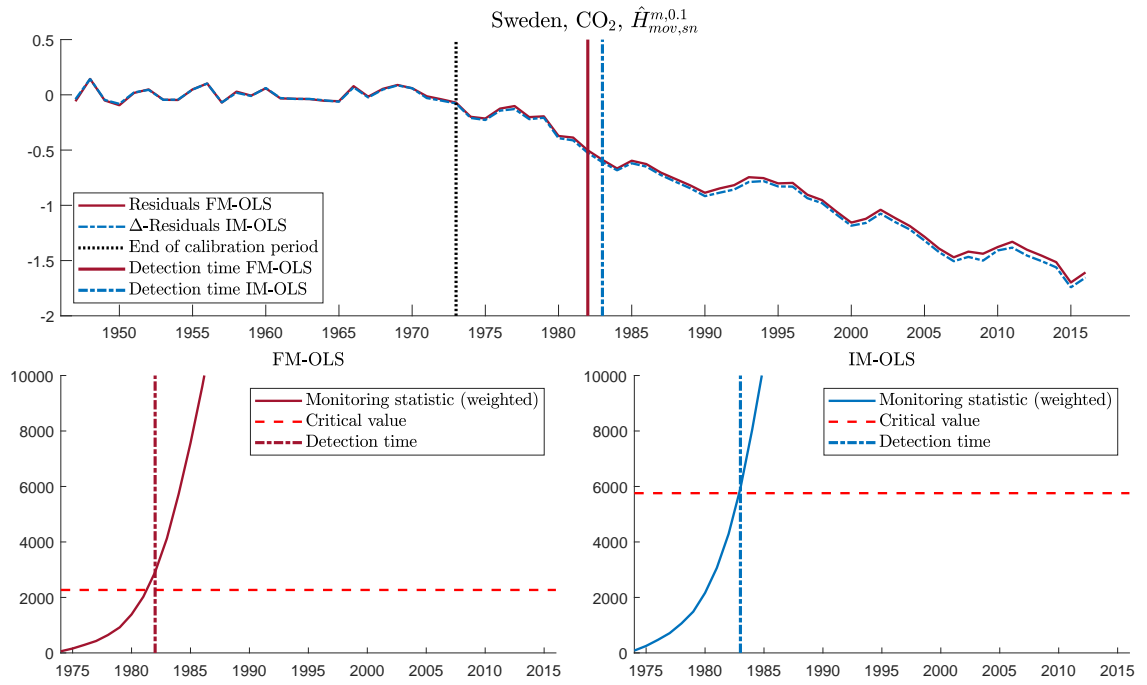


Figure S40: Monitoring results for CO<sub>2</sub> emissions of Sweden using  $\hat{H}_{mov,sn}^{m,0.1}$  with both FM-OLS and IM-OLS in the linear specification. For further explanations see notes to Figure S32.

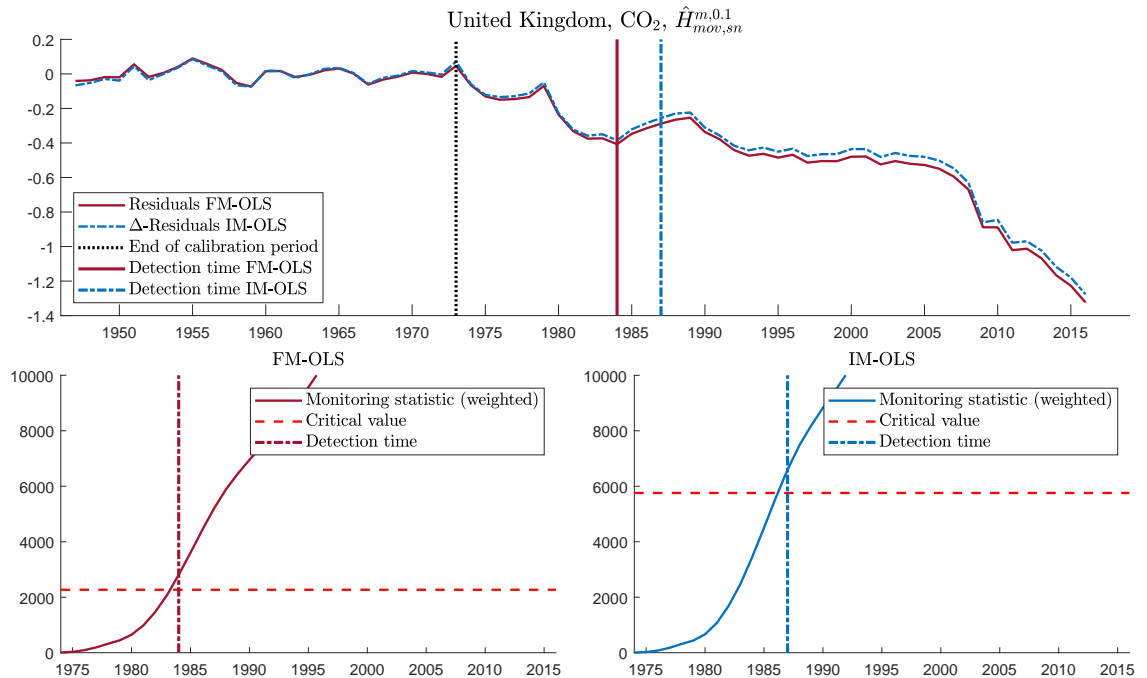


Figure S41: Monitoring results for CO<sub>2</sub> emissions of the United Kingdom using  $\hat{H}_{mov,sn}^{m,0.1}$  with both FM-OLS and IM-OLS in the linear specification. For further explanations see notes to Figure S32.

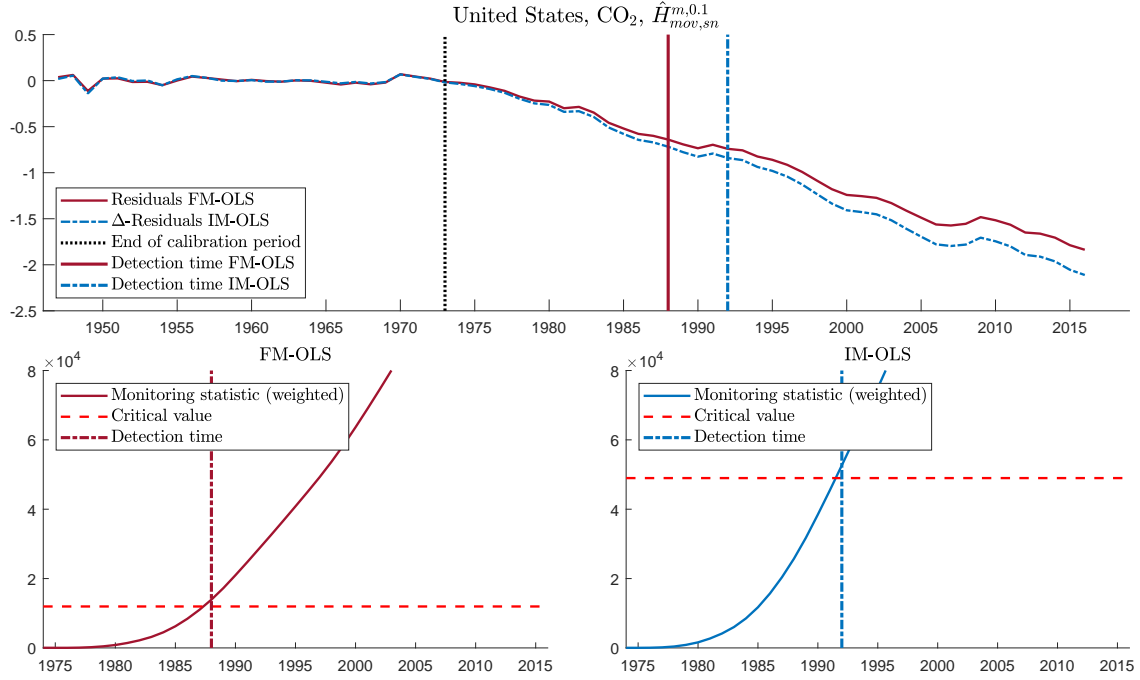


Figure S42: Monitoring results for  $\text{CO}_2$  emissions of the United States using  $\hat{H}_{\text{mov},sn}^{m,0.1}$  with both FM-OLS and IM-OLS in the quadratic specification. For further explanations see notes to Figure S32.

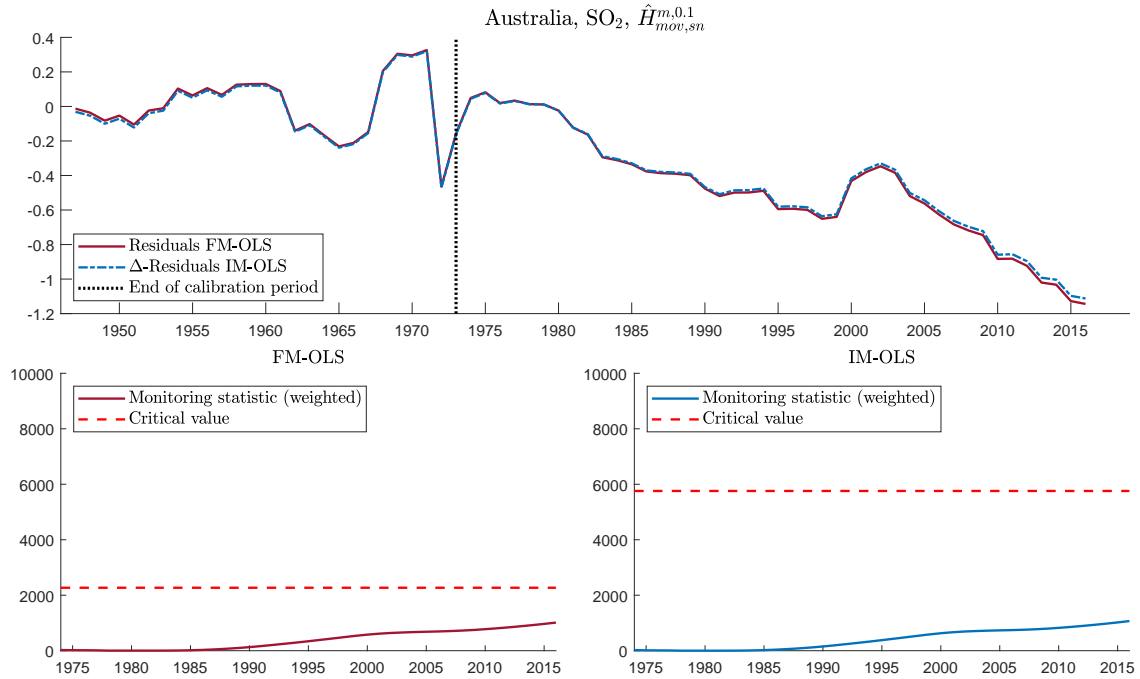


Figure S43: Monitoring results for  $\text{SO}_2$  emissions of Australia using  $\hat{H}_{\text{mov},sn}^{m,0.1}$  with both FM-OLS and IM-OLS in the linear specification. For further explanations see notes to Figure S32.

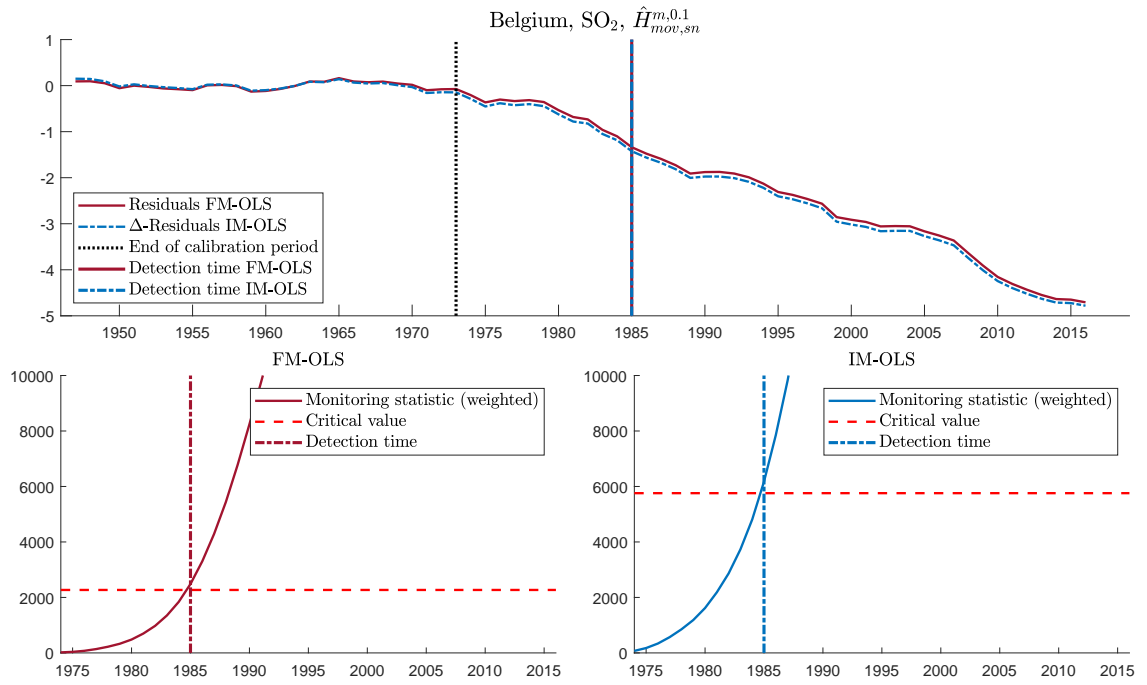


Figure S44: Monitoring results for  $\text{SO}_2$  emissions of Belgium using  $\hat{H}_{\text{moving},sn}^{m,0.1}$  with both FM-OLS and IM-OLS in the linear specification. For further explanations see notes to Figure S32.

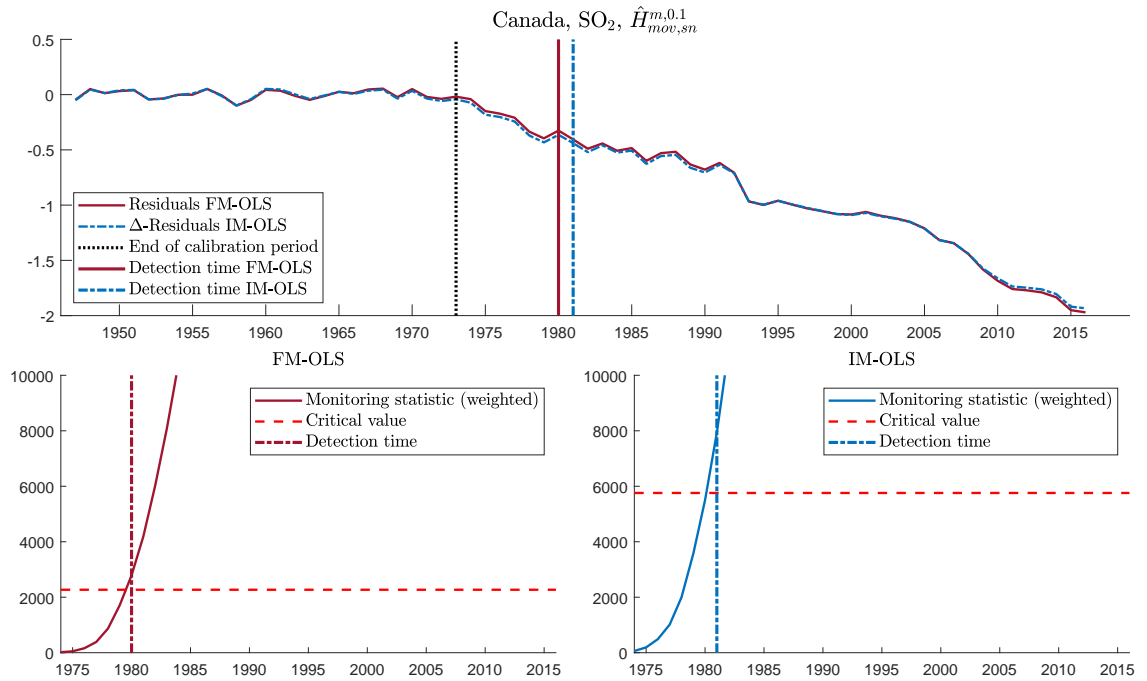


Figure S45: Monitoring results for  $\text{SO}_2$  emissions of Canada using  $\hat{H}_{\text{moving},sn}^{m,0.1}$  with both FM-OLS and IM-OLS in the linear specification. For further explanations see notes to Figure S32.

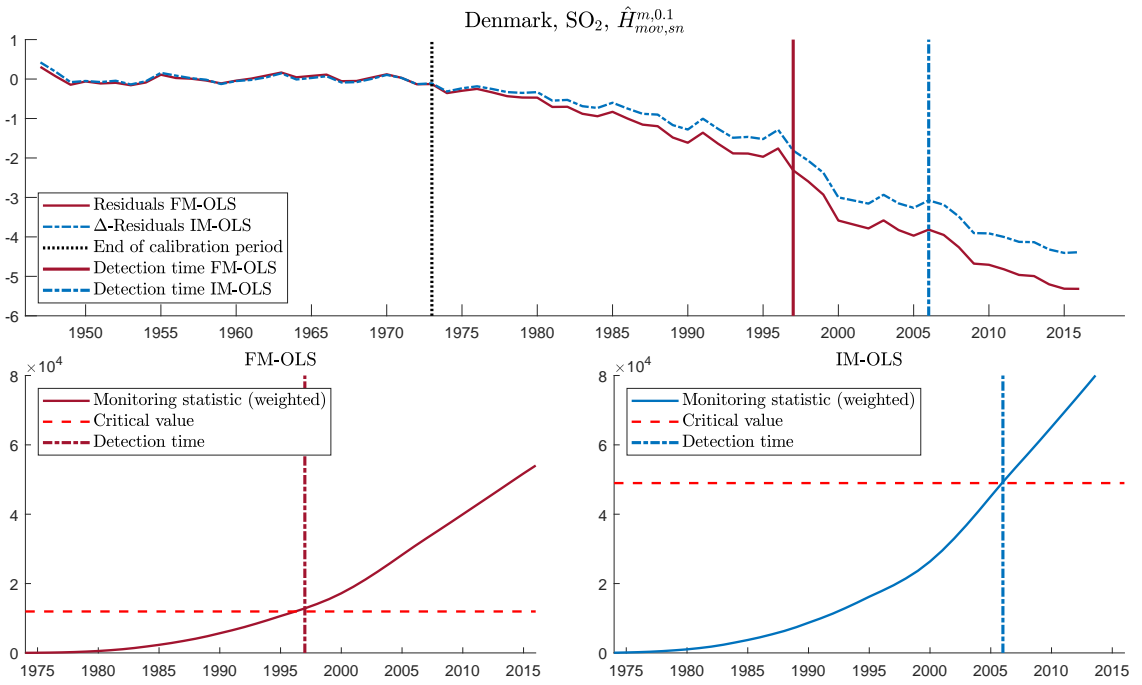


Figure S46: Monitoring results for SO<sub>2</sub> emissions of Denmark using  $\hat{H}_{mov,sn}^{m,0.1}$  with both FM-OLS and IM-OLS in the quadratic specification. For further explanations see notes to Figure S32.

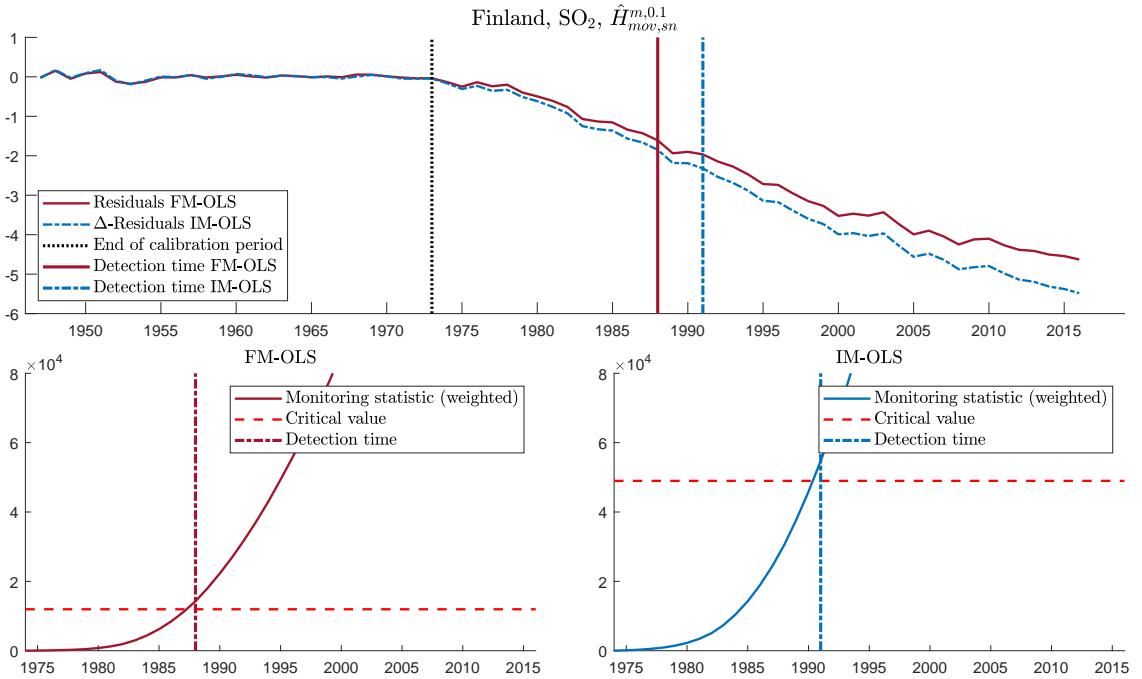


Figure S47: Monitoring results for SO<sub>2</sub> emissions of Finland using  $\hat{H}_{mov,sn}^{m,0.1}$  with both FM-OLS and IM-OLS in the quadratic specification. For further explanations see notes to Figure S32.

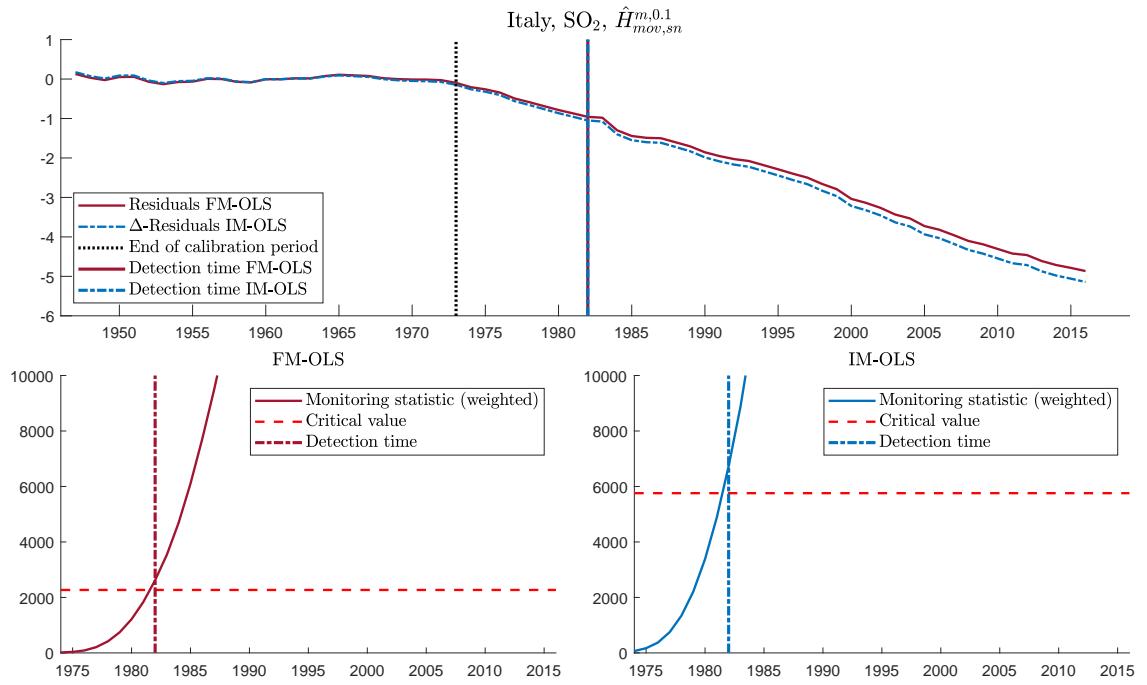


Figure S48: Monitoring results for  $\text{SO}_2$  emissions of Italy using  $\hat{H}_{\text{mov},sn}^{m,0.1}$  with both FM-OLS and IM-OLS in the linear specification. For further explanations see notes to Figure S32.

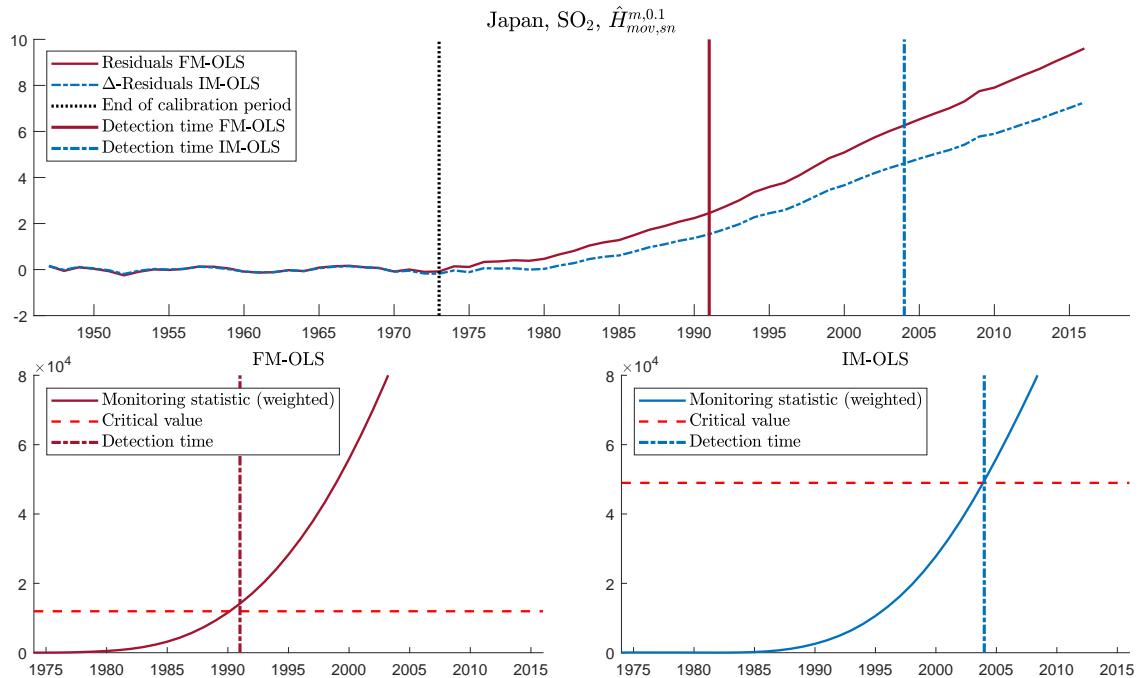


Figure S49: Monitoring results for  $\text{SO}_2$  emissions of Japan using  $\hat{H}_{\text{mov},sn}^{m,0.1}$  with both FM-OLS and IM-OLS in the quadratic specification. For further explanations see notes to Figure S32.

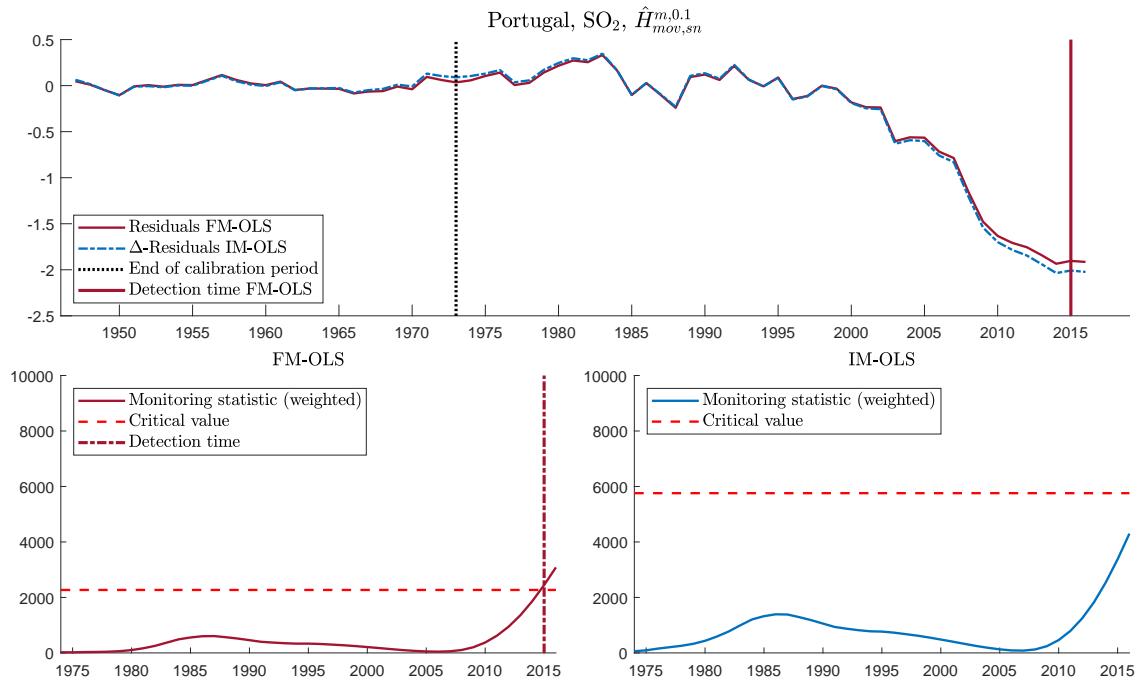


Figure S50: Monitoring results for  $\text{SO}_2$  emissions of Portugal using  $\hat{H}_{\text{moving},sn}^{m,0.1}$  with both FM-OLS and IM-OLS in the linear specification. For further explanations see notes to Figure S32.

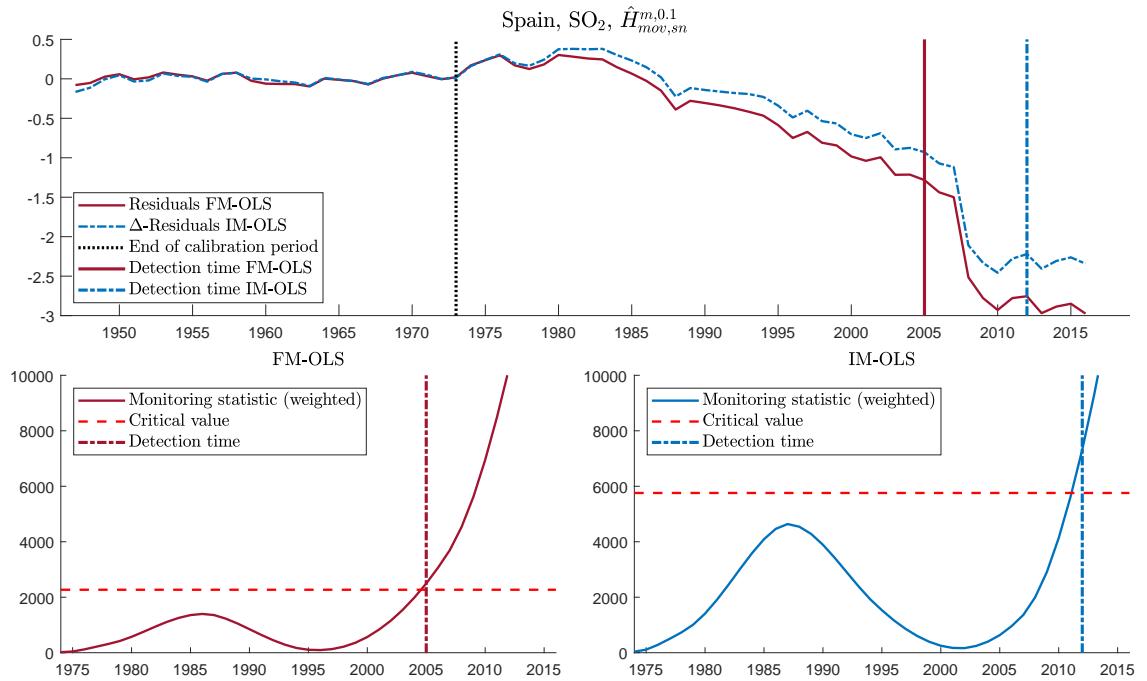


Figure S51: Monitoring results for  $\text{SO}_2$  emissions of Spain using  $\hat{H}_{\text{moving},sn}^{m,0.1}$  with both FM-OLS and IM-OLS in the linear specification. For further explanations see notes to Figure S32.

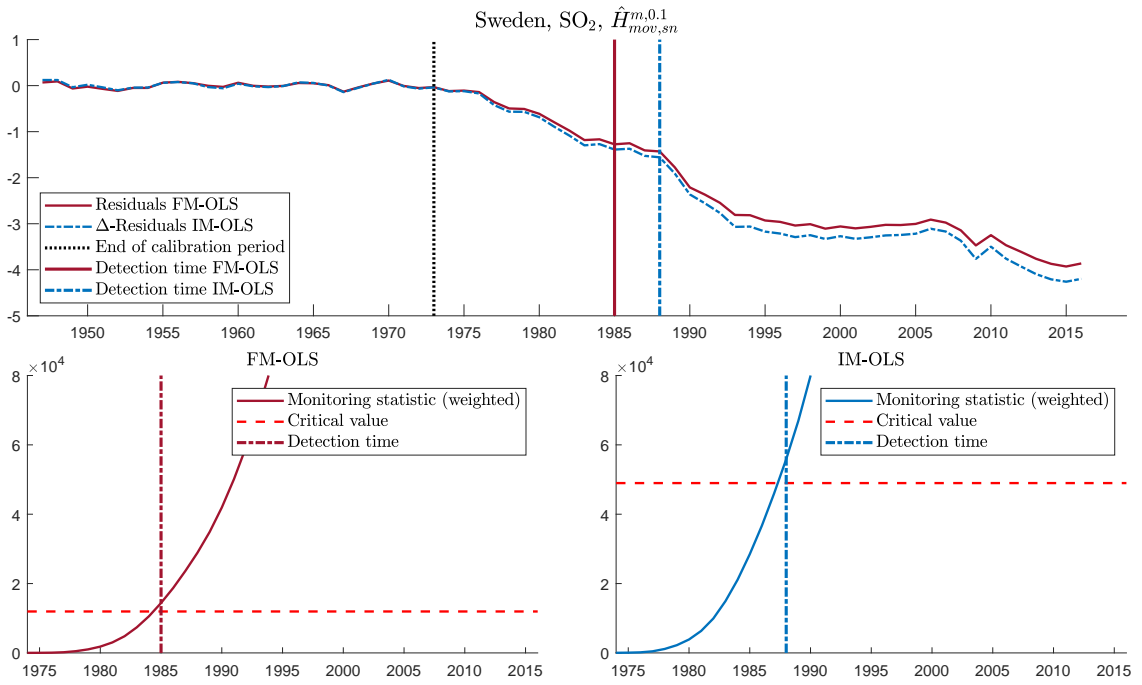


Figure S52: Monitoring results for SO<sub>2</sub> emissions of Sweden using  $\hat{H}_{mov,sn}^{m,0.1}$  with both FM-OLS and IM-OLS in the quadratic specification. For further explanations see notes to Figure S32.

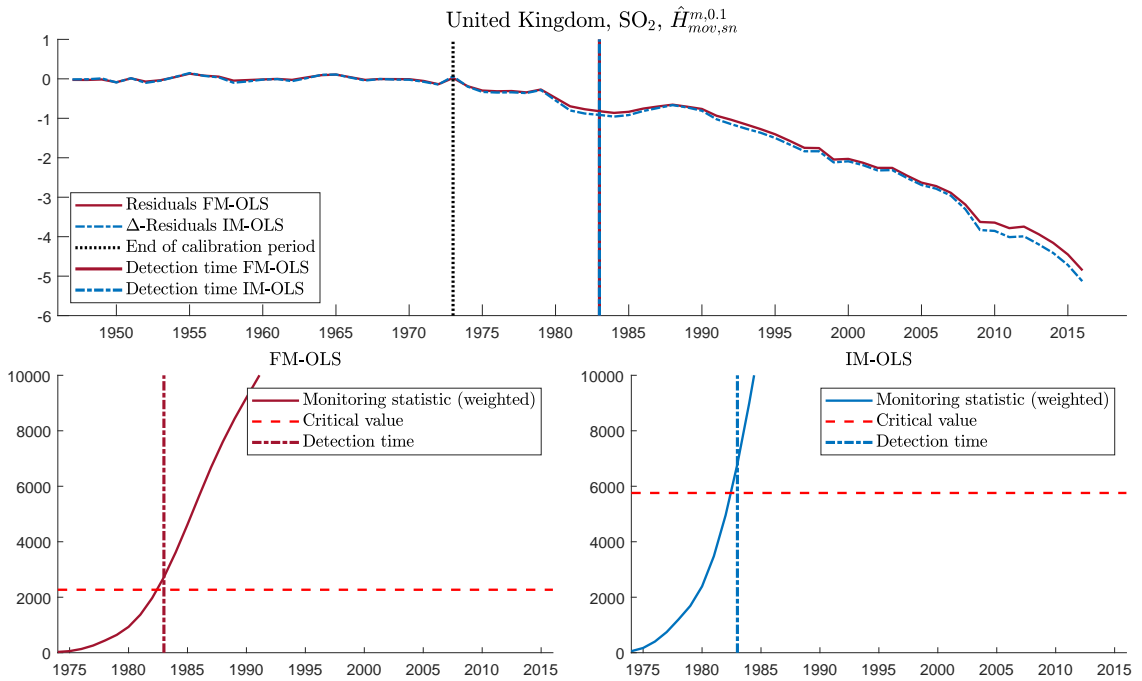


Figure S53: Monitoring results for SO<sub>2</sub> emissions of the United Kingdom using  $\hat{H}_{mov,sn}^{m,0.1}$  with both FM-OLS and IM-OLS in the linear specification. For further explanations see notes to Figure S32.

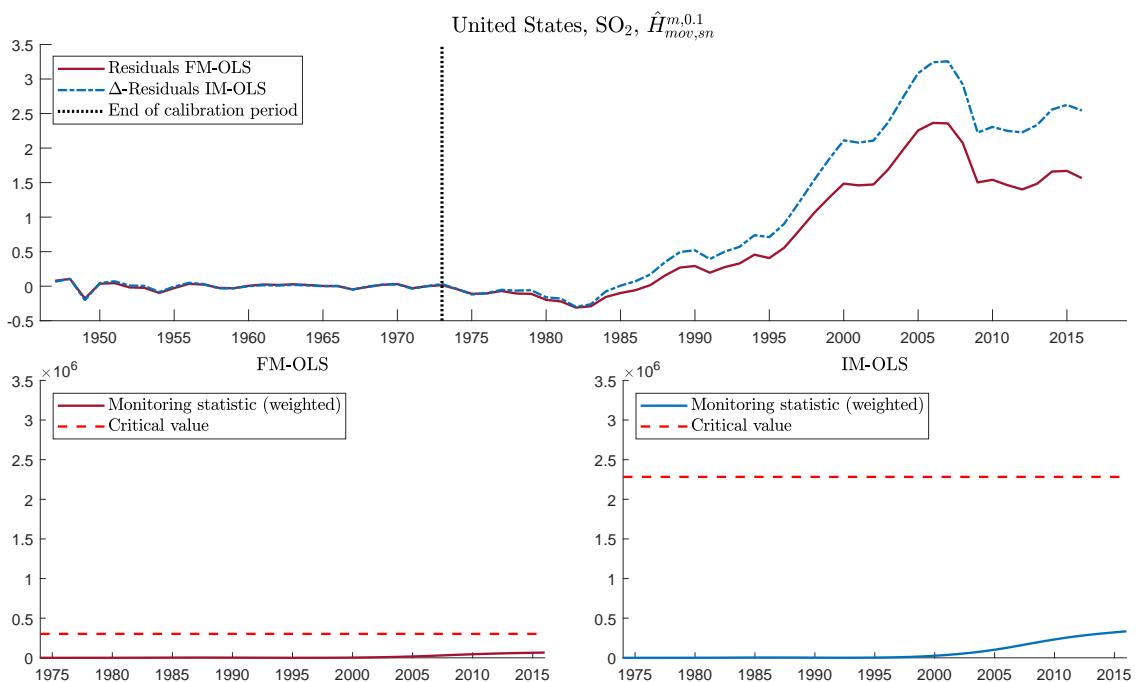


Figure S54: Monitoring results for  $\text{SO}_2$  emissions of the United States using  $\hat{H}_{\text{mov},sn}^{m,0.1}$  with both FM-OLS and IM-OLS in the cubic specification. For further explanations see notes to Figure S32.

## References

- Dickey, D.A. and W.A. Fuller (1981). Likelihood Ratio Statistics for Autoregressive Time Series with a Unit Root. *Econometrica* **49**, 1057–1072.
- Johansen, S. (1995). *Likelihood-based Inference in Cointegrated Vector Autoregressive Models*. Oxford University Press, Oxford.
- Phillips, P.C.B. and P. Perron (1988). Testing for a Unit Root in Time Series Regression. *Biometrika* **75**, 335–346.
- Shin, Y. (1994). A Residual Based Test for the Null of Cointegration Against the Alternative of No Cointegration. *Econometric Theory* **10**, 91–115.
- Vogelsang, T.J. and M. Wagner (2014a). Integrated Modified OLS Estimation and Fixed- $b$  Inference for Cointegrating Regressions. *Journal of Econometrics* **178**, 741–760.
- Wagner, M. (2020). Residual Based Cointegration and Non-Cointegration Tests for Cointegrating Polynomial Regressions. Revised and resubmitted to *Empirical Economics*.
- Wagner, M. and D. Wied (2017). Consistent Monitoring of Cointegrating Relationships: The US Housing Market and the Subprime Crisis. *Journal of Time Series Analysis* **38**, 960–980.